ANALYSIS OF THE EFFECT OF SMALL-SCALE TURBULENCE ON THE PHYTOPLANKTON DYNAMICS IN THE OPEN OCEAN

Modeling and Numerical Simulation
in the Vertical Dimension

Jesús E. Gabaldon Casasayas

Universitat Politècnica de Catalunya
Departament de Física Aplicada

ANALYSIS OF THE EFFECT OF SMALL-SCALE TURBULENCE ON THE PHYTOPLANKTON DYNAMICS IN THE OPEN OCEAN

Modeling and Numerical Simulation
in the Vertical Dimension

Jesús E. Gabaldon Casasayas

Ph.D. Dissertation

Directed by: Dr. José Manuel Redondo

Universitat Politècnica de Catalunya
Departament de Física Aplicada

"Life began in the ocean,
and most of the many forms of life
that ever existed on Earth lived,
or still live, in the ocean.[1]*"*

"But the upcoming days
are the wisest witness of Truth.[2]*"*

[1] Grant (1933).
[2] Pindar, V b.C.

CONTENTS

AKNOWLEDGMENTS

Besides all the people I ever talked with about science, I am very glad to express my gratitude to the people who directly, or indirectly, helped me in finding my *niche* in scientific research.

I feel sincerely indebted to Dr. Antonio Cruzado, from the Centre d'Estudis Avançats de Blanes (CSIC), who gave me the first chance in entering the field of modelling of aquatic ecological processes. I shared with him more than two years of good humor and work. I want also to thank to Dr. Ramiro Varela, now at the Universidade de Vigo. Both they became my first teachers and partners in modelling and numerical simulation. As a matter of fact, this Ph.D. started in the CEAB's atmosphere.

In Blanes, I was also lucky to meet Dr. Tarzan Legović, from the Rudjer Bosković Institute (Zagreb, Croatia), and his wife Emine. I am indebted to their stimulating experience, fine sense of humor and enthusiasm.

In 1995 I moved to the Applied Physics Department, at the Universitat Politècnica de Catalunya (UPC), where I initially found a suggesting atmosphere for developping my research work. There, I started my Ph.D. on the study of the influence of small-scale turbulence on phytoplankton dynamics. As a biologist, I want to thank the professors of the department not to make me feel like a stranger among them.

I specially want to express my gratitude to Dr. Jordi Vilà Guerau de Arellano. I enjoyed luckily further than his friendship, but his real mastery and talent. He and Dr. Gerber van der Graaf, both contributed in building a creative environment in the Fluid Dynamics Reasearch Group. Their loss was painfully felt by the Group.

I thank also Dr. Cèlia Marrasé and Dr. Marta Estrada, from the Institut de Ciències del Mar (CSIC), Barcelona, and Dr. Tim Granata, from the Centre d'Estudis Avançats de Blanes (CSIC)[3], and Dr. Marta Alarcon, from the UPC. They provided me with data and, more than that, with their fruitful comments.

Finally, my work was stimulated by the long stage (two years, almost) at the Limnologisches Institut from the Universität Konstanz, Germany. Its long-term biological and physical database of Lake Constance provided me with a deeper understanding of the biology of aquatic ecosystems.

I also wish to thank Dr. Ursula Gaedke for giving me the oportunity of collaborating in the project *Entwicklung eines dynamischen Simulationsmodells mit komplexer Nahrungsnetzstruktur für die Freiwasserzone mitteleuropäischer Seen* (Development of a dynamical simulation model with a complex food-web structure for the central-european

[3] Now he is back to the Department of Civil and Environmental Engineering and Geodetic Science, at Ohio State University.

lakes).

I feel also indebted with Dr. Beatriz Vidondo for the “summer advice note”, and her fruitful conversations. I also keep very happy memories of a lot of friends who, somehow, positively influenced my work, among them: Dr. Thomas Gries, Dr. Tinus Wessels, Dr. Dietmar Straile, Angelika Siegfried, Markus Holzmann, Stefan Hoernchen, Karin Roggenbrodt, Kerstin Bitner, Christoph Wittkugel... In Catalonia, I do not forget mentioning Dr. Jordi López, Ferran Pauné, Cèsar Guitiérrez and Oriol Martí, for their long friendship and support. And, how could I (anybody) forget Maria Ozilea Bezerra Menezes; for the shared experiences at the Applied Physics department.

Finally, this thesis was provided with data yielded by the next research projects:

- MODB Project funded by the European Commission, as part of the MAST-II program, contract EUR MAS2-CT93-0075-BE.
- Project funded by the spanish CICYT, contract MAR 91-0359.

Part I

INTRODUCTION

INTRODUCTION

The oceans cover nearly 71% of the surface of the Earth and play an important role over the climate variability. They are pointed out as a key issue in topics like global warming. Indeed, we know of the potential impact of changes of the ocean circulation over the global climate.

Physical processes related with ocean currents may affect marine communities at any level, and they exert a strong effect over the global biogeochemical carbon cycle (Schlesinger, 1997; Gruber, 1998; Field *et al.*, 1998; and references cited therein). Nevertheless, the relationship between the role of climatic variation and the regulation of marine phytoplankton populations and communities is not well understood yet, and the biological consequences of climatic variability of the atmosphere and oceans are still largely unknown (McGowan *et al.*, 1998).

Ocean primary producers, which account for 32% of the global net primary production (Whittaker, 1975), are located at the bottom of the marine food web. They control the carbon fixation process by means of the photosynthetical process. Photosynthesis process needs light and dissolved mineral salts (often called *nutrients* by the oceanographic scientific community).

Light and nutrients are not equally distributed throughout the ocean water column. As a matter of fact, they are not equally distributed in the vertical dimension almost anywhere, both in aquatic and terrestrial environments. Sunlight comes from above and decreases downwards, following the well known Beer-Lambert law. Contrarily, nutrients are usually more abundant in depth. Similar trends can be observed in the alpine tundra, in tropical rain forests, and in the open ocean. Aquatic and terrestrial photosynthetic organisms, both face up with the same opposite distribution. Let us see an example: trees get most of the light they need for photosynthesizing from above, whilst mineral salts, which available, remain dissolved far down into the soil. But trees need necessarily to bring light and nutrients together to the leaves. They can do little for bringing light to the leaves; just trying to get as much as possible, and efficiently use it, afterwards. However, they do heavily struggle for pumping nutrients up, higher and higher, in order to avoid shading from neighbouring light competitors.

In aquatic environments it occurs a similar process than in terrestrial environments: the analogous uneven distribution of radiation and nutrients. Nevertheless, the physical processes play a more relevant role in fluid environments which is worth to be briefly introduced at this stage.

The vertical transport of matter is a fundamental process in the biosphere that applies

to all the possible environments in the Earth. The essential chemical elements (C, N, S, P, Si) are vertically transported upward within the ecosystems, while assimilation products (organic matter) are spread down from the level where they were synthesized. Vertical transport is fundamentally an *external* process in aquatic ecosystems (Margalef, 1991), which means that it is driven by external physical mechanisms. This is because most of the carbon fixed in the open ocean is carried out by structurally very simple and free-living photosynthetical organisms called phytoplankton, which accounts for many different small ($\sim$0.4–200 μm) species with very limited swimming capabilities, or none. Phytoplanktonic organisms can be found as single cells or colonies, and they can only develop where both light and nutrients are simultaneously available (as far as nutrients are not *internally* transported within the organism). Alternatively, phytoplankton has to fundamentally rely on external physical mechanisms for the vertical transport of nutrients from the rich but dark deeper layers to the uppermost illuminated layer called *euphotic zone*[1].

On the basis of the stability provided by a solid medium, terrestrial ecosystems succeeded in internalizing some of the most sensitive vertical transport processes and, thus, becoming less dependent on environmental fluctuations.

One may try to figure it out how relevant life transport phenomena in the Earth are, by looking at the asymmetry between the vertical and horizontal gradients of the living organisms (or biomass) and, specially, by looking at the very thin layer where one of the most fundamental life processes (photosynthesis) takes place; it occurs anywhere in a layer usually not thicker than 100 or 150 meters. Such layer is surprisingly thin in comparison with the horizontal distribution of the photosynthetic organisms all over the Earth's surface. Environmental conditions vertically confine the assimilation layer to such a reduced space, with its upper boundary limited by gravity and its lower one limited by the penetration of sun irradiance.

But we shall do not intend to cope with all the underlying mechanisms that make the photosynthetic layer so thin. We shall just focus on the analysis of the role of the mixing processes, which are known to exert the major control over the vertical transport of matter in aquatic environments and, consequently, over the carbon fixation rate and nutrient utilization by the phytoplankton (called *primary production* of phytoplankton).

Light penetration in the water and, specifically, the vertical distribution of light throughout natural waters, has been thoughtfully studied (Mobley, 1994). In parallel, the relationship between irradiance and aquatic primary production has been also explored and rigorously investigated by many authors (*see* Falkowski & Woodhead, 1992; Kirk, 1994).

However, as mentioned above, the radiative energy provided by the sun is not the only necessary resource required by the phytoplankton for growing (Figure 0.1); nutrient input is a key-factor which usually becomes limiting for the synthesis of biomass by the primary producers.

Phytoplankton takes up nutrients from the boundary waters; under optimal condi-

[1] The euphotic zone (or layer; z_{eu}) is known as the uppermost layer of the water column, within which irradiance falls to around 1 or 2% of subsurface irradiance.

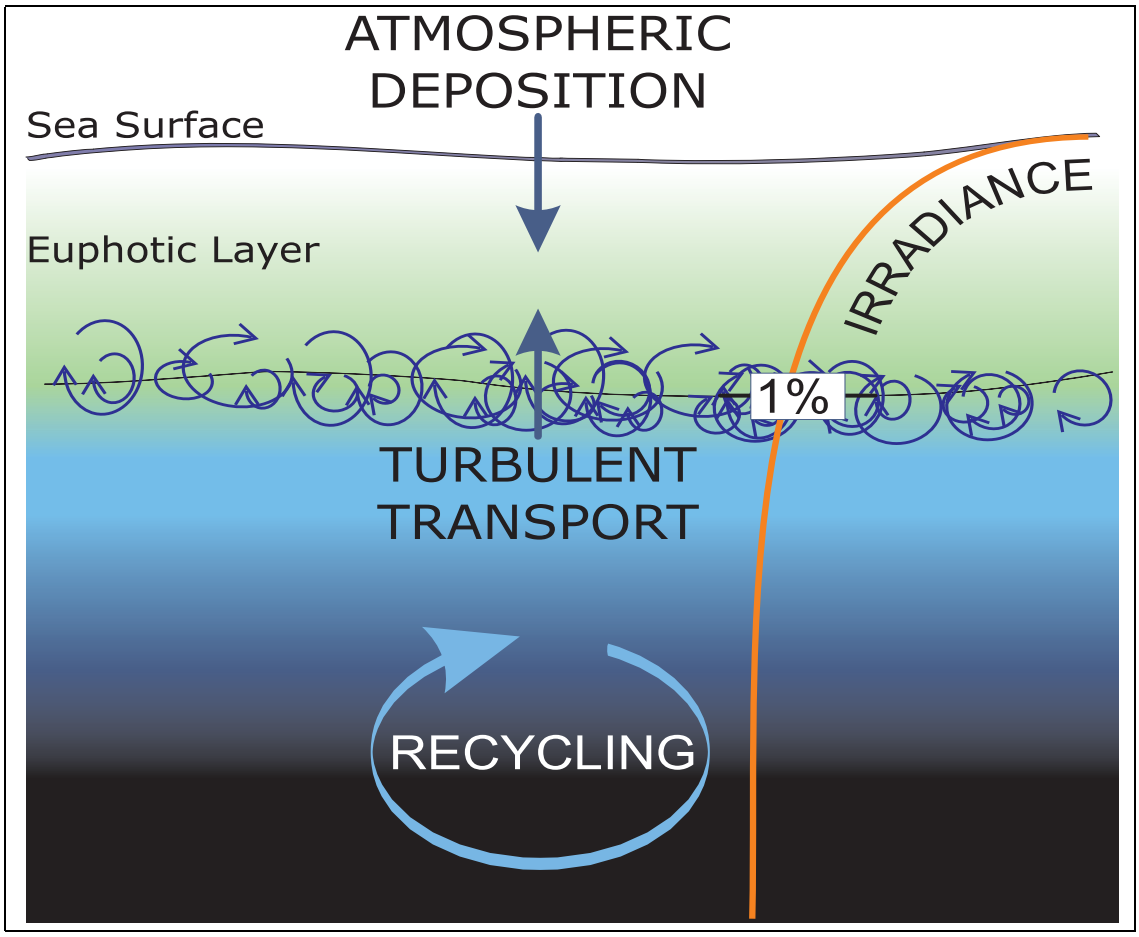

Fig. 0.1: Scheme of the main driving environmental mechanisms affecting the productivity of the phytoplankton in the open ocean: namely, nutrient inputs (nutrients upwelled from deeper layers and atmospheric deposition) and irradiance. The productive *euphotic layer* ranges from the sea surface down to the depth where 1% of subsurface irradiance is reached.

tions, they take up the most limiting one until depletion[2], or light limitation. However, terrestrial (or benthic) ecosystems follow quite different strategies than the pelagic ecosystems.

Evolution of higher plants is closely related with the advantage of living on a relatively more stable (solid) substrate: higher plants partially internalized the vertical transport of nutrients into the same organism (*xylematic* transport), thus partially avoiding the stressing effect of short period environmental fluctuations. On the other side, as most of the phytoplanktonic species show a very limited (or null) swimming capacity, phytoplankton communities basically rely on external physical mechanisms for the upwelling of nutrients (Margalef, 1991). Consequently, phytoplanktonic communities, as the lowest

[2] *See* footnote 3, and next paragraphs.

trophic level of the pelagic ecosystems, do strictly experience the impact of atmospheric phenomena and stationality, as evidenced by the seasonal alternation of functional groups (diatoms, autotrophic flagellates, etc.).

Stationality and severe meteorological events (such as storms) heavily influence the hydrodynamical conditions of the uppermost layers of the water column. Therefore, we must emphasize, as well, that the physical environment also influences the lowest levels of the pelagic ecosystems. This influence is basically exerted through the vertical transport of nutrients by means of turbulent mixing processes.

In the classical paradigm of biological oceanography, nitrogen is regarded as the *limiting*[3] nutrient for phytoplankton growth (Gruber & Sarmiento, 1997; and references cited therein; *see* also Tyrrell, 1999). The main statements for assessing whether nitrogen or phosphorus is more likely to be limiting are three: first, the preferential loss from the euphotic layer of nitrogen or phosphorus due to biogeochemical processes; second, the extent to which any relative deficit in nitrogen availability is made up through nitrogen fixation as an alternative source of nitrogen and, third, the ratio of nitrogen to phosphorus in external nutrient inputs (Howarth, 1988).

Despite the close relationship between hydrodynamical processes and phytoplankton primary production evidenced by oceanographers and aquatic ecologists since a long time ago (Eppley & Sloan, 1966; Eppley, 1972; Keller, 1989; Denman & Gargett, 1983; Dugdale *et al.*, 1989), hydrodynamics does not significatively play a direct role on light penetration (Platt *et al.*, 1991; Hoge & Swift, 1993). In consequence, phytoplankton dynamics was early evidenced that was fundamentally controlled by the upwelling of nutrients from deeper layers (Dugdale, 1967; MacIsaac & Dugdale, 1969; Walsh, 1975; Cullen & Eppley, 1981; Zimmerman *et al.*, 1987).

However, not all the kinetic energy contained in large hydrodynamical processes contribute to the mixing in the open ocean. Most of the energy contained in the hydrodynamical processes of large period and scale (typically, synoptic and mesoscale phenomena) is mainly invested in the transport of large amounts of water. However, the mixing of water and other scalars is mainly driven by the small structures of these motions, namely the turbulent diffusion transport. Therefore, the main physical process responsible for the vertical transport in the ocean is the so-called *small-scale* turbulence, which is characterized by processes times that range from seconds to minutes (Figure 0.2).

Among all the physical mechanisms involved in ocean hydrodynamics, small-scale turbulence has been evidenced as the most essential mechanism for the vertical transport of matter in the open ocean (Hopfinger, 1987; Gargett, 1997). This statement is supported not only by direct transport estimates (*op. cit.*), but also by different field studies (Platt, 1972; Powell *et al.*, 1975, Seuront *et al.*, 1999). These studies concluded that over small scales within the range (20–1000 s, and 12–540 m; from Seuront *et al.*, 1999) the spectral density of phytoplankton shows a similar scaling regime than temperature and

[3] We define the concept of *nutrient limitation* as the limitation of the potential rate of net primary production. As phytoplankton aggregates play the role of unique primary producers in this thesis, such definition allows for possible shifts in the composition of the phytoplanktonic community, thus not referring to one single species, or group.

salinity. This results evidence a strong relationship between small-scale turbulence and spatio-temporal phytoplankton dynamics at these small scales. Therefore, in this thesis we mainly focused on the effect of small-scale turbulence over the dynamics of these organisms.

The main nutrient input to the euphotic zone in the open ocean is basically the transport from deeper layers. However, during the last decades, the increasing trend of atmospheric deposition to the open ocean (Figure 0.1) has been also stated as an additional nutrient input (Duce *et al.*, 1991; Taylor & Penner, 1994; Prospero *et al.*, 1996; Paerl, 1997; Herut *et al.*, 1999).

In the Northwestern Mediterranean Sea, nitrate presents a permanent maximum concentration at nearly 800 meters. During the warm season nitrate, like other major nutrients (phosphorus, and silicate), show a decreasing trend towards the surface as a consequence of the depletion by the primary producers. At that time phytoplankton may almost completely deplete the uppermost layers of the water column. Ocean surface layers will not be replenished again till the next winter mixing events. Despite that nitrogen input from atmospheric deposition can not be neglected in some areas (Taylor & Penner, 1994; Herut *et al.*, 1999), the main input of nitrate to the surface waters comes from the deeper layers. The replenishment process of the surface waters takes place every year by turbulent mixing and remineralization, and at a lower scale, by atmospheric deposition. Therefore, we will mainly focus on the vertical turbulent transport as the most essential mechanism for the limitation of phytoplankton primary production.

Rationale

Growth rate is commonly considered as a relevant indicator of phytoplankton productivity or metabolic activity. Its characteristic time scale ranges approximately from less than half a day to a few days. However, the characteristic time scale of turbulent transport of matter in the ocean is several orders of magnitude smaller than growth rate's. This implies that phytoplankton can not directly react to single turbulent events in terms of turbulent nutrient transport (analogously, trees do not significatively react when a cloud just passes by shading sunlight). Nevertheless, this short period environmental phenomena may influence somehow biological processes characterized by longer period; likewise (e.g.), a few days long cloudy periods may give a slower phytoplankton growth rate.

Such a pronounced separation of scales (two orders of magnitude) does not suggest a direct causal relationship. In consequence, we assume that phytoplankton growth rate has to be related with relevant environmental factors like nutrient transport, by means of intermediate faster biological process of similar time scales. This argument immediately raises the question of what is the biological mechanism of phytoplankton with a similar characteristic time scale to the nutrient turbulent diffusion transport; furthermore, we may infer that it has to be a biological mechanism closely related with nutrient transport dynamics. Time scale analysis of the most relevant physical and biological processes suggested that this mechanism can be nutrient uptake. Characteristic time scales of nitrate

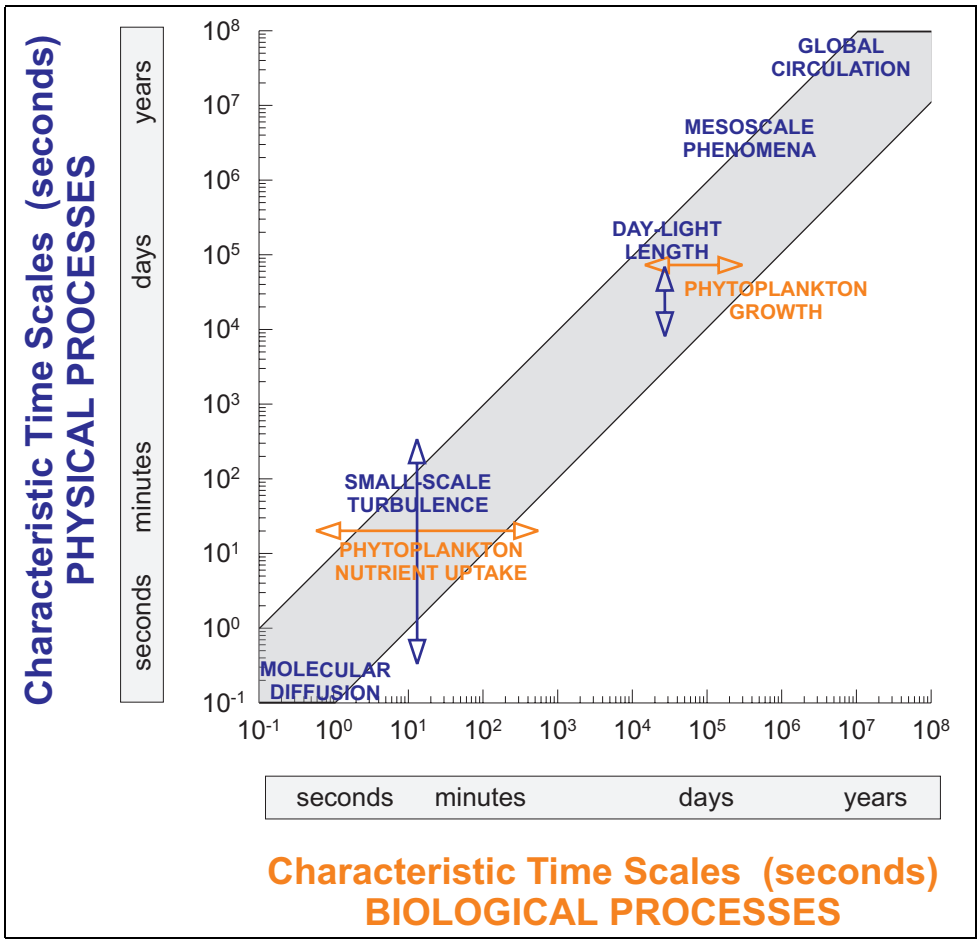

Fig. 0.2: Characteristic time-scales of some marine physical processes *versus* characteristic time scales of some relevant biological processes of the phytoplankton.

uptake and other nutrients are similar to the typical values of small-scale turbulence in the open ocean (Figure 0.2).

Despite any synthesis effort, the set of parameters involved in the biological processes considered in this work is far too large to be measured during the same cruise or oceanographic campaign, in order to be representative of similar environmental conditions. Some of the parameters require long processing methods or complex sensors to be acquainted with (i.e.). Therefore, modeling became the most suitable approach for our purposes, aware of that modeling of physical and biological processes involved in phytoplankton dynamics can be successfully achieved (*see* Franz *et al.*, 1991; and Evans & Garçon, 1997). In addition, models allow us to study the interaction dynamics of different processes. Mathematical models can also be powerful predictive tools. They can also improve our ability to monitor and quantify large (synoptical and global) spatial and

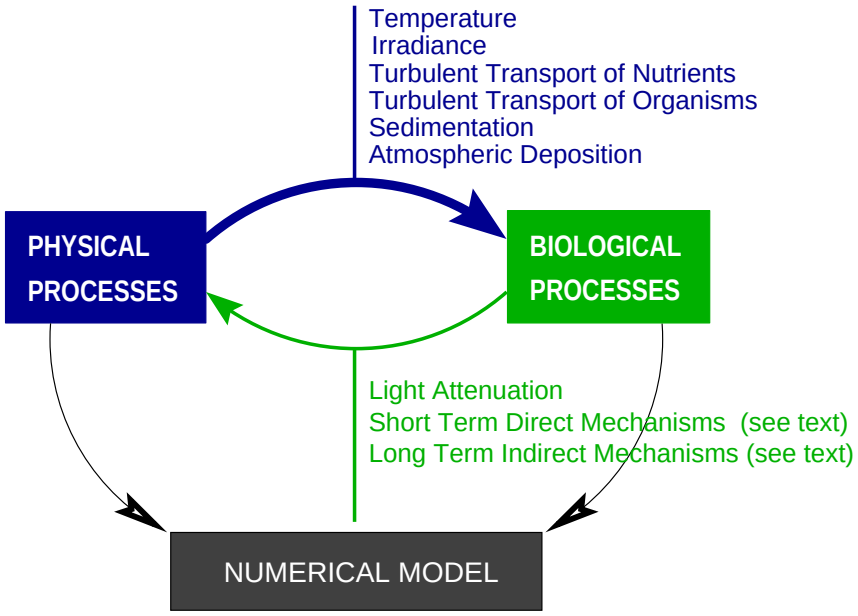

Fig. 0.3: Schematic representation chart of the coupled global physical-biological system developed in this study for the marine phytoplankton. Above (blue) are shown the main physical controlling factors affecting phytoplankton growth considered in this work. Below (green), the main feedback processes that, directly or indirectly, influence the physical environment. Phytoplankton exert a weak *direct* influence over the physical processes mainly because of the relative low concentration of organisms, particulated organic matter, and dissolved substances. On the other side, the physical-biological system represented by the marine environment and the phytoplankton shows a close long term *indirect* non-linear global interaction at climatological time scales; though this interaction has not been rigorously quantified yet. After the evaluation of the numerical results against depth, the model provide an output that can be piped into different large scale models, like *GCMs*.

temporal scale processes[4].

We have defined the physical-biological system (Figure 0.3), first, by the concentration of a *phytoplankton aggregate*; this is, by the concentration of an heterogeneous assemblage of phytoplanktonic species (measured in units of chlorophyll *a* concentration). And second, by the two fundamental resources necessary for the phytoplankton growth, namely, light and nutrients. Roughly speaking, the system is controlled by the co-occurrence at each depth of the limiting nutrient, and the necessary energy input for the synthesis of biomass (sun irradiance).

Phytoplankton shows very different dynamics in the vertical and horizontal spatial scales. Models concerned with large horizontal scales like *General Circulation Models* (GCMs) still lack of spatial resolution, specially in the vertical dimension. In the horizon-

[4] *See* the U.S. JGOFS Synthesis and Modeling Project Implementation Plan for a further insight.

tal dimensions, this drawback has been usually overcome with the aim of remotely sensed high resolution images from satellites and aircrafts. However, it is necessary to vertically integrate the carbon and nutrient distributions in order to estimate global fluxes and budgets. The vertical distributions of biological variables, like phytoplankton primary production, can be estimated and properly simulated with the aim of coupled physical-biological numerical models. Therefore, we focused our research on the vertical dimension, as far as it usually shows the highest gradients and, consequently, they need to be more carefully estimated.

We strived to build up a flexible biological model that could react and adapt to the fast environmental changes due to small-scale turbulence. Thus, the reasons for writing a new eco-physiological *sub*-model instead of taking one from the literature were several. The first one was to uncouple nutrient uptake and growth. Though growth and nutrient uptake have very different characteristic temporal scales, phytoplankton growth rate has been often described as a function of external nutrient concentration, according to the well known Michaelis-Menten (or Monod) equation. A first advantage of uncoupling those processes is to allow nutrients to accumulate in the cell, according to the internal nutrient requirements. This enables growth to be estimated according to the internal nutrient concentration, which is a more realistic approach indeed. Second, we also uncoupled photosynthesis (carbon fixation) and growth (synthesis of biomass). In this case, we achieved that the synthesis of biomass could be maintained during night time. On the other hand, it has been demonstrated that nutrient limitation is not globally exerted at each physiological or biochemical levels. This is (e.g.), nutrient limitation does not significatively affect carbon fixation, unless severe limiting conditions exist, but the synthesis of biomass (Cullen, 1990). Therefore, uncoupling the synthesis of biomass from carbon fixation allows nutrient limitation to be exerted over the growth rate, thus, not directly affecting photosynthesis. Finally, the coupling between the physical and the biological processes in the present model ensures the variability of the relevant time scales to be accurately resolved.

Outline of the Thesis

Chapter 1 introduces the governing equations of the physical processes and the whole physical-biological system. There, the main working hypothesis are stated. We also introduce the non-dimensional numbers suited for quantitatively classifying the relationships between the physical and biological processes.

Part II of this thesis deals with the basic concepts on turbulence. Its definition and characteristics, are introduced in chapter 2, as well as the main differences between molecular and turbulent diffusivities. Finally, we also briefly introduce the most relevant characteristic length and time scales of turbulence.

Chapter 3 deals with parameterizations of turbulent diffusivities of matter considered in this study. We compare them under stratified and non-stratified conditions. In

addition, related concepts like mixing efficiency and the kinetic energy dissipation are also introduced and discussed.

Two chapters of this thesis (Chapters 4 and 9) deal with the physical processes related with mass transport below Kolmogorov length scale (*see* Chapter 2). Chapter 4 presents the basic framework for the estimation of the physical processes affecting the transport of nutrients and CO_2 within the *Diffusive Boundary Layers* (DBLs) around phytoplanktonic organisms. Chapter 9 shows some relevant results about the physical limitations of nutrient transport rates through the surrounding DBLs regarding Redfield ratios.

Chapters 5 and 6 are specifically devoted to the modeling of the biological processes. Chapter 4 describes the fundamental equations of the bio-optical models, according to the characteristics of the photosynthesis *vs.* irradiance relationship, and the spectral absorption of light by the phytoplankton, taking into account the *inherent* and *apparent* properties of both, phytoplankton and water.

The main characteristic of bio-optical models is that the carbon fixation process is directly related with PAR (*Photosynthetical Available Radiation*) absorption according to two different non-linear relationships, under different ecological and physiological assumptions.

The biological (*sub-*)model for the phytoplankton is described in Chapter 5, with the exception of the equation for carbon fixation, which has been described in the previous chapter. The model treats independently carbon and nitrogen compounds, since they follow different pathways. Consequently, the model can also simulate variability of the internal nutrient quota due to nutrient limiting conditions. It explicitly describes the nutrient uptake, the synthesis of biomass, respiration and loss terms, as the characteristic matter flows of the model.

The different discretization schemes used for solving the physical (diffusion and advection) and biological (net phytoplankton growth) terms of the driving equations have been described in Chapter 7. The coupling scheme and convergence criteria have been described in this chapter, as well.

Numerical results are discussed in Chapters 8 and 9. Chapter 8 describes the numerical analysis of the biological model. It has been run alone in *one-box*, with constant nutrient in and out flows under different environmental conditions (temperature, day and night oscillation), forced by real irradiance time series. The response of the phytoplankton aggregate against different nutritional status has also been explored, and results appear at the end of this chapter. Results of transport rates within DBLs around phytoplanktonic organisms and the constraints set up by the physical environment, are finally described in Chapter 9.

Chapter 10 centers the full interaction between the physical and biological processes considered in this thesis. The model includes the effect of small-scale turbulence, expressed in terms of matter transport, over the phytoplankton primary production. Different runs simulate the environmental conditions at different locations within the Northwestern Mediterranean Sea, between Barcelona and the Balearic Islands, and they show the differential response under different stability conditions of the water column.

Overall results and conclusions are presented and discussed in Part V.

We include a description of FRONTS-1992 dataset and forcing time series in Appendix A. The parameter values of used by the biological model are shown in Appendix B. Additionally, Appendix C includes a long list of vertical attenuation values of Chlorophyll *a* at different world sites, while Appendix D shows a mathematical derivation with the aim of presenting how the two types of bio-optical models can be related.

Part II

METHODOLOGICAL BACKGROUND

1. PHYSICAL FRAMEWORK

1.1 The Conservation Equation

The water movements of the ocean are the driving mechanisms to transport and mix the majority of the planktonic organisms. In order to properly model the spatial and time scales which influence phytoplankton dynamics the small scales of the transport terms should be taken into account. In our approach to the subject, the conservative variables (velocity, temperature, salinity) are prescribed and the main emphasis is focused on the representation of the state variables of the system (nutrient and phytoplankton concentrations). Consequently, in this thesis we shall study the physical and biological processes that occur in the upper part of the oceans by means of a numerical model.

The governing equation of this model is a conservation equation for nitrate and an heterogeneous phytoplankton aggregate. In this chapter we derive the main governing equations and each term of which is discussed afterwards in detail.

If one assumes horizontal homogeneity, the instantaneous conservation equation reads

$$\frac{\partial \rho_i}{\partial t} + w\nabla\rho_i = D_i\nabla^2\rho_i + f_i(\rho_1, \ldots, \rho_n) \tag{1.1}$$

where ρ_i is a scalar, in units of concentration (dimensions $[\mathrm{ML}^{-3}]$); the subindex i refers to the state variable, $i = 1, \ldots, n$, being n the number of state variables of the system. w is the vertical velocity of the fluid and D_i is the molecular diffusion coefficient of the i^{th} state variable. The first term is the rate of change of the scalar property. The second term on the left hand side, namely the advection term, accounts for the vertical displacement of the fluid, carrying on dissolved substances and particles. Like the other terms, it is defined in units of mass transport $[\mathrm{ML}^{-3}\mathrm{T}^{-1}]$. The first term on the right hand side is the molecular diffusion term. Finally, $f_i(\rho_1, \ldots, \rho_n)$ accounts for the instantaneous sources and sinks due to biological processes for each one of the n state variables.

The driving equations of the coupled physical-biological model will be determined by the time-averaged equations that we will derive from equation (1.1).

First, one applies the Reynolds decomposition, $\rho = \overline{\rho} + \rho'$, $w = \overline{w} + w'$, where $\overline{\rho'} = \overline{w'} \equiv 0$, which means that the state variable ρ and the vertical velocity w are decomposed in the mean components, $\overline{\rho}$ and $\overline{w}$, and the fluctuating ones, ρ' and w', respectively (Reynolds, 1895; *see* also Tennekes & Lumley, 1972). Introducing this decomposition in

(1.1) yields

$$\frac{\partial(\overline{\rho}+\rho')}{\partial t}+\underbrace{(\overline{w}+w')\frac{\partial(\overline{\rho}+\rho')}{\partial z}}_{\boxed{\Upsilon}}=D\nabla^2(\overline{\rho}+\rho')+f\left(\left(\overline{\rho_1}+\rho_1'\right),\ldots,\left(\overline{\rho_n}+\rho_n'\right)\right) \quad (1.2)$$

The advection term $\boxed{\Upsilon}$ can be further developed

$$(\overline{w}+w')\frac{\partial(\overline{\rho}+\rho')}{\partial z}=\underbrace{\overline{w}\frac{\partial}{\partial z}\overline{\rho}+\overline{w}\frac{\partial}{\partial z}\rho'+w'\frac{\partial}{\partial z}\overline{\rho}+w'\frac{\partial}{\partial z}\rho'}_{\boxed{\aleph}}$$

and then substitute $\boxed{\aleph}$ back into equation (1.2), which now reads

$$\frac{\partial(\overline{\rho}+\rho')}{\partial t}+\overline{w}\frac{\partial}{\partial z}\overline{\rho}+\overline{w}\frac{\partial}{\partial z}\rho'+w'\frac{\partial}{\partial z}\overline{\rho}+w'\frac{\partial}{\partial z}\rho'=D\nabla^2(\overline{\rho}+\rho')+f\left(\left(\overline{\rho_1}+\rho_1'\right),\ldots,\left(\overline{\rho_n}+\rho_n'\right)\right) \quad (1.3)$$

The last term of the left side of the previous equation can be expressed in the flux form using $\frac{\partial}{\partial z}w'\rho'=w'\frac{\partial}{\partial z}\rho'+\rho'\frac{\partial}{\partial z}w'$. In the case of an incompressible fluid the continuity equation reads

$$\frac{\partial\overline{w}}{\partial z}=\frac{\partial w'}{\partial z}=0 \quad (1.4)$$

whence, we conclude that

$$w'\frac{\partial}{\partial z}\rho'=\frac{\partial}{\partial z}w'\rho'$$

One can average equation (1.3) and eliminate the average of the fluctuacting terms

$$\overline{\frac{\partial(\overline{\rho}+\rho')}{\partial t}}+\overline{\overline{w}\frac{\partial}{\partial z}\overline{\rho}}+\overline{\overline{w}\frac{\partial}{\partial z}\rho'}+\overline{w'\frac{\partial}{\partial z}\overline{\rho}}+\overline{\frac{\partial}{\partial z}w'\rho'}=\overline{D\nabla^2(\overline{\rho}+\rho')}+\overline{f\left(\left(\overline{\rho_1}+\rho_1'\right),\ldots,\left(\overline{\rho_n}+\rho_n'\right)\right)}$$

Finally, the resulting averaged equation can be written as

$$\frac{\partial\overline{\rho}}{\partial t}+\overbrace{\overline{w}\frac{\partial\overline{\rho}}{\partial z}}^{\boxed{\text{Advection}}}=\underbrace{-\frac{\partial}{\partial z}\overline{w'\rho'}}_{\boxed{\text{Turbulent Diffusion}}}+\overbrace{D\,\nabla^2\,\overline{\rho}}^{\boxed{\text{Molecular Diffusion}}}+\underbrace{f\left(\overline{\rho_1},\ldots,\overline{\rho_n}\right)}_{\boxed{\text{Biological term}}} \quad (1.5)$$

where $f\left(\overline{\rho_1},\ldots,\overline{\rho_n}\right)$ represents now the averaged biological term.

1.1.1 The Advection Term

The advection term accounts for the external forcing such as water upwelling or sinking. Consequently, it affects in the same way to all kinds of scalar properties, whatever they are dissolved substances, isotropic particles, etc.

$$\overline{w}\frac{\partial\overline{\rho}}{\partial z} \tag{1.6}$$

where $\overline{w}$ is the mean vertical velocity of the fluid [MT^{-1}].

This term is actually set to zero ($\overline{w}=0$) for all the simulations, but it is included in the general governing equation (1.5) in order to be able to reproduce future non-homogeneous situations.

1.1.2 The Diffusion Terms

Equation (1.5) presents the classical *closure* problem with the non-linear term $-\overline{w'\rho'}$. In order to solve the governing equation, this term needs to be parameterized. A common parameterization was introduced by Boussinesq[1] in 1878. Then, the vertical turbulent diffusion transport is parameterized as a function of an exchange coefficient and the mean gradient

$$-\overline{w'\rho'} = K_\rho \frac{\partial}{\partial z}\overline{\rho} \tag{1.7}$$

where K_ρ is the vertical turbulent diffusion coefficient of the given scalar property ρ.

Within the usual range of Reynolds number values in the ocean $K_\rho \gg D$, in such a way that $K_\rho \approx K_\rho + D$. Thus, both the molecular and the turbulent diffusion terms can be rewritten together as

$$\frac{\partial}{\partial z}\left(K_\rho + D\right)\frac{\partial\overline{\rho}}{\partial z} \equiv \underbrace{\frac{\partial}{\partial z}K_\rho\frac{\partial\overline{\rho}}{\partial z}}_{\boxed{\Lambda}} \tag{1.8}$$

This means that global diffusion transport is mainly achieved by turbulent diffusion, and it is quantitatively controlled by K_ρ. Introducing in (1.5) the final term of turbulent diffusion yields

$$\frac{\partial\overline{\rho}}{\partial t} + \overline{w}\frac{\partial\overline{\rho}}{\partial z} = \frac{\partial}{\partial z}K_\rho\frac{\partial\overline{\rho}}{\partial z} + f\left(\overline{\rho_1},\ldots,\overline{\rho_n}\right) \tag{1.9}$$

[1] Although the cross-product $\overline{w'\rho'}$ can be solved by Large Eddy Simulation (LES) and Direct Numerical Simulation (DNS) techniques, it can be, in any case, also parameterized by higher order *closure* schemes (*see* Mellor & Yamada, 1974; and Bougeault & André, 1986; for a further development).

$\overline{w'\rho'}$ is also called Reynolds flux because it arises when Reynolds decomposition is applied.

1.1.3 The Sedimentation Term

It is assumed that the dissolved nitrate and other nutrients do not sink. However, it is possible for some functional groups of phytoplankton to show a sedimentation velocity $|w_S|$ greater than zero. In such a case, the sedimentation flux $\overline{w_S\rho}$ has to be defined with the aim of an additional advection term that will be added to the turbulent transport term.

If we apply now the continuity equation [1.4] to the new advection term, we may define the sinking term as

$$\overline{w_S}\frac{\partial}{\partial z}\overline{\rho} = \underbrace{\frac{\partial}{\partial z}\overline{w_S\rho}}_{\boxed{\blacksquare}} \tag{1.10}$$

where $\overline{w_S\rho}$ is the mean local sinking flux of concentration [$\mathrm{ML^{-2}T^{-1}}$].

1.1.4 An Overall Transport Term

We may finally collect for sedimenting particles both the common terms of sinking $\boxed{\blacksquare}$ and vertical turbulent difussion $\boxed{\Lambda}$ in a global one accounting for both mechanisms

$$\frac{\partial}{\partial z}\left(\overline{w_S\rho} + K_\rho\frac{\partial\overline{\rho}}{\partial z}\right) \tag{1.11}$$

This global term is relevant only for particles, as far as it is assumed that dissolved nutrients have a negligible sinking value.

1.2 Governing Equations

We can now summarize the governing equations of the coupled physical-biological model become as follows:

$$\frac{\partial\overline{N}}{\partial t} + \overline{w}\frac{\partial\overline{N}}{\partial z} = \frac{\partial}{\partial z}K_N\frac{\partial\overline{N}}{\partial z} + F_N \tag{1.12}$$

$$\frac{\partial\overline{P}}{\partial t} + \overline{w}\frac{\partial\overline{P}}{\partial z} = \frac{\partial}{\partial z}\left(\overline{w_S P} + K_P\frac{\partial\overline{P}}{\partial z}\right) + F_P \tag{1.13}$$

---

where $\overline{N}$ and $\overline{P}$ are, respectively, the averaged concentrations of nitrate [mg-at $\mathrm{N\,m^{-3}}$] and phytoplankton in terms of carbon [mg $\mathrm{C\,m^{-3}}$]: therefore, we deal independently with two different units of mass. K_N and K_P are the vertical turbulent transport coefficients of nitrate and phytoplankton, respectively.

The non-conservative terms F_N and F_P account for the sink and source processes as a consequence of the biological activity of the living phytoplanktonic organisms, and they are computed by the biological sub-model. F_N is essentially a sink term which removes the nitrate from the water throughout nutrient uptake by the phytoplankton. F_P includes both source and sink processes. F_N and F_P are described in detail in Chapter 6.

1.3 Further Bio-Physical Considerations

Determining the terms of the governing equations of our model requires some physical assumptions which will be discussed in the next sections.

1.3.1 Diffusion Transport

As we have seen above we may actually consider turbulent diffusion transport as the most relevant diffusion process in the water column. However, diffusion transport of matter formally accounts for two different phenomena: a small scale fluid-dependent mechanism, namely *molecular diffusion*, and a very complex flow-dependent mechanism known as *turbulent diffusion*. Molecular diffusion is actually present in both laminar and turbulent flows, but turbulent diffusion characterizes transport in turbulent flows. Turbulent diffusion, in any case, occurs on spatial scales much greater that molecular diffusion and at much faster temporal scales than molecular diffusion could account for. Equation (1.7) is the averaged generic expression to describe the vertical transport by turbulent diffusion. The relevance of molecular and turbulent diffusion transport is described below.

Molecular diffusion depends on the properties of the scalar in a determined fluid, but not on the properties or characteristics of the flow. In other words, the molecular diffusion coefficient of a scalar depend on the arising properties of the interaction between the scalar and the fluid.

In this study we are specifically concerned, from a biological point of view, with nitrate (NO_3^-) and phytoplankton. These two scalars are the state variables of the coupled physical-biological model. The molecular diffusion coefficient of nitrate D_{NO_3} is known to be 1.7×10^{-9} m^2 s^{-1}, at 20°C (Li & Gregory, 1974), which is several orders of magnitude smaller than usual eddy diffusion coefficient values. This means that the molecular diffusion process is of the order of $\sim 10^9$ seconds a meter, this is, 19 years! Evidently, this can not be the most relevant underlying nutrient transport mechanism because it does not either reflect the the seasonal variability of the physical-chemical conditions of the water column, nor even its faster response to meteorological events.

Nevertheless, as we shall see in the next chapters, molecular diffusion plays a fundamental role at the length scales of planktonic organisms like bacteria, most of the phytoplanktonic species, and many other small aquatic organisms. The sizes of many of these small organisms (usually up to a few microns) often fall below Kolmogorov and Batchelor scales[2], which means that below such scales transport is essentially driven by molecular

[2] *See* chapter 2 for the definitions.

diffusion. Thus, below Batchelor scale diffusion transport is dominated by molecular diffusion, and, consequently, transport depends to a final extent on the characteristics of the molecules that are being transported.

Regarding the phytoplankton, we may force the molecular diffusion term to include a scalar that is several orders of magnitude larger than dissolved molecules. However, the model rest on the assumption that in both cases the movements of molecules or particles are purely random.

On the other hand, we can not give a specific value for D_P (namely, the *molecular* diffusion coefficient of phytoplankton) because in this study we consider phytoplankton as an *heterogeneous aggregate* (or an *assemblage*) of species. The phytoplanktonic species that can be found in a water sample usually show large differences in size, shape, etc., indeed every species or functional group show different ecological preferences and physiological characteristics, which are supposed to determine a different interaction with the environment.

The reason why we are mainly concerned on heterogeneous aggregates and not on phytoplankton monospecific *populations* is because we are usually estimating phytoplankton biomass through bulk properties like chlorophyll *a* concentration, and common measurements of chlorophyll *a* do not discriminate among species, taxa or functional groups.

Because of the classic argument in turbulence research which states that turbulent diffusion transport does not depends on the characteristics or properties of the fluid, we assume that $K_N \sim K_P$.

Before further studies provide us with a more rigorous determination of the turbulent diffusion coefficients, in principle, we may assign the same value to the two coefficients K_N and K_P, computed as a function of the coefficient of turbulent diffusion of momentum K_m. Then, we need an estimation of such coefficients taking the usual assumption $K_N, K_P \propto K_m$.

K_N and K_P are linearly related with the turbulent diffusion coefficient of momentum K_m by the turbulent Schmidt number S_{Tc}, as

$$K_N, K_P = \frac{K_m}{S_{Tc}} \tag{1.14}$$

We take $S_{Tc} = 1$ as in preceding works (Bougeault & Lacarrère, 1989; Gaspar *et al.*, 1991). This choice is consistent with laboratory experiments (Mellor & Yamada, 1982) and with some few available estimates deduced from oceanic measurements (Gregg, *et al.*, 1985; Peters, *et al.*, 1988). Therefore, an expression of K_m is now required. Chapter 3 discusses in detail on the parameterization of K_m.

Despite the relevance of turbulent or eddy diffusion to the overall diffusion transport in the water column we need to keep in mind that turbulence somehow reflects the characteristics of the flow, and that turbulent flows are inherently irregular, and spatially heterogeneous. Their characteristics show a sort of strong space and time dependency (*see* Chapter 2).

1.3.2 Sedimentation Transport

Sedimentation velocity of phytoplankton $\overline{w_S}$ can be greater than zero for diatoms, as well as for other functional groups (Bienfgang *et al.*, 1982); specifically, the vertical flux of diatoms to depth is disproportionate to their abundance in the euphotic zone. However, nano and picoplankton, which are the smallest fraction of the planktonic photosynthetic organisms, not only numerically dominate during long periods of time in oligotrophic areas, but they are responsible for most of the total ocean primary production (Behrenfeld, *pers. comm.*). The low proportion of nano and picoplankton found in sediment traps indicates that these groups are numerically less relevant in terms of biomass sedimentation than larger organisms; though further research should be addressed on the improvement of filter analysis techniques for preventing the losses or degradation of the samples.

Information on phytoplankton species composition were not available, however we can infer from silicate profiles and (NO_3:PO_4) dissapearance ratios that the chemical conditions at the euphotic zone were not dominated by diatoms. The mixed layer was still nutrient depleted in all the biological stations considered in this thesis (*see* chapter A, for the dataset description), but silicate concentrations at the depth of the *Deep Chlorophyll Maximum* were too high to become the signature of an assemblage dominated by diatoms.

As stated above, in this thesis we are dealing with heterogeneous phytoplankton aggregates, thus considering other phytoplanktonic species apart from diatoms. However, as an average, we shall consider in this thesis the phytoplankton assemblage to be neutrally buoyant.

Aggregation of particles may also exert an effect on the sedimentation rate, specially in the case of senescent or dead organisms (Bienfgang *et al.*, 1982; Thingstad & Sakshaug, 1990; Waite *et al.*, 1992). Degradation and aggregation processes, and their effect on the sedimentation fluxes, falls beyond the scope of this thesis, but in some circumstances may represent quantitatively a significative vertical flux of matter (Culver & Smith, 1989; Riebesell, 1991a, 91b, 92); such circumstances should be carefully assessed and, hence, sedimentation fluxes not to be neglected.

1.4 Effect of the Turbulent Diffusion Transport on the Phytoplankton Dynamics

The mixing of nitrate and phytoplankton is driven by turbulent diffusion transport. In consequence, turbulent diffusion exerts an influence on phytoplankton spatio-temporal dynamics. It is very convenient in our study to quantify such influence of turbulent transport on the biology by defining non-dimensional control parameters.

In the general conservation equation for nitrate and phytoplankton, the last term of the right hand side accounts for the eco-physiological processes. In order to carry out our development we assume at this stage a simple decay of the state variable ρ_i, for $i = 1, \ldots, n$, as follows

$$f_{(\rho_i)} = q_i \rho_i$$

where q_i is the net change rate coefficient, of dimension $[T^{-1}]$, and n the number of state variables of the system. The dimensionless form of this term provide us the non-dimensional numbers which account for the influence of turbulence on the relevant biological processes.

Defining a characteristic time scale of the fluid flow $\tau = \frac{L}{v}$ for a characteristic length L and the velocity of the fluid v, and defining additionally an average concentration for a generic scalar ρ_j where $j \neq i$, the non-dimensional function $f^*_{(\rho_i)}$ now reads

$$f^*_{(\rho_i)} \;=\; q_i\,\tau\,\frac{1}{\overline{\rho}_j}\,\rho_i$$

The asterisks denote non-dimensional terms. If we now multiply this term by $\overline{\rho}_i/\overline{\rho}_i$ it leads to

$$f^*_{(\rho^*_i)} \;=\; q_i\,\tau\,\frac{\rho_i}{\overline{\rho}_i}\,\frac{\overline{\rho}_i}{\overline{\rho}_j} \;=\; T^*_B N^* \rho^*_i$$

where the two non dimensional numbers are:

$$T^*_P \;=\; q_i\,\tau \;=\; \frac{\tau}{\tau_B} \tag{1.15}$$

$$N^* \;=\; \frac{\overline{\rho}_i}{\overline{\rho}_j} \tag{1.16}$$

The first one T^*_P, accounts for the interaction of physical and biological processes; the inverse number will be defined as $T^*_B = (T^*_P)^{-1}$.

One can establish a classification based on the number T^*_B:

$\boxed{T^*_B < 1}$	The characteristic time scale of the biological processes are slower than the one of turbulent transport, which means that the scalar property is uniformly mixed.
$\boxed{T^*_B \simeq 1}$	The turbulent transport limits the relevant biological processes.
$\boxed{T^*_B > 1}$	The characteristic time scale of the biological processes is faster than the physical ones, and in consequence the biology can be in local equilibrium.

The other number N^* defines a concentration ratio of the state variables. In our study it accounts for the concentration of phytoplankton *vs.* concentration of nutrients. This ratio may hold, from the physical as well as the biological point of view, a meaningful interpretation for the biological processes.

2. CONCEPTS IN TURBULENCE

2.1 "What's Turbulence?"

> *"In the customary description of turbulence, there are always more unknowns than equations (...)"* (Tennekes & Lumley, 1972).

Some characteristic effects of turbulence on plankton ecology have been already widely explored and described by many authors in the last years (Marrasé *et al.*, 1990; Sundby & Fossum, 1990; MacKenzie & Leggett, 1991; Belayev, 1992; Saiz *et al.*, 1992; Thomas & Gibson, 1992; Saiz, 1994; Saiz & Kiørboe, 1995); in more theoretical approaches (Rotschild & Osborn, 1988; Granata & Dickey, 1991). All these works have delivered clear proofs of the close relationship between some relevant biological processes and turbulence.

As the main goal of this study is related with the impact of physical conditions on the marine phytoplanktonic primary production in the open ocean we shall focus on the mechanisms which are relevant at the uppermost layers of the water column down to the euphotic depth. The deep-ocean processes developed far away from the surface, which do not show any significative effect in the upper layers, fall beyond the scope of this thesis. Coastal processes will either be considered, nor will be the large horizontal scales which would be affected by rotation or fronts.

Let us first make clear some introductory remarks about the different kinds of turbulent processes which can be properly identified according to their properties or general characteristics. Turbulence is mainly defined as a three-dimensional process, but as we shall briefly review in the next sections there is also a *geostrophic turbulence* developed in the horizontal plane that is principally described as a two-dimensional turbulent process. The effect of stratification also produces two-dimensional structures and allows the propagation of internal waves, which in turn may also trigger turbulent mixing events.

2.1.1 Definition and Characteristics

There is no unique definition of turbulence, thus I will first borrow some definitions from different authors to introduce this section.

> The turbulent movement of a fluid is an irregular condition of the flow, where the different variables show an aleatory variability in time and space. (Hinze, 1959).

> Turbulence is not a property of the fluid, but of its state of motion.
> (Gargett, 1997).

And explicitly referring to turbulent flows,

> Turbulence is not a feature of fluids but of fluids flows. Most of the dynamics of turbulence is the same in all fluids, whether they are liquids or gases.
>
> The major characteristics of turbulent flows are not controlled by the molecular properties of the fluid in which the turbulence occurs.
>
> Since every flow is different, it follows that every turbulent flow is different, even though that all turbulent flows have many characteristics in common. (Tennekes & Lumley, 1972).

All these definitions stress the fact that turbulence depends on the characteristics of the flow, but not in the fluid itself. There are different classes of turbulent flows. We can go a little bit further by describing some of the characteristics and properties of turbulent flows.

Intermitency

Turbulence consists of random velocity fluctuations. In practice, such an *irregularity* or *intermitency*[1] in amplitude makes prediction impossible, so that we need a statistical approach to the study of turbulence. For this purpose the Reynolds decomposition $u = \bar{u} + u'$ of the quantity u in a mean value $\bar{u}$ and fluctuations with zero mean u' is of general use (page 18). Mean values in turbulence research are usually time averages, that correspond to the experimental conditions in the laboratory; in such a case measurements are taken at fixed points. In an inhomogeneous flow such as most of real turbulent flows, a time average is a function of position, so that the use of spatial averages would be inapropiate for most purposes.

Three-Dimensionality

Because of the rotational nature of turbulence, characteristic random vorticity fluctuations that appear in two-dimensional flows such as cyclones are not in a strict sense considered as turbulence themselves (Tennekes & Lumley, 1972). Even though, their characteristics may be influenced strongly by small-scale turbulence (generated somewhere, by shear or buoyancy). Nowadays the techniques applied to 3-D turbulent flows are also used in 2-D "quasi-turbulent" flows.

[1] Intermitency is also often described as *irregularity*.

Large Reynolds numbers

Turbulence develops in a laminar flow when Reynolds numbers become large. Turbulence appears in a pipe when Reynolds numbers reach a value of near 2000, although higher values may be reached carefully controlling the boundary conditions of the flow. Turbulence often originates as an instability in laminar flows, and develops according to the non-linearity of the viscous and inertia terms of the Navier-Stokes equation. However, turbulent flows should be independent of the Reynolds number if they are scaled properly.

Dissipation

Turbulent flows dissipate the kinetic energy transferred from large eddies into smaller ones. Finally, the energy of the smallest eddies is dissipated as heat by viscous friction forces. The amount of kinetic energy dissipated ε, assuming planar isotropy ($u' = v'$), is approximately

$$\varepsilon \approx \nu \overline{\frac{\partial w'}{\partial z} \frac{\partial u'}{\partial x}} \tag{2.1}$$

or, for isotropic turbulence, in the sense of Kolmogorov (1941)

$$\varepsilon \approx \nu \overline{\left(\frac{\partial w'}{\partial z}\right)^2} \tag{2.2}$$

where ν is the kinematic viscosity, and u' and w' are respectively the relevant fluctuations of the velocities of the water (*see* also section 3.3).

Viscosity is the utmost responsible mechanism for dissipation. Turbulent flows are always dissipative, and they need a continuous supply of energy; otherwise, turbulence rapidly decays. The major distinction between random waves and turbulence is that waves are essentially non-dissipative.

Self-similarity

The geometrical characteristics of the spatial structure of turbulence is suitable to be described within a limited range by a definite fractal dimension (Redondo, 1990). The fractal dimension D_i of an isoline like the sharp interface of a picnocline of a stratified fluid may be calculated, and its measured length L will show a power law dependence on the measuring yardstick σ as:

$$L \propto \sigma^{1-D_i} \tag{2.3}$$

where the subindex i refers to the embedded Euclidean space, and the fractal dimension being defined as

$$D_i = \frac{\log N}{\log \sigma^{-1}} \tag{2.4}$$

N is the number of self-similar parts or covering boxes at size σ. See also Redondo (1990), McComb (1990), Jou (1997), and the comprehensive review of Sreenivasan (1991) for

deeper study of the fractal dimension of turbulence. Such works state that turbulence show spatial irregularities presenting strongly convoluted areas among *smooth* areas. It is further deduced that matter and energy fluxes are not constant and spatially non-uniformly distributed.

Diffusivity

Diffusivity is the mechanism that causes mixing in fluids. It is not just a random process, e.g. if a flow looks random but does not exhibit a spread of velocity fluctuations through the surrounding fluid, it is surely not turbulent. Diffusivity increases momentum transfer between winds and ocean currents, and it is the source of the resistance of flow in pipelines.

Quantitatively, turbulent diffusivity is several orders of magnitude higher than molecular diffusivity. Diffusivity in turbulent flows can also be 10^3 to 10^5 times higher than in laminar flows.

Turbulent diffusivity is, in fact, one of the most striking characteristic of turbulence which exerts a direct effect over the biological processes.

2.1.2 Molecular Viscosity and Turbulent Diffusivity

Turbulence always promotes diffusion. However, viscosity behaves like a mechanism against the dissipation of the kinetic energy, this is, against turbulence. Viscosity, in fact, is likely to reduce turbulent diffusion; in the same way, turbulence will greatly increase viscosity (Boussinesq, 1870; *in* Frisch, 1995). Indeed, viscosity may be considered as the diffusivity of momentum.

Taylor showed in 1932 that in equilibrium the input of kinetic energy due to turbulence per unit of volume is equal to the dissipation of energy by viscosity, plus the potential energy increment of the system. In other words, kinetic energy of a turbulent flow can hardly be transported; it can only be saved as an increment of potential energy. But, in stably stratified fluids, mean vertical turbulent velocities are often too small for producing a significative increment of potential energy.

An interesting characteristic of viscosity is that it can be negative. This was initially proposed by Kraichnan (1976) and later described by Starr (1988), as an interpretation of the inverse cascade of energy in two dimensions. Vergassola *et al.* (1993) and Gama *et al.* (1994) showed that eddy viscosity can be frequently negative, and leads to large-scale instabilities. This mechanism may be related to the process defined in stratified fluids by the relationship between the flux Richardson number R_f against the gradient Richardson number R_i, which states that if the slope is negative the mass flux is inversely proportional to the density gradient, in such a way that the instabilities are maintained (Posmentier, 1977)[2].

[2] *See* chapter 3 for the definitions of R_f and R_i.

2.2 Two-Dimensional Phenomena

Two-dimensional phenomena are represented in the ocean by mesoscale processes characterized by large Reynolds numbers. Because of the large-scale specificity we shall not deal with large scale processes in this thesis, although this statement does not imply the assumption that mesoscale phenomena can not be a significative process to be taken into account in the modeling of biological processes, regarding specially horizontal spatial patterns (*see* McGillicuddy & Robinson, 1997). In this work we mainly focus on vertical mixing and small-scale mechanisms (*cf.* Abraham, 1998; for an interesting advance on the simulation of horizontal phytoplankton pattern formation in the ocean).

2.3 Characteristic Scales of Turbulence

Although real turbulent flows are not isotropic the mathematical techniques developed by Taylor (1921) proved suitable for describing small scales of turbulence. Kolmogorov (1941), following Richardson's idea of energy cascade, hypothesized that the statistics of smallest eddies in a turbulent isotropic flow depend only on two parameters, namely viscosity and the rate of dissipation[3].

2.3.1 Length Scales

Kolmogorov Scale

The size of the smallest turbulent eddies is defined by the Kolmogorov (or viscous) length scale

$$L_K = \left(\frac{\nu^3}{\varepsilon}\right)^{1/4} \tag{2.5}$$

where ν is the molecular viscosity [L^2T^{-1}], and ε the rate of kinetic energy dissipation [L^2T^{-3}]. Below this scale viscosity dominates, resulting in laminar shear, and fluctuations are considered to be homogeneous, isotropic and nearly steady (Monin & Yaglom, 1975).

Lazier & Mann (1989) showed that the eddies containing the maximum energy density are about 40 times the size of Kolmogorov length, and that the smallest energy-containing eddies are 5 to 10 times larger than Kolmogorov scale. This estimation gives us an idea about the relevant length scales in turbulent flows. In general, the ratio of small to large length scales depends on the Reynolds number.

Batchelor Scale

Batchelor introduced in 1959 an additional length scale L_B relevant to molecular diffusion D [L^2T^{-1}] of the scalar property. This length scale is smaller than L_K because mass transfer requires displacement of molecules, while momentum can be transferred in successive

[3] For a historical overview of the related concepts we refer the reader to Monin & Yaglom (1975), and Yaglom (1994).

molecular collisions without as much net displacement; for dissolved nutrients like nitrate and phosphate $D \ll \nu$ by several orders of magnitude.

$$L_B = \left(\frac{\nu D^2}{\varepsilon}\right)^{1/4} \tag{2.6}$$

The analysis of Batchelor (1959) showed that the scalar property is distributed in the fluid in long thin streams lying parallel to the flow, and on the average exhibit gradients across the shear on the spacing of L_B. Thus, it may be expected that below L_B turbulent flows are not significatively different from laminar ones and, consequently, both velocity and scalar gradients are extremely small.

2.3.2 Time Scales

Time scales of turbulence are specially relevant in this study because they will enable us to characterize the interaction between physical processes and some relevant biological ones, according to the non-dimensional number (1.15) defined in Chapter 1. The Kolmogorov length scale has its own counterpart time scale τ_K. It is defined as

$$\tau_K = \left(\frac{\nu}{\varepsilon}\right)^{1/2} \tag{2.7}$$

It can be stated that turbulence is dissipated as heat beyond the limit defined by the Kolmogorov scale.

As we have pointed out at the beginning of this chapter, small-scale turbulence is the main physical mechanism responsible for the vertical transport of energy and matter in the ocean. Thus, the vertical transport of nutrients is heavily influenced by such mechanisms. Indeed the vertical transport of nutrients is the key-factor of the interaction between phytoplankton dynamics and turbulence and, consequently, τ_K is used for characterizing the time scale of the such relevant physical processes. For such a purpose we take the smallest characteristic time scale as the reference time scale of the physical processes which we assume to be the most relevant ones for the vertical transport of matter in the ocean.

It can be demonstrated for a given scalar property that Kolmogorov and Batchelor time scales, τ_K and τ_B, are equivalent. If we start with the Batchelor length scale [2.6] and we operate with it, in such a way that

$$L_B = \left(\frac{\nu^2}{\nu^2}\frac{\nu D^2}{\varepsilon}\right)^{1/4}$$

we obtain that

$$\left(\frac{D^2}{\nu^2}\frac{\nu^3}{\varepsilon}\right)^{1/4}$$

This equation can be then rewritten as

$$\left(S_{Tc}^{-2}\,\frac{\nu^3}{\varepsilon}\right)^{1/4}$$

where $S_{Tc} = \frac{\nu}{D}$ is the Schmidt number. The previous equation can be further simplified, yielding

$$L_B = S_{Tc}^{-\frac{1}{2}} L_K \tag{2.8}$$

Assuming that the Batchelor time scale refers to the time that a scalar takes for covering a Batchelor length scale, at a rate determined by the molecular diffusivity, the later can be transformed in a time scale by setting the right hand term of the previous equation up to two, and dividing it by the molecular diffusion coefficient D

$$\tau_B = \frac{\left(S_{Tc}^{-\frac{1}{2}} L_K\right)^2}{D} = \frac{\nu^{\frac{1}{2}} D}{D \varepsilon^{\frac{1}{2}}} = \left(\frac{\nu}{\varepsilon}\right)^{\frac{1}{2}} = \tau_K$$

Therefore, the characteristic time scale of a given scalar property transported in a fluid is determined by the Kolmogorov time scale.

3. TURBULENT DIFFUSION AND MIXING IN THE OCEAN

fluid mechanics mainly deals with processes at a macroscopic scale. But what it is known by *molecular diffusion* occurs, or it has its own origin, at a microscopical scale. Some properties of a fluid, like velocity, show a dramatical non-uniform variability depending on the considered scale. Other properties apparently describe a more uniform behavior at different scales, and empirically validate the continuum hypothesis; this could be the view of Kelvin, and it is clearly stated by Lamb (1932). Turbulent transport of momentum might be regarded in an analogous way to molecular transport, with the small-eddies playing the role of molecules.

The origin of the idea of eddy viscosity (or turbulent viscosity) seems to be in Boussinesq (1870), as it has been referred later by Monin & Yaglom (1975). Boussinesq assumed that the turbulent shear stress is proportional to the velocity gradient, just as viscous shear stress in a laminar flow.

In the nineteenth century the distinction between eddy and molecular viscosity was faint, as eddies were probably considered like *fictious fluid molecules*. At the beginning of this century, after the works of Prandtl (1925) and von Kármán (1930), all these ideas moved towards a statistical description of the turbulence under the analogy of the kinetic theory (*see* Brusch, 1976; and Frisch, 1995; for a more in depth revision of the field).

Some theoretical approaches describe eddy viscosity as a factor of scale: after Richardson (1922) turbulence was described arising as a dissipative structure. The energy flows from large eddies of scale L_0 and dissipated later in smaller ones of scale L_K, the Kolmogorov's scale (section 2.3).

According to the previous idea, the characteristic velocity $v_{(L)}$ for eddies of scale L is

$$v_{(L)} \sim (\varepsilon L)^{1/3} \tag{3.1}$$

where ε is the energy transfer per unit of mass, or kinetic energy dissipation. This scaling was later used by Kolmogorov to derive from dimensional arguments the well known dependence of the spectral energy density $E_{(L)}$ on the eddy size

$$E_{(L)} \sim \varepsilon^{2/3} L^{5/3} \tag{3.2}$$

Such an approach becomes analogous in terms of the effect of a fluid moving around an organism. It can be empirically stated that the scale-factor exerts a strong effect on the

behaviour of some planktonic species (Alcaraz *et al.*, 1988; Thomas & Gibson, 1990; Berdalet, 1992; Alcaraz *et al.*, 1994). In a more intuitive way, what happens to be a disruptive and stressing storm for a small organism may be considered a providential phenomena for a larger one.

The scale-factor also plays a major role on the spatial distribution of the planktonic species. Moreover, it determines the further development of the population in terms of temporal evolution.

Thus, according to this point of view a planktonic population could be ideally transported by a large scale hydrodynamical processes without any apparent effect on the population. But the same population could be effectively dispersed by the turbulence produced as a consequence of the dissipation at smaller scales of the energy of the large eddies.

The effect of turbulence on the planktonic species depends on both the spatial scale and the biological process under consideration. However at the scale of small phytoplankton species, turbulence in the ocean seems to be fully developed at the three space dimensions.

Small-scale turbulence is in fact, the essential mechanism in the vertical energy and mass transport in the ocean. We can state the estimation of the vertical fluxes is still a difficult task, as turbulence occurs intermittently (by shear instability, internal wave breaking or convection), is often spatially inhomogeneous, and generally undergoes a transition to a quasi two-dimensional motion under the action of stratification. Gibson (1980) called this transition process *fossilization* of turbulence, and turbulence can persist for a rather long time in these conditions, becoming a non-linear process.

3.1 Vertical Transport of Matter

Small-scale turbulence is quantitatively the most important agent for the vertical transport of matter in the ocean (Hopfinger, 1987; Gargett, 1997).

Vertical fluxes of nutrients play a fundamental role over the whole pelagic community by the way of the primary producers (DeAngelis, 1992; Valiela, 1995). Therefore, the estimation of vertical fluxes remain as a key-process for the dynamics of aquatic ecosystems. This is strictly true for the areas where the mixing mechanisms are not very strong, and specially during the period of stratification.

Nevertheless, the estimation of the vertical nutrient fluxes in the aquatic environment is still a rather difficult task due to the special characteristics of the turbulent mixing process.

The estimation of the vertical fluxes of nutrients in the upper part of the ocean is a fundamental task, as far as nutrient concentrations in the euphotic zone mainly controls, roughly speaking, the maximum phytoplankton primary production to a large extent. Due to the irregular character of small-scale turbulence, the mixing process, as described in the second chapter, is an intermittent mechanism which is also irregularly distributed in space. Additionally, when the water column appears to be stratified, the well developed three-dimensional turbulence progressively undergoes to a two-dimensional motion process. This transition makes the evaluation of the intensity of mixing and the vertical transport

process even more difficult; one must necessarily establish some restrictions to the study of turbulence to estimate the vertical transport.

As it has been already stated above small-scale turbulence is a dissipative process, which needs of a continuous energy input. One can take advantage of this characteristic to estimate turbulence as a function of the contribution kinetic energy input mechanism, a fraction of which is transformed into turbulence.

Many approaches have been proposed for this purpose and for trying to estimate the overall contribution of turbulence to the turbulent diffusive transport process, whether the transport accounts for momentum, matter or heat.

3.2 Parameterization of Turbulent Diffusion

It is necessary to state that we can not longer take any longer a fixed turbulent diffusion coefficient for the whole water column. Unfortunately, it doesn't exist either a canonical relationship for properly parameterizing turbulent diffusion.

McCreary (1981) described a parameterization based on a stability factor (accounted by the Brunt-Väisälä frequency, N), valid for areas dominated by strong shear currents. This can be the case of near-equatorial latitudes (within a range of 5° North and Southwards from the Equator)

$$K_m = K_h = K_{min} N^{-2} \tag{3.3}$$

where K_m and K_h are the turbulent diffusion coefficients for momentum and heat, respectively, and

$$K_m = K_h = 5.5 \times 10^{-5} \ \ [m^2 s^{-1}]$$

K_{min} takes this value where N is maximum. This usually happens near the point where the shear velocity is highest (e.g. near the thermocline). The Brunt-Väisälä frequency N [s^{-1}] is defined for $\frac{\partial \overline{\rho}}{\partial z} > 0$ as

$$N^2 = -\frac{g}{\rho_0} \frac{\partial \overline{\rho}}{\partial z} \tag{3.4}$$

g is the gravity acceleration (9.80665 $m\,s^{-2}$), $\overline{\rho}$ is the averaged density and ρ_0 is the density of reference.

Pacanowski & Philander (1981) defined a different relationship for the momentum and heat turbulent diffusion coefficients

$$K_m = \frac{O}{(1+5R_i)^2} + 10^{-4} \tag{3.5}$$

and

$$K_h = \frac{K_m}{1+5R_i} + 10^{-5} \tag{3.6}$$

where $O = 0.005$. R_i is the gradient Richardson number (*see* next section).

3.2.1 The Balance of Turbulent Kinetic Energy

The assessment of the equilibrium states of a system is probably still today one of the major underlying goals in dynamical systems research. So far, water in natural environments is never at rest. If homogeneous turbulence is assumed, the turbulent kinetic energy TKE can be defined as

$$TKE = \frac{1}{2}\sum_i \overline{u_i'^2} \tag{3.7}$$

and the rate of change of the turbulent kinetic energy (TKE) can be described in a general way by the next equation, notating the spatial coordinates and fluid velocities, respectively, as $(u',v',w') = (u_1',u_2',u_3')$ and $(x,y,z) = (x_1,x_2,x_3)$, thus

$$\frac{\partial TKE}{\partial t} = \underbrace{\sum_{i,j} \overline{u_i'u_j'}\,\frac{\partial \overline{u_i}}{x_j}}_{P} \overbrace{-\overline{\rho' u_3'}\,\frac{g}{\rho}}^{B} \underbrace{-\nu \sum_{i,j} \overline{\left(\frac{\partial u_i'}{\partial x_j} + \frac{\partial u_j'}{\partial x_i}\right)\frac{\partial u_i'}{\partial x_j}}}_{\varepsilon} + T \tag{3.8}$$

where ν is the molecular viscosity, and ρ the density of water. The first term of the right side of the equation P is the shear production of TKE. The second term B is the buoyancy flux and expresses the fraction of TKE converted to potential energy. This term can be either positive or negative; we follow the same sign convention as for velocities (downward velocities are negative). The third term ε is the main sink (output) term of the equation and it represents the dissipation of TKE; it will be explored in depth in the next sections. Finally, T indicates the transport of TKE. This term is often taken as zero, as far as TKE quickly dissipates, but it is included in the equation for consistency.

The Flux Richardson Number

The *flux* Richardson number R_f describes the kinetic energy fraction absorbed by the stratification, as a ratio of the buoyant kinetic energy production B to stress kinetic energy production P

$$R_f = \frac{B}{P} \tag{3.9}$$

This ratio reflects the increase in potential energy of the fluid divided by the production of turbulent kinetic energy; thus, it determines how efficiently a fluid is mixed. As far as there is always some dissipation in all turbulent fluxes ($\varepsilon > 0$), if we assume $T = 0$, then $P > B$, consequently $R_f < 1$.

The cross-product $\overline{\rho' u_3'}$ from the buoyancy flux B, has been parameterized in (1.7) in the vertical dimension as $\overline{w'\rho'} = K_m \frac{\partial \overline{\rho}}{\partial z}$. Hence, B can be expressed as

$$B = K_m \frac{g}{\rho}\frac{\partial \overline{\rho}}{\partial z} \tag{3.10}$$

Collecting this expression together with (3.4) results in

$$B = K_m N^2 \tag{3.11}$$

If the buoyancy flux $B \neq 0$ it implies the movement of the gravity center of the water column. Hence, the flux Richardson number R_f describes the efficiency of the transfer of kinetic energy to buoyancy flux.

As far as we mainly deal with the vertical dimension in this work, the Reynolds stress production P can be expressed as

$$P = -\overline{u'w'}\,\frac{\partial \overline{u}}{\partial z} \tag{3.12}$$

For local stationary conditions we can state that all the turbulent kinetic energy is dissipated ($\varepsilon = P + B$). The Reynolds stress production and dissipation terms are always positive, whereas the buoyancy term can take on either sign. For $B < 0$ mixing is against the density gradient, which means that the potential energy of the water column is increased. In the opposite way, if $B > 0$ mixing is produced by the sinking of heavier water masses and the upwards circulation of lighter ones.

The Mixing Efficiency

The flux Richardson number *is* the *mixing efficiency* concept, defined as a measure of the fraction of the available kinetic energy of a flow used to mix the fluid, and raise its potential energy. It can be determined by measuring the density gradient before and after all motion has occurred. A measure of the mixing efficiency can also be estimated by means of the scale defined by Ozmidov (1965) L_o. It represents the scale of motion at which buoyancy forces become of the same order as inertial forces

$$L_o = \left(\frac{\varepsilon}{N^3}\right)^{\frac{1}{2}} \tag{3.13}$$

Thus, the maximum vertical movement of a fluid particle from its equilibrium position will be of the order of the L_o. Typical values of Ozmidov scale fall within the range of 0.01 to 1 meters.

Another parameter related to the mixing efficiency can also be defined in a different way as the ratio between the kinetic energy produced by buoyancy and the dissipation of kinetic energy[1] (Gibson & Schwarz, 1963; Gargett, 1989).

$$\gamma = \frac{B}{\varepsilon} \tag{3.14}$$

[1] Gargett (1989) defined γ (therein notated as η) as the *efficiency of turbulence*. This definition introduced some confusion interpreting this term as mixing efficiency. The two definitions R_f and γ are equal only under steady-state no-mixing conditions, when $P = \varepsilon$. The concept of mixing efficiency, as defined above, will be developed further in the next sections.

therefore,

$$\gamma = \frac{\overline{\rho' w'} \frac{g}{\rho}}{\varepsilon} \equiv \frac{K_m N^2}{\varepsilon} \tag{3.15}$$

Alternatively, if we deal with (3.8) simply as $\frac{\partial TKE}{\partial t} = P - B - \varepsilon + T$ we can easily deduce γ in a rather simple way: under steady state conditions, and assuming no energy transport ($T = 0$), we have that

$$\begin{aligned} \frac{P}{\varepsilon} &= \frac{B}{\varepsilon} + 1 \\ 1 &= \frac{B}{P} + \frac{\varepsilon}{P} \end{aligned}$$

If we now substitute (3.14) and (3.9) back we have that

$$\begin{aligned} \frac{P}{\varepsilon} &= \gamma + 1 \\ 1 - R_f &= \frac{\varepsilon}{P} \end{aligned}$$

After collecting both equations we obtain

$$\left(1 - R_f\right)(\gamma + 1) = 1 \tag{3.16}$$

The main check for stably stratified flows is that $0 < R_f < 1$, as there is always some dissipation ($\varepsilon > 0$). Thus, we finally get that

$$R_f = 1 - \frac{1}{\gamma + 1} = \frac{\gamma}{\gamma + 1} \tag{3.17}$$

$$\gamma = \frac{1}{1 - R_f} - 1 = \frac{R_f}{1 - R_f} \tag{3.18}$$

Normal values in the ocean of R_f are usually less than unity, and often fall within the range $0.11 < R_f < 0.25$. Panofsky & Dutton (1984) report a critical value of R_f at which turbulence ceases to be self-supporting ($R_f \simeq 0.25$) since dissipation is usually larger than shear production of kinetic energy. Higher values of R_f would imply stronger stratification conditions. Such conditions would indicate that turbulence is about to dissipate.

The Gradient Richardson Number

The *gradient* Richardson number R_i may be derived rewriting the *flux* Richardson number using Boussinesq's proportionality between fluxes and gradients. After eliminating the viscosity and diffusivity terms is defined by

$$R_i = \frac{N^2}{\left(\frac{\partial \overline{u}}{\partial z}\right)^2} \tag{3.19}$$

where $\overline{u}$ is the averaged horizontal velocity. Then, it holds the relationship

$$R_f = \frac{K_h}{K_m} R_i \tag{3.20}$$

3.2.2 The Dissipative Method

It is possible to calculate the vertical fluxes across density gradients according to measurements (or estimations) of the different dissipation scales. This method mainly applies in the case of weak stratification and high turbulence levels. Thus, when turbulence is maintained for a long time one may assume homogeneity, therefore

$$-\left(1-R_f\right)\overline{u'w'}\cdot\frac{\partial\overline{u}}{\partial z}=\varepsilon \tag{3.21}$$

where R_f is the flux Richardson number, and ε is the kinetic energy dissipation term. Equation (3.21), expressed in terms of the turbulent diffusion coefficient of momentum K_m, becomes

$$\overline{u'w'}=K_m\frac{\partial\overline{u}}{\partial z} \tag{3.22}$$

hence we deduce that

$$K_m=\frac{\varepsilon}{\left(1-R_f\right)\left(\frac{\partial\overline{u}}{\partial z}\right)^2} \tag{3.23}$$

If the stratification is weak, then R_f would be very small and , it may be sometimes neglected. This method should not be applied when it is presumed that internal wave breaking occurs. In this case the next parameterization better serves the purpose of modeling diffusivities in a stratified layer.

3.2.3 Parameterization of Osborn

Osborn (1980) introduced a different method for estimating the turbulent diffusivity through a density gradient. Considering the parameterization (1.7) and taking into account the equation (3.23), the turbulent diffusion coefficient K_m can be defined as

$$K_m=\frac{R_f\cdot\varepsilon}{\left(1-R_f\right)N^2} \tag{3.24}$$

and assuming $R_f\leq 0.15$ (Osborn, 1980), then

$$K_m<0.2\frac{\varepsilon}{N^2}$$

C C As far as the flux Richardson number is sometimes rather difficult to estimate, (3.24] is usually expressed according to the buoyancy to dissipation ratio γ, yielding

$$K_m=\gamma\frac{\varepsilon}{N^2} \tag{3.25}$$

Assuming the Richardson's hypothesis, which is to say that the turbulent Schmidt number $S_c=1$ or, assuming that density depends only on temperature and neglecting the effect of salinity and any other scalar, γ can be expressed as a function of the kinetic energy dissipation ε and term χ_T, that describes the rate at which the fluctuations of temperature

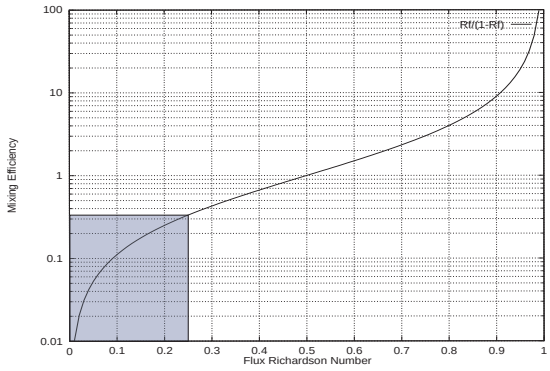

Fig. 3.1: Plot of the also called *mixing efficiency* γ *vs.* the Flux Richardson number R_f according to the equation (3.18). The shadowed area indicates the phases-space below the R_f critical value (*see* text).

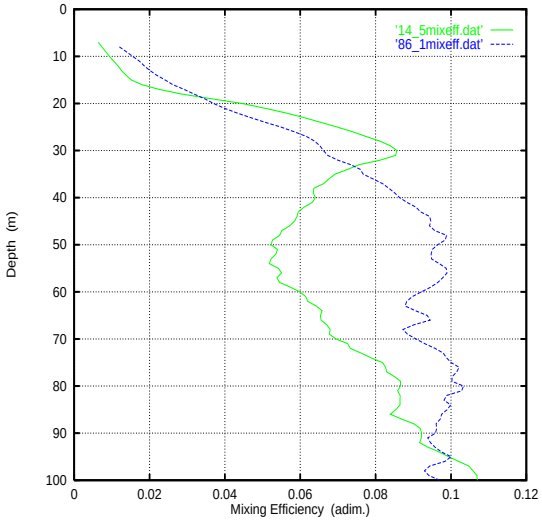

Fig. 3.2: Estimated γ profiles under strongly (station 14.5; green solid line) and weakly (station 86.1; blue broken line) stratified conditions, computed using the equation (3.26). The Cox number has been approximated according to Gregg (1987).

T diffuse in a fluid. A value of $\kappa_T = 1.4 \times 10^{-7}$ m^2 s^{-1} is usually considered; thus, the ratio of buoyancy to dissipation γ can also be calculated for temperature stratification as

$$\gamma = \frac{\kappa_T C_T N^2}{\varepsilon} \tag{3.26}$$

where C_T is the Cox number, which decreases with N with a slope between N^{-1} and N^{-2} (Gregg, 1987). The Cox number is defined as

$$C_T = 3 \frac{\overline{\left(\frac{\partial T'}{\partial t}\right)^2}}{\left(\frac{\partial T}{\partial z}\right)^2} \tag{3.27}$$

where T is the temperature of the fluid, and T' are their fluctuations over the time.

Thus, for $\varepsilon \propto N^1$ to $N^{1.5}$, regarding to equation 3.25, then $C_T \propto N^{-1}$ to $N^{-0.5}$. We can actually take the Cox number as $C_T = 0.025 \cdot N^{-1.5}$ (Gregg, 1987).

Since the seventies it has been published many estimations for the mixing efficiency. Lilly *et al.* (1974) assumed $R_f = 0.25$. Upon this estimation it is deduced that $\gamma = 0.33$. Osborn (1980) assumes that the flux Richardson number for oceanic turbulence is $R_f = 0.15$, which implies that $\gamma \leq 0.2$. Weinstock (1978) assumed $\gamma = 0.8$, a value certainly high. In the eighties, after simultaneous measurements of temperature and kinetic energy dissipation Oakey (1982) found $\gamma = 0.24 \pm 0.12$. Also Gregg *et al.* (1986)

got values between $\gamma = 0.18$ and $\gamma = 0.2$, from two different data series. Moum *et al.* (1989) estimated $0.12 \leq \gamma \leq 0.48$. And Weinstock (1987) found an approximated value of $\gamma = 0.25$ that seems to be in good agreement with many oceanographic measurements.

3.2.4 Parameterization of Gaspar, Grégoris and Lefevre

This method is based in the model published by Bougeault & Lacarrèrre (1989), developed for the study of turbulence in the atmosphere. It is, in fact a new parameterization for the turbulent mixing in the vertical dimension. The method described by Gaspar *et al.* (1990) (GGL) assume the efficiency term as defined in (3.18) which can also be directly deduced from equation (3.24), and the flux Richardson number (3.9) definition.

Gaspar *et al.* (1990) also assumed like Lilly *et al.* (1974) that $R_f = 0.25$, which also implies $\gamma = 0.33$. Nevertheless, as we realized in the previous section, there exists some disparity in the values of γ and, correspondingly, in the mixing efficiency R_f; so Gaspar *et al.* (1990) finally took $\gamma = 0.25$, according to Weinstock (1987).

The same authors (*op. cit.*) define a new parameterization for the turbulent diffusion coefficient of momentum K_m as

$$K_m = 2^{1/2} P_r^{-1} C_K \overline{e} N^{-1} \tag{3.28}$$

this is, without explicitly considering the kinetic energy dissipation term ε, although it is considered in further computations. P_r is the turbulent Prandtl number, defined as $K_h = K_m/P_r$, where K_h is the turbulent vertical diffusion coefficient for temperature. The same authors (*op. cit.*) define ε in such a way that

$$\varepsilon = 2^{-1/2} c_\varepsilon \overline{e} N \tag{3.29}$$

taking $c_\varepsilon = 0.7$. According to Bougeault & Lacarrère (1989) $\overline{e}$ can be neglected at the points where the kinetic energy is being produced. Anyway, as an attempt to converge to some previous estimations from Gargett (1984) it can be estimated a minimum $\overline{e}$ as $e_{min} = 10^{-6}$ m^{2}s^{-2}. Taking this value equations (3.28) and (3.29) yield, respectively, $K_m = 1.4 \times 10^{-7} N^{-1}$ and $\varepsilon = 5 \times 10^{-7} N$.

Dividing the equation (3.28) by (3.29) we found again the known parameterization of Osborn (3.25); and the buoyancy to dissipation ratio is expressed as

$$\gamma = 2 C_K c_\varepsilon^{-1} P_r^{-1} \tag{3.30}$$

Thus, considering $P_r = 1$, and taking $\gamma = 0.3$ according to Moum *et al.* (1989) (implicitly assuming $R_f = 0.23$), we deduce a value of $C_K = 0.1$, which is not far from an empirical estimation (Figure 3.2).

3.3 A Direct Estimation of

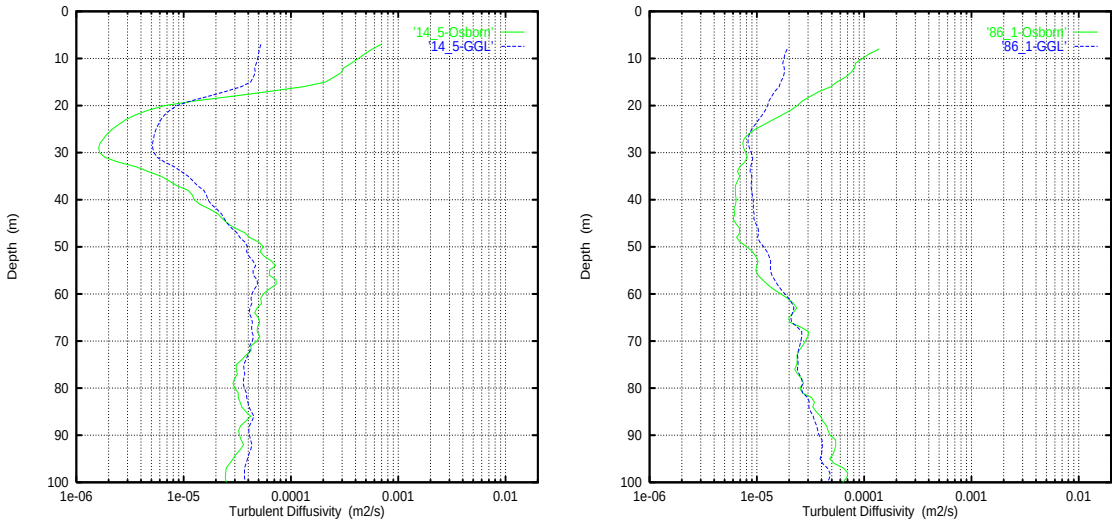

Fig. 3.3: Profiles of turbulent vertical diffusion coefficients for a strong and weak stratification conditions during the period of study estimated by the parameterizations of Osborn (green solid line) and GGL (blue broken line). In Osborn profiles ε has been estimated according to equation (3.36), taking the wind velocities U_{10} as 3.1 and 3.7 $\mathrm{m\,s^{-1}}$, for the stations 14.5 (left) and 86.1 (right), respectively (*see* figures 10.2.2 and 10.2.2 for the density profiles).

the Kinetic Energy Dissipation

The kinetic energy introduced to the water column by the wind takes place by creating a (wind-) stress τ_0 on the water surface [$\mathrm{N\,m^{-2}}$], which is usually assumed to be constant within a layer extending from the air into the water, can be expressed in the ocean as

$$\tau_0 \;=\; \rho_{air}\,\overline{u'_{air}w'_{air}} \;=\; \rho\,\overline{u'w'} \tag{3.31}$$

where u'_{air} and w'_{air} are the horizontal and vertical velocity fluctuations of the air, respectively, while u' and w' refer to the water column.

As soon as τ_0 is difficult to measure directly, it is commonly parameterized by the square of the wind velocity U_{10} [$\mathrm{m\,s^{-1}}$], measured at a standard height of 10 meters above the water surface:

$$\tau_0 \;=\; \rho_{air}\,C_{10}\,U_{10}^2 \tag{3.32}$$

where ρ_{air} is the density of the air ($\approx$ 1.2 $\mathrm{kg\,m^{-3}}$ at 20°C) and C_{10} is the so-called drag coefficient. C_{10} is not really constant because the coupling between air and water depends on the roughness of the interface. In the ocean or in large lakes C_{10} is expected to be larger than in a small lake. Also because wave heights increase with increasing wind speed, C_{10} should be larger for large U_{10}. Amorocho & deVries (1980) identified three wind-speed regimes for C_{10}:

$\boxed{U_{10} \leq 7}$ Where waves do not break, $C_{10} \approx 0.001$.

$\boxed{7 < U_{10} \leq 20}$ In an intermediate regime characterized by the onset of breaking waves C_{10} linearly increases up to a value of 0.0025.

$\boxed{U_{10} > 20}$ At higher wind speeds breaker saturation is attained and C_{10} becomes constant, thus equal to 0.0025.

The energy flux from the atmosphere to the air-water interface, at a height of 10 meters above the water surface P_{10} [$\mathrm{W\,m^{-2}}$] is given by

$$P_{10} \;=\; \tau_0\, U_{10} \;=\; \rho_{air}\, C_{10}\, U_{10}^3 \tag{3.33}$$

It is generally found that just a small fraction χ of approximately 1-2% of P_{10} is transferred to the water and is available for mixing in the surface layer (Denman & Miyake, 1973). Thus the kinetic energy flux from the wind into the water is

$$TKE \;=\; \chi\, \rho_{air}\, C_{10}\, U_{10}^3 \tag{3.34}$$

where $\chi \sim 0.01$-0.02.

Additionally, when the wind is the main mixing agent at the surface of the water column Yamazaki & Kamikowski (1991) estimated the kinetic energy dissipation term ε according to the friction velocity u_*, defined by

$$u_* = f_c U_{10} \tag{3.35}$$

where f_c is an empirical coefficient, estimated in 0.00123 by Oakey & Elliott, (1982).

Thus, under pure wind-stress forcing, the rate of dissipation of kinetic energy should follow

$$\varepsilon_{(z)} = \frac{u_*^3}{\kappa z} \tag{3.36}$$

κ is the von Kármán's constant ($\kappa \approx 0.4$) and z is the depth. This simple formula proved to describe well the observations reported by Dillon (1981) in lakes, and in the ocean by Osborn & Lueck (1985).

4. SMALL-SCALE MASS TRANSPORT

The coupling between carbon fluxes and vertical nutrient transport still contains open questions. Vertical turbulent diffusion transport remains as the most fundamental physical driving mechanism for the upwelling of nutrients in the open ocean and large freshwater systems. However, the early works of Gavis (1976), Berg & Purcell (1977), Purcell (1977, 1978), Lazier & Mann (1989) and Kiørboe (1993), firmly stated for the limited influence of turbulence within the boundaries of small planktonic organisms ($\sim 1\mu$m) over the transport of small diffusible molecules.

This subject was review by Karp-Boss *et al.* in 1996, focusing to the fine interaction between the turbulent environment and planktonic organisms considered as perfect osmotrophs, thus providing an updated theoretical basis for the study of the Diffusive Boundary Layers (DBLs) around living organisms. The analysis of Karp-Boss *et al.* (1996) and Karp-Boss & Jumars (1999) based on steady shear flow experiments, although it can not be directly applied to field data because turbulence is not fully developed under the conditions carried out in these studies, they provide a fundamental theoretical background that fully covers the *state-of-the-art* knowledge of this field both for still and moving organisms. Later on, Ploug *et al.* (1997, 1999a,b) presented experimental evidences of DBLs' role on mass transport and characterized them in the case of *Phaeocystis* sp. colonies.

The pH gradients measured within DBLs around still and sinking *Phaeocystis* colonies by Ploug, *et al.* (*op. cit.*) allow us to carefully analyze and review the deep implications of a previous work by Riebesell *et al.* (1993). As pointed out in the references cited above, the mass transport within DBLs is driven by mechanisms of different nature than the overall mean turbulent fluxes which dominate transport in the water column. The main resource fluxes which are relevant for the phytoplankton development in the water column (fundamentally, C , N and P), do not necessarily match the fluxes across the DBLs. Riebesell *et al.* (1993) considered the hypothesis of diatom growth rate can be limited by low CO_2 supply through DBLs, comparing the ratios of maximum potential fluxes through the DBL and the Redfield's elemental molar ratio C:N:P of organic matter composition taken as 106:16:1 (Redfield, 1958).

In a turbulent environment concentration and momentum fluctuations dissipate below Kolmogorov (or viscous) length scale L_K, equation (2.5) (*cf.* Tennekes & Lumley, 1972; Lazier & Mann, 1989). The kinematic viscosity of water ($\nu \simeq 10^{-6}$ m^2 s^{-1}) is equivalent to the molecular diffusivity of momentum. The values of the turbulent kinetic energy dissipation rate ε (Oakey, 1982; Oakey & Elliot, 1982), usually fall within

the range of approximately 10^{-11}–10^{-5} $\mathrm{W\,kg^{-1}}$ [$\mathrm{L^2T^{-3}}$]. In the open ocean L_K normally ranges from 1–6 mm. This implies that momentum and mass transport through parcels or *particles* of water smaller that Kolmogorov length scale is dominated by molecular diffusion.

By definition solid bodies submerged in a fluid are surrounded by DBLs. Because DBLs are very thin (up to 10-fold the radius of the organism, under pure diffusion conditions; *see* Karp-Boss *et al.*, 1996) transport within these layers occurs only by molecular diffusion. However, the effective thickness of the DBLs around small planktonic organisms whose size is also smaller than L_K, are significatively large compared to their own sizes, and strong implications are derived from this statement.

Considering a small spherical and planktonic organism of radius r_o, the radial flux of mass J [$\mathrm{ML^{-2}T^{-1}}$] through its surrounding DBL is defined by the Fick's first law, as

$$J = D\frac{\mathrm{d}C}{\mathrm{d}r} \tag{4.1}$$

where D is the molecular diffusion coefficient of a solute whose concentration is C, in Mol or mg per unit of volume, and r is the radial distance from the surface of the organism. J expresses the transport of mass by means of only molecular diffusion.

If we consider now the transport within the DBL of a dissolved nutrient which is (let us assume, by now) passively and totally absorbed by the organism at its surface (as a perfect osmotroph), δ_{eff} can be defined at steady-state as the *effective* DBL length that yields a mass flux equal to J, thus, the transport becomes maximum. Then, equation (4.1) can be discretized in such a way that

$$J = D\frac{C_\infty - C_0}{\delta_{eff}} \tag{4.2}$$

where C_∞ is the bulk concentration of nutrient, and C_0 is the concentration at the organism's surface ($r = r_0$), where r_0 is the radius of the organism (*see* Lazier & Mann, 1989; Karp-Boss *et al.*, 1996; and Ploug *et al.*, 1997).

The area-integrated flux Q at the surface of the organism is

$$Q = 4\pi r_0^2 D\frac{\mathrm{d}C}{\mathrm{d}r} = 4\pi r_0^2 D\frac{(C_\infty - C_0)}{\delta_{eff}} \tag{4.3}$$

Taking

$$Sh = \frac{r_0}{\delta_{eff}} \tag{4.4}$$

where Sh is known as the Sherwood number (Sherwood *et al.*, 1975). In the case of spherical organisms equation (4.3) can be then rewritten as

$$Q = Sh\,4\pi r_0 D\,(C_\infty - C_0) \tag{4.5}$$

The Sherwood number describes the relative increase of the area-integrated mass transport due to flow, regarding pure diffusional flux. In stagnant fluid it is defined $Sh = 1$, while flux is proportionally enhanced by the flow (e.g., sinking) for $Sh > 1$.

Some authors implicitly assume that Q expresses pure diffusional transport, thus no sinking or advection processes are considered (Lazier & Mann, 1989; Riebesell *et al.* 1993; Karp-Boss *et al.*, 1996; Rau *et al.* 1996); in that case, equation (4.5) can be also properly written as

$$Q = 4\pi r_0 D\,(C_\infty - C_0) \tag{4.6}$$

If we define the total inward flux normal to the organism's surface as the area-integrated gradient of the nutrient concentration

$$Q_T = D \iint \mathbf{n}\nabla C \,\mathrm{d}x\,\mathrm{d}y \tag{4.7}$$

where $\mathbf{n}$ is a unit vector normal to the cell surface.

Then, the Sherwood number can be perhaps more intuitively defined (*see* Karp-Boss *et al.*, 1996) as

$$Sh = \frac{Q_T}{Q} \tag{4.8}$$

As far as in this study we are mainly dealing with small-scale processes below Kolmogorov scale, it holds that $\nabla(D\nabla C) = D\nabla^2 C$, for any given solute.

4.1 Transport of Dissolved Inorganic Carbon (DIC) within the Phytoplanktonic DBL

Among all the biological processes occurring in the uppermost layers of the oceanic water column CO_2 fixation by the marine algae plays a fundamental role on global climate which is under deep quantitative analysis.

Diatoms account for a large proportion of the marine phytoplankton, specially in coastal waters. Sediments deposited in the deep open ocean containing a record of past environments are also dominated by silicate clay minerals, which indicate a relevant role of diatoms over geologic time (Schlesinger, 1997). Because of their predominant role in the ocean's primary production and the vertical carbon fluxes, diatoms also play a central role in the biological pump (Eppley & Peterson, 1979) transferring carbon dioxide from surface to deep waters. For such a reason, during the last years attention has been payed on the environmental conditions which limit diatom growth rate and primary production.

Equations (4.5) or (4.6) apply directly to nutrients like NO_3^- and PO_4^{3-}. However, in the case of CO_2 it is necessary to take into account the whole carbonate system. Following DOE (1994) standards by Dickson & Goyet, the reactions that take place when carbon dioxide dissolves in water can be represented by the following series of equilibria

$$\mathrm{CO_2}(g) \rightleftharpoons \mathrm{CO_2}(aq) \tag{4.9}$$

$$\mathrm{CO_2}(aq) + \mathrm{H_2O}(l) \rightleftharpoons \mathrm{H_2CO_3}(aq) \tag{4.10}$$

$$\mathrm{H_2CO_3}(aq) \rightleftharpoons \mathrm{H^+}(aq) + \mathrm{HCO_3^-}(aq) \tag{4.11}$$

$$\mathrm{HCO_3^-}(aq) \rightleftharpoons \mathrm{H^+}(aq) + \mathrm{CO_3^{2-}}(aq) \tag{4.12}$$

where the notations (g), (l) and (aq) refer to the state of the species: a gas, a liquid, and an aqueous solution, respectively. Unfortunately, it is difficult to distinguish between the species $CO_2(aq)$ and $H_2CO_3(aq)$ by analytical means. It is thus usual to lump the concentrations of $CO_2(aq)$ and $H_2CO_3(aq)$ together and to express this sum as the concentration of a hypothetical species CO_2^*. Redefining reactions (4.9), (4.10) and (4.11) in terms of this species they become

$$CO_2(g) \rightleftharpoons CO_2^*(aq) \tag{4.13}$$

$$CO_2^*(aq) + H_2O(l) \rightleftharpoons H^+(aq) + HCO_3^-(aq) \tag{4.14}$$

From an experimental perspective the CO_2 system in seawater is characterized by four measurable parameters: the total DIC CO_2 ($\Sigma CO_2 = [CO_2^*] + [HCO_3^-] + [CO_3^{2-}]$), the total alkalinity[1] (TA), the pH, and either the partial pressure of CO_2 pCO_2, or the fugacity of CO_2 (fCO_2). The knowledge of any two of these parameters, along with the temperature, salinity, pressure, the abundances of other constituents of seawater (necessary for the evaluation of the TA), and the relevant equilibrium constants, allows the determination of the other two (Lewis & Wallace, 1998).

As soon as CO_2 is enters the organism and, thus the partial pressure of CO_2 is reduced within the DBL, the whole set of equilibrium reactions move leftwards and a fraction of the dissolved HCO_3^- is converted to CO_2.

The relative contribution to the CO_2 flux which is converted spontaneously from HCO_3^- and H_2CO_3 within the DBL is given by the ratio r_0/r_k, where r_k is the so-called reacto-diffusive length (Rau *et al.*, 1996)

$$r_k = \sqrt{\frac{D_{CO_2}}{k'}} \tag{4.15}$$

D_{CO_2} is the molecular diffusion coefficient of CO_2 in seawater. k' is the overall inverse reaction rate of the conversion from CO_2 to HCO_3^- and

$$k' = k_1[OH^-] + k_2 \tag{4.16}$$

where k_2 accounts respectively for the inverse conversion rate of reaction (4.10), and k_1 for the direct reaction

$$CO_2 + OH^- \rightleftharpoons HCO_3^- \tag{4.17}$$

[1] The total alkalinity (TA) of a sample of sea water is a form of mass-conservation law for the hydrogen ion.

$$TA = [HCO_3^-] + 2[CO_3^{2-}] + [B(OH)_4^-] + [OH^-] + [HPO_4^{2-}] + 2[PO_4^{3-}] + [SiO(OH)_3^-] +$$
$$[NH_3] + [HS] + \ldots - [H^+]_F - [HSO_4^-] - [HF] - [H_3PO_4] - \ldots$$

where the ellipses stand for additional minor acid or base species that are either unidentified or present in such small amounts that they can be safely neglected. $[H^+]_F$ accounts for the *free* concentration of hydrogen ion. TA is rigorously defined as the number of moles of hydrogen ion equivalent to the excess of proton acceptors (bases formed from weak acids with a dissociation constant $K \leq 10^{-4.5}$, at 25°C and zero ionic strength) over proton donors (acids with $K > 10^{-4.5}$) in one kilogram of sample (DOE, 1994).

Values of k_1 and k_2 at 25°C are, respectively, ∼8500 $m^3\,Mol^{-1}\,s^{-1}$ and 0.025–0.04 s^{-1} (Stumm & Morgan, 1996). Reaction (4.17) is insignificant at pH values below 8, but it progressively contributes above this value, and it definitely dominates the CO_2 hydration above pH=10 (Stumm & Morgan, 1996).

The concentration of the hydroxyl ion OH^- is computed from the pH value, according to $K_W = [H^+]\,[OH^-]$, holding that $H_2O(aq) \rightleftharpoons H^+(aq) + OH^-(aq)$, where K_W is the dissociation constant that can be computed from DOE (1994)

$$\ln(K_W) = \frac{-13847.26}{T_K} + 148.9652 - 23.6521\ln(T_K) + \left[\frac{118.67}{T_K} + 1.0495\ln(T_K)\right] S^{1/2} - 0.01615\,S \tag{4.18}$$

S is the salinity (in p.s.u.).

The temperature correction for the constants k_1 and k_2 can be introduced by

$$k_{(T_K)} = k_{(T_{K_0})} \frac{e^{-\left(\frac{E_K}{RT_K}\right)}}{e^{-\left(\frac{E_{K0}}{RT_{K0}}\right)}} \tag{4.19}$$

where the reference temperature is $T_{K_0} = 298\,K$ (25 °C), and $R = 8.314510\ J\,K^{-1}\,Mol^{-1}$ (Cohen & Taylor, 1986; *in* DOE, 1994).

The diffusion coefficients also show a strong temperature dependence. In the case of D_{CO_2}we take the correction introduced by Jähne *et al.* (1987), given by

$$D_{CO_2} = 5.019 \times 10^{-6} e^{-\left(\frac{E_D}{RT_K}\right)} \tag{4.20}$$

with $E_D = 19510\,J\,Mol^{-1}$. Nevertheless, this relationship is valid for freshwater. Therefore, in order to correct for the differences in the dynamics viscosity of freshwater and seawater (Li & Gregory, 1974) D_{CO_2} has to multiplied by

$$\frac{\nu_{fw}}{\nu_{sw}} = 0.9508 - 7.389 \times 10^{-4} T_C \tag{4.21}$$

where ν_{fw} and ν_{sw} are the dynamical viscosities of freshwater and seawater, respectively, and T_C is the temperature in Celsius degrees (Rau *et al.*, 1996).

The temperature dependency of the molecular diffusion coefficients of bicarbonate, nitrate and phosphate can be estimated for the usual range of temperature (5 to 30 °C) with the linear relationship given by the Stokes-Einstein equation (Table 4.1) (*see* Li & Gregory, 1974).

In order to account for the total CO_2 transport Q_C within the DBL the spontaneous conversion $HCO_3^- \rightarrow CO_2$ must be added to equation (4.6), then

$$Q_C = 4\pi r_0 D \left(1 + \frac{r_0}{r_k}\right)(C_\infty - C_0) \tag{4.22}$$

Ions			Function
Bicarbonate	$D_{HCO_3^-}$	=	$5.39 \times 10^{-10} + 2.56 \times 10^{-11}\, T_C$
Nitrate	$D_{NO_3^-}$	=	$9.72 \times 10^{-10} + 3.65 \times 10^{-11}\, T_C$
Phosphate	$D_{PO_4^{3-}}$	=	$2.79 \times 10^{-10} + 1.23 \times 10^{-11}\, T_C$

Tab. 4.1: Temperature dependency functions of the molecular diffusion coefficients of dissolved ions. *See* text for the molecular diffusion coefficient of CO_2 .

Equation (4.6) remains unchanged for HCO_3^- and nutrients (NO_3^-, PO_4^{3-}). In the case of nitrate and phosphate the ratio $\frac{C_0}{C_\infty}$ may be estimated from the lowest C_0 values observed for a given species or phytoplankton aggregate. But in the last case we should further assume that phytoplankton is the responsible depleting agent for keeping the nutrient concentration at the low value C_0.

As far as the molecular diffusion coefficients are different for every chemical species, the thickness of the DBLs do not necessarily have to be the same. On the other side, the nutrient uptake rates may show quite a large time variability depending on metabolic requirements. Therefore, the maximum thickness of the DBL around an organism δ^{max} may be estimated as

$$\delta^{max} = \sqrt{\frac{D}{\langle u \rangle}} \tag{4.23}$$

where $\langle u \rangle$ is the averaged uptake rate [T^{-1}], and the angles $\langle\ \rangle$ indicate time average.

In equation (4.23) we are implicitly assuming that the organisms growing under optimal light and nutrient conditions can take up as much nutrients and carbon that can reach the plasmatic membrane. And that phytoplanktonic species are genetically adapted (both genotypically and phenotypically) to the physical constraints superimposed by the presence of the DBL around every single cell or colony. However, each species probably are able to optimize their transport kinetics by rate/efficiency considerations to specific natural environmental conditions. Transport rates per unit of surface[2] reported by different authors (Riebesell *et al.*, 1993; Ploug *et al.*, 1999b) of around 5–10 μMol C m^{-2} s^{-1} are Check of the same order than the fluxes through transport proteins (1–10 μMol C m^{-2} s^{-1}) given by Raven & Smith (1980) and Raven (1984, 1985) in laboratory experiments.

However it is necessary to point out the theoretical limitations of the latest approach for the estimation of the thickness of the DBLs: (e.g.), they mainly apply to steady state conditions, but the rapidly adaptable metabolic rates (specially uptake rates) seem to make such state difficult to reach. Parallel, carbon and nutrient gradients around the organism may change too. Size is a relevant parameter for the *effective* transport within the DBLs. It represents a fundamental key factor for the phytoplanktonic species to adapt to different turbulent conditions (Margalef, 1978; Estrada & Berdalet, 1997); and shape, which is not even considered or parameterized in the present model, may also significatively contribute

[2] Dividing equations (4.6) or (4.22) by the sphere's area: $4\pi r_0^2$.

to the same role (*see* Pahlow *et al.*, 1997).

Symbol	Definition	Value	Units
E_k	Activation Energy (reaction rates k_1, k_2)	6.28×10^{-4}	$\mathrm{J\,Mol^{-1}}$
E_D	Activation Energy ($\mathrm{D_{CO_2}}$)	19510	$\mathrm{J\,Mol^{-1}}$
Q_S	CO_2 Surface Diffusion Transport	-	$\mathrm{Mol\ m^{-2}s^{-1}}$
Q_C	Overall CO_2 Diffusion Transport	-	$\mathrm{Mol\ CO_2\ s^{-1}}$
R	Perfect Gas Constant	8.31451	$\mathrm{J\,K^{-1}\,Mol^{-1}}$
S	Salinity	35	p.s.u.
Sh	Sherwood Number	1	(adim.)
T_C	Temperature (in Celsius degrees)	17	$^\circ$C
T_K	Temperature (in Kelvin degrees)	290.15	K
$\mathrm{D_{CO_2}}$	Molecular Diffusion Coeff. CO_2	1.4478×10^{-9}	$\mathrm{m^2\,s^{-1}}$
$D_{HCO_3^-}$	Molecular Diffusion Coeff. HCO_3^-	9.7420×10^{-9}	$\mathrm{m^2\,s^{-1}}$
$D_{NO_3^-}$	Molecular Diffusion Coeff. NO_3^-	1.5925×10^{-9}	$\mathrm{m^2\,s^{-1}}$
$D_{PO_4^{3-}}$	Molecular Diffusion Coeff. PO_4^{3-}	4.8844×10^{-10}	$\mathrm{m^2\,s^{-1}}$
r_k	Diffusion-Reaction Length	-	m
k'	$HCO_3^-\rightarrow CO_2$ Overall Conversion Rate	-	s^{-1}
k_1	Reaction (4.17) Conversion Rate	8500	$\mathrm{m^3\,Mol^{-1}\,s^{-1}}$
k_2	Reaction (4.10) Conversion Rate	0.03	$\mathrm{s^{-1}}$
T_{K_0}	Reference Temperature	298.15	K
J	Fick's Diffusion Transport	-	$\mathrm{Mol\ m^{-2}s^{-1}}$

Tab. 4.2: Listing of the definitions, symbols, values and units of variables and parameters described in the text.

4.2 Nutrient Upwelling Fluxes and Abundance of Organisms: A Coupling Hypothesis

We can describe an equilibrium state of the nutrient-phytoplankton system where the nutrient taken up by the phytoplankton balances the upwelling nutrient flux. This situation is usually reached in sub-tropical areas as well as in temperate seas during the warm season. In fact, the *Deep Chlorophyll Maximum* (DCM) reflects such balanced situation as a typical feature of oligotrophic waters (Anderson, 1969; Banse; 1987).

Under the assumption of a negligible phytoplankton sinking rate $\overline{w_S} = 0$ and the lack of net advective processes, the governing equations for the nutrient (1.12) allow us to represent the equilibrium conditions which lead to the DCM as

$$\overline{w'N'} = F_N \tag{4.24}$$

where the phytoplankton nutrient uptake F_N balances the upward turbulent diffusion transport $\overline{w'N'}$. Otherwise, when $\overline{w_S} < 0$ it holds that the net upward flux equals diffusion transport minus phytoplankton sinking $c_N\,\overline{w_S P}$ (in terms of nitrogen), hence

$$\underbrace{\overline{w'N'} - c_N\,\overline{w_S P}}_{Net\ Nutrient\ Upward\ Flux} \;=\; F_N \tag{4.25}$$

c_N is a conversion factor from mg $\mathrm{C\,m^{-3}}$ to mg-at $\mathrm{N\,m^{-3}}$, taken as the Redfield N:C ratio ($\simeq 0.0126$ mg-at N mg $\mathrm{C^{-1}}$), which is analogous to the biomass nutrient internal quota defined by the ratio of nitrogen against carbon biomass phytoplankton composition (chapter 6). The dimensions of the fluxes are $[\mathrm{ML^{-2}T^{-1}}]$. As soon as diatoms were not quantitatively relevant during FRONTS'92 campaign (*cf.* section 1.3.2) we assume that the phytoplankton aggregate shows a negligible sedimentation rate, therefore taking (4.24) as the representative equation.

The equilibrium solution determined by both equations assume that all the nutrient upwelling flux by turbulent diffusion is totally consumed by the phytoplankton, thus neglecting the influence of any other possible competitor for the same nutrient. This statement may represent sometimes an oversimplification of the nutrient pathway in the pelagic ecosystem. However, from a theoretical point of view, the present analysis introduces an suggesting coupling hypothesis between diffusive nutrient transport and phytoplankton uptake.

The time-averaged nutrient uptake of the whole phytoplankton aggregate can be estimated as the uptake of a single individual Q multiplied by the concentration of organisms B. Assuming no competition for the nutrient by other organisms and that the nutrients are efficiently taken up by the phytoplankton, we may infer at steady state that

$$\ell\, F_N \;=\; Q\, B \tag{4.26}$$

ℓ is the length scale where the balanced nutrient flow takes place; where nutrients and light reach optimal proportions, which is around the DCM's depth. Therefore, ℓ is defined by the thickness of the DCM.

Under near-equilibrium conditions the nutrient flux entering the euphotic layer can be estimated according to (1.7). As the thickness of the euphotic layer and the vertical nutrient flux are closely related (Banse, 1987), the vertical turbulent diffusion nutrient flux is determined by the largest vertical concentration gradient, this is, at the nutricline.

Substituting (4.6) into (4.26) we get that

$$\ell\, F_N = \; 4\pi r_0 D \langle C_\infty \rangle \left(1 - \frac{C_0}{C_\infty}\right) B \tag{4.27}$$

If we now isolate B it becomes that

$$\frac{\ell\, F_N}{4\pi r_0 D \langle C_\infty \rangle \left(1 - \frac{C_0}{C_\infty}\right)} \;=\; B \tag{4.28}$$

As stated above, the equilibrium conditions where (4.27) applies is mostly reached around the DCM. Consequently, a possible statistical verification is to check up the predicted abundances at the DCM, for each one of the biological stations during FRONTS'92 cruise against chlorophyll *a* concentrations, also at the DCM's depth (Table 4.1).

Station	N Flux	$\langle C_\infty \rangle$	ℓ	B	Chl *a*
14.1	2.08×10^{-6}	0.24	30	835.56	0.50
45.1	4.10×10^{-6}	0.01	20	26365.06	0.40
61.1	7.83×10^{-6}	0.09	30	8392.06	0.49
65.1	4.53×10^{-6}	0.12	30	3639.66	0.46
76.1	5.06×10^{-6}	0.09	20	3618.23	0.56
86.1	4.03×10^{-6}	0.13	30	2988.70	0.49

Tab. 4.3: The upward diffusion transport at the nutricline N Flux, is expressed in mg-at $\mathrm{N\,m^{-2}\,s^{-1}}$, $\langle C_\infty \rangle$ is the average nitrate concentration at the DCM, in mg-at $\mathrm{N\,m^{-3}}$. The DCM's thickness ℓ is expressed in meters, while B is the number of organisms per milliliter, and Chl *a*, is the chlorophyll *a* concentration at the DCM, in mg $\mathrm{m^{-3}}$. The absorption capacity $\frac{C_0}{C_\infty}$ is taken for this computations as 0.5 (adim.).

Chl *a* against B shows a negative Pearson correlation index r = -0.7691. On the other hand, the upward nutrient flux is interestingly not directly correlated with Chl *a* concentration at the DCM ($r = 0.1111$).

Former studies mainly focused on the physical environmental description (Lazier & Mann, 1989; Karp-Boss *et al.*, 1996, 1998) assumed organisms to be *perfect absorvers*, which means that $\frac{C_0}{C_\infty}$ equals zero. Nevertheless, as it has been indicated, living organisms adjusts their nutritional requirements to their own metabolic rates. Consequently, we must point out that further research on the fine coupling between diffusional delivery of nutrients and the biological requirements is needed; because either $\langle C_\infty \rangle$ is constant, nor is expected the absorption capacity $\frac{C_0}{C_\infty}$ to be, as well. So that an evident key point would be to determine how much $\langle C_\infty \rangle$ varies according to the turbulent characteristics of the flow.

The analysis presented in this chapter can also provide us with an additional estimation of the stabilization time for the DCM structure. A simple computation yields an approximated period between a few hours and 2–3 days for shallow DCM, depending on the stability of the water column and mixing events.

5. MODELING PHOTOSYNTHESIS

5.1 Photosynthesis vs. Irradiance

Photosynthesis is probably one of the the most fundamental processes in the biosphere, and it is definitely the most relevant one in the biological context of this thesis. The mathematical estimation of the carbon fixation rate by the photosynthetical process becomes also a fundamental part of the present work, as I will present in the next chapters devoted to the biological sub-model.

The relationship between **I**rradiance and carbon fixation (**P**hotosynthesis) shows a typical saturable function, which is presented in its general form in Figure 5.1. Several functions have been published over the last twenty years as an attempt to describe this relationship. The references about this subject are numerous. Here I shall give just a brief description about the subject, referring to others for further explanations.

It is worth to stress the importance of this direct relationship between light and photosynthesis in primary production models because it reflects the key-point of the radiative to chemical energy conversion. Phytoplankton growth has been modeled in many different ways over the last years, but often some parameterizations mix concepts like *light-limitation* and *nutrient-limitation* that should be considered separately. Parameterizations should always try to use functional relationships, with preferable experimental or empirical support, as far as the main goal of mathematical modeling in scientific research is not just fitting a function to the available data, but to attempt to understand the underlying mechanisms involved in each process.

Among all the functions which are intended to describe the asymptotic relationship between light and photosynthesis I shall introduce the two most commonly used, although the first attempts to parameterize the P/I curve appear at the beginning of this century (*see* Kirk, 1983, for an overall introduction; and Häse, 1996, for a more updated review).

Webb *et al.* presented in 1974 a function which is still widely used. This function introduces all the relevant parameters for the P/I curves described in Figure 5.1.

$$P^B_{(z)} \;=\; P^B_{max} \cdot \left(1 - e^{-\frac{\alpha^B \cdot I}{P^B_{max}}} \right) \tag{5.1}$$

where the gross carbon assimilation process (vertically integrated) $P^B_{(z)}$ is often expressed in mg C mg chl $a^{-1}\,\mathrm{m}^{-3}\,\mathrm{day}^{-1}$ (the exponent B means *normalized* to biomass, in terms of chlorophyll *a*). I is the irradiance $\mu\,\mathrm{E}\,\mathrm{m}^{-2}\,\mathrm{day}^{-1}$, and α^B represents the initial slope of the

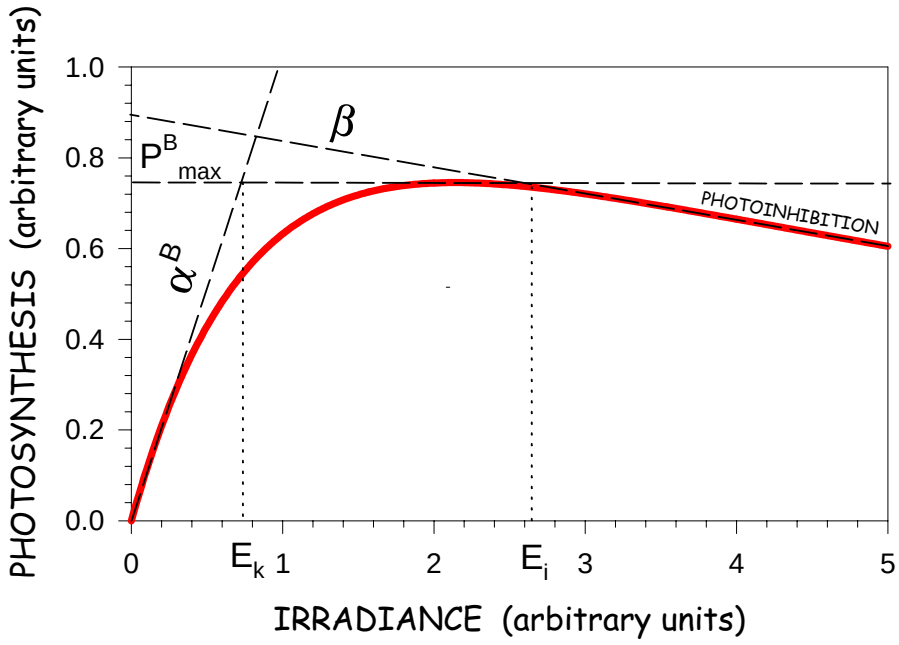

Fig. 5.1: Typical P/I curve with the main descriptive parameters. E_k and E_i are called onset saturation and inhibition parameters, respectively.

function normalized to chlorophyll *a* [mg C mg chl a^{-1} m^{-3} day^{-1} (μ E m^{-2} day^{-1})$^{-1}$]. P^B_{max} is the maximum photosynthetical rate at some defined temperature (mg C mg chl a^{-1} day^{-1}).

The initial slope of the curve α^B and the onset of saturation E_k both reflect how efficiently the light is used by the phytoplankton for fixing CO_2, in terms of specific rate of photosynthesis. It can also be easily shown that the initial slope reflects a linear relationship between production and irradiance, $\alpha^B = P^B/E_k$. Thus, E_k and α^B are also linearly related parameters.

The previous function can be modified by introducing a new term which accounts for photoinhibition (Platt *et al.*, 1980), thus

$$P^B_{(z)} = P^B_{max} \cdot \left(1 - e^{-\frac{\alpha^B \cdot I}{P^B_{max}}}\right) \cdot \left(e^{-\frac{\beta \cdot I}{P^B_{max}}}\right) \tag{5.2}$$

where β is the photoinhibition parameter [mg C mg chl a^{-1} m^{-3} day^{-1} (μ E m^{-2} day^{-1})$^{-1}$] (Figure 5.1).

Jassby & Platt (1976) introduced a new function for describing phytoplankton primary production, which is commonly referred as the *tangents hyperbolicus* function

$$P^B_{(z)} = P^B_{max} \cdot \tanh\left(\frac{\alpha^B \cdot I}{P^B_{max}}\right) \tag{5.3}$$

This function can also be modified by introducing a photoinhibition term like in equation (5.2).

Some of the functions described in the literature may provide a better fit to experimental or empirical data than others, but the selection can be somehow arbitrary as far as they do not introduce any significative difference in the dynamics of the model.

5.1.1 The Effect of Temperature on the Photosynthetical Process

The photosynthetical capacity (maximum photosynthetical rate) P^B_{max} show a temperature dependence (Li, 1980; Falkowski, 1981; Li *et al.*, 1984) on the basis of the temperature dependence of the activities of Ribulose-1,5-bisphosphate carboxylase RuBPC (or RubisCO) and phosphoenolpyruvate carboxylase PEPCK enzymes. This relationship is quantitatively very relevant not only because the reaction it catalyzes, but also because it seems to be by far the most abundant protein on earth. Consequently, it will be explicitly considered in the biological model (chapter 6).

The temperature dependence of P^B_{max} is usually modeled as a function of Q_{10} factor

$$P^B_{max} = P^B_{max10} \cdot Q_{10}^{\left(\frac{T-10}{10}\right)} \tag{5.4}$$

P^B_{max10} is the photosynthetic capacity at 10°C (Falkowski, 1980). Q_{10} is the metabolic proportionality factor for the effect of temperature.

Li *et al.* (1984) points out that the measurements from phytoplankton species from arctic waters are similar that the ones from temperate phytoplankton at low temperatures (data from Williams and Murdoch, 1966; Mandelli *et al.*, 1970 and Durbin *et al.*, 1975). This relationship reflects a lack of genotypic adaptation to overcome the effect of low temperatures on enzymatic rates of photosynthesis.

5.2 Bio-optical Models of Phytoplanktonic Carbon Fixation

The photosynthetical process begins when a photon the incident solar radiation is captured by a phytoplankton cell. The conversion from light energy to chemical energy in the form of carbohydrate is accounted by the chloroplast to reduce a CO_2 molecule, and it can be described as a function depending on two factors: the *absorption coefficient* $\chi_{(\lambda,z)}$, this is the ability of capturing a photon by the phytoplankton or rate of capture of quanta, and the efficiency of conversion of the absorbed light. The second factor is described as the *quantum yield* $\phi_{(z)}$.

Kiefer & Mitchell (1983) proposed a simple model based on the absorption coefficient and the quantum yield[1] as

$$P^B_{(z)} = \xi_C \cdot \phi_{(z)} \cdot \underbrace{a_p(\lambda,z) \cdot E_d(\lambda,z)}_{\chi_{(\lambda,z)}} \tag{5.5}$$

[1] Both terms expressed following Kirk's, (1983, 1994) notation.

where $P^B_{(z)}$ is the daily integrated rate of photosynthesis (mg C m^{-3} day^{-1}) at depth z; $\phi_{(z)}$ is the *in situ* quantum yield, and it is expressed in mol C·E^{-1}, and ξ_C is the conversion factor from mols of carbon to milligrams of carbon, which is equal to 12000. Finally, $\chi_{(z)}$ is the photosynthetically absorbed radiation E m^{-3} day^{-1}, equivalent to the absorption coefficient of the phytoplankton $a_p(\lambda,z)$ by the downward radiation $E_d(\lambda,z)$, (*see* next section). Kirk (1983) uses the notation $\chi_{(z)}$, in W·m^{-3}, MJ m^{-3} h^{-1}, or converted to quanta m^{-3} s^{-1} or μE m^{-3} s^{-1} using the relation $\frac{Q}{W} = 2.77 \times 10^{18}$ quanta·s^{-1} W^{-1}, after Morel & Smith (1974); the relationship, computed for a wave length of $\lambda = 550$ nm, taken as the center of the PAR spectra 400–700 nm, yields the conversion factor 4.599696 ($\approx$ 4.6) μE m^{-2} s^{-1}/W m^{-2}.

5.2.1 Light Absorption by the Phytoplankton

Just a fraction of the light irradiance that reaches the water surface penetrates below the surface. A fraction between 2–6% of the incident light irradiance is reflected. Globally, the *albedo* accounts for a small influence in the efficiency use of light by the phytoplankton.

In this work I shall consider just ocean waters in which the reflection by the bottom has no meaning, but this case can be specially important in shallow waters like estuaries or shallow lakes and ponds. In this case a large fraction of the incident light may be reflected out of the water column, and thus to be not usable by the phytoplankton or macrophyta. This is specially significative in the case of very shallow waters and white sediments that even with large irradiances and no nutrient limitation the productivity of the water column can be very low.

Let us consider at this stage that the major fraction of the incident light absorbed by the phytoplankton is absorbed by the pigments present in chloroplasts.

The energy absorbed by the phytoplankton $\Phi_p(z)$ per unit of volume v, at a depth z can be described as

$$\frac{d\Phi_p(z)}{dv} = \int_{400}^{700} a_p(\lambda,z) \cdot E_0(\lambda,z)\, d\lambda \tag{5.6}$$

where $a_p(\lambda,z)$ is the phytoplankton absorption coefficient at the wave length λ and depth z. $E_0(\lambda,z)$ is the scalar irradiance at the same wave length and depth[2].

As we often deal with the downward irradiance E_d instead of scalar irradiance E_0 a correction must be introduced, as $E_0 < E_d$. The correction $g(\lambda,z)$ was computed by Morel (1991) for phytoplankton biomasses between the range of 0.1–1.0 mg chl$a$ m^{-3}, and for the range of maximum light absorption by the photosynthetical process (400-570 nm). This factor corrects the underestimation of considering only the light that reaches the cell from its upper side, while it is also possible to receive some amount of upward

[2] The term Φ describes the *radiative flux* in W, J s^{-1} or quanta s^{-1}.

Irradiance is the incident radiative flux on a infinitesimal surface point divided by its area, in W m^{-2}, J m^{-2} s^{-1} or quanta (=photons) m^{-2} s^{-1}.

Scalar irradiance is the irradiance at some point integrated in all directions. See Kirk (1983; Chapter 1) for a comprehensive description.

radiation. If we do not consider this correction factor we can underestimate the radiative flux that reaches a phytoplankton cell (Kirk, 1983). g varies from 1.1 to 1.5. According to this, $E_0(\lambda,z) \equiv E_d(\lambda,z) \cdot g(\lambda,z)$.

If we consider now that the total rate of absorption of radiant energy $\Phi_{(z)}$ by water per unit of volume mainly corresponds to the downward radiation, thus vanishing the upwards light flux (this can be quite safely assumed in clear ocean waters with low turbidity; Morel, 1977), K_D defining as the vertical attenuation coefficient for the downward irradiance, then

$$\frac{d\Phi_{(z)}}{dv} \simeq K_D \cdot E_d(z) \tag{5.7}$$

This function now accounts not only for the downward irradiance absorbed by the phytoplankton K_{PH} but for the whole set of attenuating factors within the PAR spectra

$$K_D = \underbrace{K_W + K_G + K_{TR}}_{k_{np}} + K_{PH} \tag{5.8}$$

K_W, K_G and K_{TR} are the downward attenuation coefficients due to the water, the dissolved colored substances (gilvin) and to the suspended particles (tripton), respectively. In this work I shall group these three first terms as k_{np}.

Now we can approximate that the attenuation coefficient due to the phytoplankton is linearly related with the concentration of phytoplankton. As a first approach we can consider the phytoplankton biomass B_c in terms of chlorophyll a ($\mathrm{mg\,Chl}\,a\ \mathrm{m}^{-3}$), together with the specific vertical chlorophyll attenuation k_c ($\mathrm{m}^2\,\mathrm{mg\,Chl}\ a^{-1}$), and this can be written as

$$K_{PH} = B_c \cdot k_c \tag{5.9}$$

To finally arrive to an estimation of the radiative energy absorbed by the phytoplankton in the water column $\Phi_p(z)$ we can use the expression

$$\frac{\Phi_p(z)}{dv} = \int_{400}^{700} \frac{a_p(\lambda,z)}{a_T(\lambda,z)} \cdot K_D(\lambda,z) \cdot E_d(\lambda,z)\, d\lambda \tag{5.10}$$

where $K_D(\lambda,z)$ is the vertical attenuation coefficient for downward irradiance at wavelength λ and depth z. $a_T(\lambda,z)$ is the total absorption coefficient; thus the ratio accounts for the proportion of light absorbed by the phytoplankton. As a simplification, it can be assumed that all the absorption process accounted by the phytoplankton is due to the chlorophyll a

$$a_p(\lambda,z) \simeq B_c(z) \cdot a_c(\lambda,z) \tag{5.11}$$

being $a_c(\lambda,z)$ defined as the specific absorption coefficient of the phytoplankton in terms of chlorophyll ($\mathrm{m}^2\,\mathrm{mg\,Chl}\ a^{-1}$). $a_c(\lambda,z)$ is also written in the literature as $a^*(\lambda,z)$ or $a_p^*(\lambda,z)$, where the asterisk means *normalized* to chlorophyll.

It is necessary to point out that $a_p(\lambda,z)$ is an *inherent* property of the phytoplankton, and may vary depending on the species composition of the heterogeneous aggregate of phytoplankton being considered; this is, the water mass. $a_p(\lambda,z)$ is determined in the laboratory using a collimated beam, trying to minimize scattering losses by using short path-length cuvettes (*see* Grum & Becherer, 1979, for further details on the standard technique; and Mobley, 1994, for a modified technique). On the other hand, k_c is an *apparent* optical property of the underwater light field, resulting from the interaction between sunlight and the phytoplankton suspended in natural waters (Schanz, *et al.*; 1997); it is usually determined *in situ* by linear regression of K_D *vs.* chl *a* concentration (Talling, 1960) with

$$K_D = k_c \cdot B_c + k_{np} \tag{5.12}$$

or using filters with increasing phytoplankton concentrations. If there is no different indication k_c is assumed to be equal to $\overline{k_c}(PAR)$, this is, the wavelength-averaged chlorophyll absorption over the photosynthetical available radiation. Both, k_c and $a_p(\lambda,z)$ depend on physical, ecological and physiological factors like the color of the water mass, species composition, geometry and cell size, packaging of pigments, photoacclimatation and nutrient status (Marra & Bidigare, 1994; *see* also Schanz, 1997; and references cited therein). So that, their values may change in time as well as in space (*cf.* Appendix C). According to inequality (5.11] we may now define the relationship $a_p(\lambda,z) \equiv B_c(z) \cdot k_c$.

Finally, the energy absorbed by the phytoplankton per unit of volume $\frac{d\Phi_p(z)}{dv}$ is also commonly denoted as $\chi_{(z)}$, so we can write equation (5.10) in the PAR spectra as

$$\chi_{(z)} \;=\; B_c(z) \cdot k_c \cdot E_d(z) \tag{5.13}$$

with $\chi_{(z)}$, in $\mathrm{W{\cdot}m^{-3}}$ or $\mu\mathrm{E\,m^{-3}\,s^{-1}}$. $\chi_{(z)}$ can be also expressed by the normalized to chlorophyll *a* concentration according to the relationship $\chi_{(z)} = B_c \cdot \chi_{c(z)}$. The rate of PAR absorption by the phytoplankton in terms of chlorophyll *a* $\chi_{c(z)}$ has the units $\mathrm{W\,mg\ Chl}\,a^{-1}$, or $\mu\mathrm{E\,mg\ Chl}\,a^{-1}\,\mathrm{s}^{-1}$.

5.2.2 The Quantum Yield, ϕ

As I have already defined above, the *quantum yield* is described as the efficiency of conversion to chemical energy of the absorbed energy of light $\chi_{(z)}$ (or $\chi_{c(z)}$), and this can be also directly expressed as the ratio

$$\phi = \frac{B_c \cdot P^B_{(z)}}{\xi_C \cdot \chi_{(z)}} = \frac{P^B_{(z)}}{\xi_C \cdot \chi_{c(z)}} \tag{5.14}$$

ϕ, in $\mathrm{mol\,C\,E^{-1}}$ (Morel, 1983). $P^B_{(z)}$ is the photosynthetic rate of fixed carbon, in $\mathrm{mg\,C\,mg\,Chl}\,a^{-1}\,\mathrm{h}^{-1}$. The photosynthetic rate can be measured by the ^{14}C technique, or measuring the oxygen release rate divided by the *photosynthetic quotient* (O_2/CO_2), which is in the range of 1.1–1.2, as far as phytoplankton is composed not only by carbohydrates but also by lipids,

proteins and nucleic acids. Then, equations (5.7) or (5.13), and equation (5.14) may be expressed as

$$\phi = \frac{P^B_{(z)}}{\xi_C \cdot k_c \cdot E_d(z)} \tag{5.15}$$

On the basis of the proportionality between the quantum yield and the ratio $P^B_{(z)}/E_d(z)$ in the initial linear part of the P/I curve, Bidigare *et al.*(1992) derived for the PAR range the next equation, which is based on Jassby & Platt (1976) equation (*cf.* equation (5.3); and appendix D for the complete deduction)

$$\phi = \phi_m \frac{E_k}{E_d(z)} \tanh\left(\frac{E_d(z)}{E_k}\right) \tag{5.16}$$

5.2.3 The Maximum Quantum Yield, ϕ_m

As stated above, the slope of P/I curves α^B is related with the CO_2 fixation efficiency, which is maximum at the lowest irradiance levels. The fixation efficiency is conceptually related with the quantum yield, and many attempts have been devoted to explore all possible theoretical relationships (Bannister & Weidemann, 1984). Thus, it is also expected the quantum yield to be maximum at the initial part of the curve. This property allow us to define a new parameter named the *maximum quantum yield* ϕ_m, with strong physiological and ecological implications (*see* Falkowski, 1981; and Kirk, 1994, for a deeper insight into the concept).

6. THE BIOLOGICAL MODEL

Any attempt to deal exhaustively with the huge amount of research devoted to the modeling of phytoplankton population dynamics would be vane. However, it is suitable to include here the main preceding works upon which this thesis stands and briefly review the main ideas and concepts. Afterwards, we shall refer to some review texts as a matter of introductory opuses, and critically discuss some of their basic statements.

Despite most theoretical or heuristic approaches, generally based on Lotka-Volterra-like equations, there is a wide variety of mathematical models and formulations on phytoplankton dynamics[1].

We shall quote a question raised by Hastings (1996), in his review of Pahl-Wostl's book entitled *The dynamic nature of ecosystems: chaos and order entwined* (1995):

> **Is it reasonable to examine properties of an ecosystem using models?** More precisely, **what properties of an ecosystem can be examined using mathematical properties?** (...) The models produced are complex and nonlinear. Work during the past two decades on nonlinear dynamics suggest that complex nonlinear systems are likely to have extraordinary complex behavior. **Unless the models are mechanistic and have some essential simplifying properties, an approach based on complex nonlinear models may not be fruitful because the model behavior may depend critically on the assumptions made.**

In other words, models must attempt to mathematically describe the processes under study by the simplest mechanistic equations, without superfluous or unnecessary terms. The use of mechanistic equations, specially when they do directly and explicitly refer to specific ecological, physiological or biochemical processes, is a clear statement that we tried to follow during the modeling exercise which we will introduce next.

There are many different types of ecological or eco-physiological mathematical models, depending on their ultimate purposes or goals. Dynamical models that intend to be useful for the study of nutrient or carbon fluxes through a community or food web tend to outline their ruling equations by simple formulations. This means that the considered processes are usually the simplest ones. However, community or ecosystem models usually attempt to cope with all the main compartments, allowing the cycling of nutrients (*e.g.*, Fasham, *et al.*, 1990; Doney *et al.*, 1996). These models mainly focus on

[1] We shall not consider in this thesis either Lotka-Volterra equations, nor their many related ones. For an extended review *see* Kingsland, 1985; Berryman, 1992; and the throughfully analysis by Goel *et al.*, 1971; devoted to the multi-specific Lotka-Volterra models, and additional comments by Hastings, 1990.

the seasonal dynamics of the functional groups or species, and on the final (averaged) global budgets; their output should be correlated with the output of steady flow-diagrams depicted by network analysis (Ulanowicz, 1980, 1986).

On the other hand, the modeling exercise follows different aims as well. The study of dynamical systems is actually the general framework here. Ecological models that are built to understand the main controlling features of the system can not usually deal with a very complex system's structure, otherwise flow and structural analysis becomes too complex. Complexity must also be obviously limited to some extent for numerical reasons; thus, the increasing complexity of some initially simple models represent a drawback whenever we include unrelevant terms. It is definitely necessary to make a critical analysis in order to discard terms which are unnecessary whenever the model increases its complexity. Obviously, this should be done before the model becomes completely unmanageable. Superfluous complexity strongly limits the capacity of the model for providing useful synthetical results and ideas about the main underlying features of the system under study.

6.1 Preceding Studies

Ecological modeling is not a young research field anymore. It is already more than thirty years old, although its origin must be related to pure mathematical analysis of dynamical systems. Aside of Lotka-Volterra model, and previous attempts like Verhulst "logistic" equation, which could be studied by analytical means (*see* Gabaldon, 1996; for an historical introduction to population models), mechanistic ecological modeling took off after the fast development of computers: this is, after the sixties. Although it is always worthwhile to attempt any analytical study of the model, in most of the cases the equations are solved by numerical algorithms, opening the field to numerical simulation (Zeigler, 1976).

The first precedents of the ecological models of aquatic systems were, in fact, just simple mathematical functions (*e.g.*, Eppley, 1972; among many others). Anyway, this kind of simple mathematical relationships allowed the first ecological models to be built.

The 2-D model developed by Walsh (1975) and the vertical 1-D models by Radach & Maier-Reimer (1975) and Jamart *et al.* (1977), are all of them well known pioneering dynamical models of marine phytoplankton. However, the physical environment was too roughly represented in all of them: for instance, the vertical stability of the water column was, in fact, determined by only one or two values (above and below the thermocline) for the whole water column. Furthermore, the assumption of a constant value of the eddy diffusion coefficient in the mixed layer does not provide, as we know now, a realistic representation of the physical environment (Jamart *et al.*, 1977). We address the reader to Patten (1968) for an historical review of the statements that led to the development of the works mentioned above.

A decade later new models were developed further with some very significative advances. Tett *et al.* (1986) described growth rate as a function of the internal nutrient concentration (the concentration inside of the organism), instead of the concentration in

the bounding fluid, commonly modeled using a *Michaelis-Menten* function[2] (Dugdale, 1967). Internal concentration is actually computed in terms of nutrient quota, or *nutrient-to-carbon* ratios. The hypothesis that internal nutrient content controls algal growth was first formally stated by Droop (1968) and Caperon (1968), supported recently by new works (Anderson *et al.*, 1994; Droop, 1973, 1977, 1983; Elser *et al.*, 1988; Elser & Hassett, 1994; Longhurst & Harrison, 1988; Painting *et al.*, 1993), and implemented in dynamical models by Olsen *et al.* (1983) and Fong *et al.* (1994), among others. However, the final formulation based on the internal nutrient quota was first published by Droop in 1974, and further developed in Droop *et al.* (1982).

In the last ten or fifteen years many new models for different purposes have been published so far, and modeling has become a useful and powerful tool in marine research, as well as in other fields. *See* Fransz *et al.* (1991) for a comprehensive revision.

6.2 Model Description

In spite of the large number of models that have been published about phytoplankton dynamics (some of them briefly reviewed in the previous section), the reasons for building up a new model on phytoplankton growth are several. The first one is to split up phytoplankton growth from nutrient uptake. Growth has been modeled in many different ways up to now. Most of them consider growth directly as a function of external nutrient concentration; this means that uptake and growth processes are not separately considered. But growth has a time scale within a range from hours to a few days, and nutrient uptake is often a much faster process, ranging from a seconds to a few hours.

Turbulence has a characteristic time scale faster than growth scale (taken as the range of ecologically meaningful values) but of the same order than nutrient uptake's time scale. Thus, if turbulence influences phytoplankton growth, it is expected that this influence is mainly exerted throughout a process of roughly the same magnitude. In principle, it can not be assumed that any further effect is relevant other than what is explicitly defined by the model, although it is obvious that the model does not discard what is not considered explicitly in it[3].

On the other hand, splitting up growth from nutrient uptake allows nutrients to accumulate in the cell[4]. This is achieved by a faster uptake rate than the rate at which nutrients are fixed in the cell as biomass. The model that we present in this chapter shows a fast nutrient uptake dynamics, closely coupled to different functional patterns.

There was another reason for building a new model, according to the main goal of this thesis. Most of the models usually deal with the biomass in terms of carbon or ni-

[2] Sometimes called *Monod* function (Monod, 1950).

[3] A model is actually built for exploring the factors which are known to influence the system's dynamics. But it is also possible (and even desirable) that a model gives rise to new hypothesis and open new questions not considered at the initial stage.

[4] Sometimes the accumulation of nutrients in the organism (Droop, 1968, 1973) has been described to be due to *luxurious* uptake. This qualification is, in fact, inexact, as far as it has not been proved that some fraction of the nutrients accumulated in the cell are definitely going to be wasted or *luxuriously* misused.

trogen (or phosphorus, although they are not usually considered all together), but it was necessary to separately follow the track of both carbon and nutrients for one fundamental reason. On one side it is necessary to calibrate carbon assimilation rate of the phytoplankton, and the most accurate way for estimating carbon assimilation rate is to use a bio-optical model (Chapter 5); carbon is usually the standard unit of biomass, as it is set up in our model. On the other side, the seasonal spatial dynamics of the phytoplankton in the vertical dimension can not be determined solely with a bio-optical model. Bio-optical models can not explicitly account for nutrient limitation conditions because they do not explicitly consider nutrients in their formulations. They were mainly developed for providing vertically integrated estimates of primary production based on light, chlorophyll and temperature, from remote sensing measurements. Thus, they can not properly describe the vertical structure of the phytoplankton without the aid of nutrients, and nutrients may still not be estimated by remote sensing. Consequently, bio-optical model by themselves are not able to infer spatial vertical structures like the *Deep Chlorophyll Maximum* (DCM, from now onwards).

As far as the vertical spatial structure of the phytoplankton in aquatic systems is determined by both light and nutrients distribution, it is necessary to explicitly account for nutrients in vertically resolved phytoplankton models. Further on, vertical fluxes of nutrients in the aquatic environment are strongly influenced by turbulence and mixing processes. Therefore, turbulence becomes the key-point that couples light-mediated mechanisms (photosynthesis and growth), and mixing-mediated mechanisms (vertical nutrient fluxes).

The main hypothesis is that turbulence exerts its influence on the spatial dynamics of the phytoplankton mainly at two different levels: the most relevant one is the control of the vertical flux of nutrients by the mixing processes. But there is still a second one that also plays an important role near the surface, which is the spreading of the organisms through the uppermost layers of the water column, and their interaction with nutrients and predators. Thus, although the biological model has a larger number of state variables, the physical and the biological model only shear the concentration of nutrients dissolved in the fluid and the phytoplankton biomass, in terms of carbon concentration.

6.2.1 State Variables

The biological model has been defined by five state variables (Figure 6.1). The state variables denoted as N_{Ext}, C_P, N_P, C_B and N_B, are, respectively, the concentration of nitrate N_{Ext}, the internal *pool* concentrations of carbon and nitrate in the organism, and the internal concentrations of carbon and nitrogen, as biomass. The units of carbon are in mg C$\cdot$m^{-3}, and the units of nitrogen are in mg-at N$\cdot$m^{-3}, both for nitrate and atomic nitrogen.

The model follows the track of carbon and nitrogen through the different eco-physiological processes considered in it. The postulated internal carbon pool C_P is a necessary key-point for uncoupling carbon assimilation and growth. This transient carbon pool, as *non-permanent biomass*, was first proposed by Zonneveld *et al.* (1997). It can be inter-

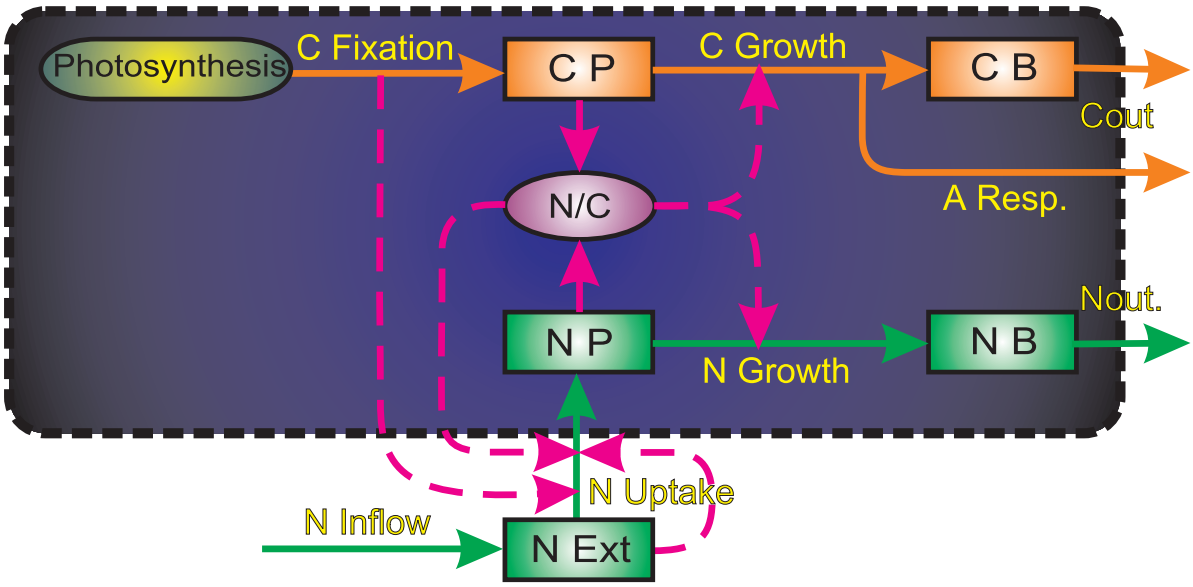

Fig. 6.1: Conceptual scheme of the biological model. N_{Ext}, C_P, N_P, C_B and N_B are the compartments (state variables) of the system. Solid lines indicate carbon (orange) and nitrogen (green) fluxes. Broken lines indicate functional relationships among compartments and functional variables like the internal pool nutrient quota $\frac{N}{C}$. Photosynthetical carbon assimilation rate is accounted by a bio-optical model (*see* text).

preted physiologically as a functional reservoir for saving photosynthetical output products (principally tricarboxylic carbohydrates). These intermediate substances do work as the basic energy source for growth in the model.

N_P is the counterpart of C_P. Both are transient pools and their contents respond very sensitively to environmental variability; and they buffer most of it. They also allow a balance between carbon and nitrogen pathways within a physiologically plausible range of variation. N_P accounts for the reservoir of the nutrient in vacuoles.

The parallel occurrence of carbon and nitrogen at the pool and biomass stages enables the possibility of computing two different types of quotas. The first one, the *pool nutrient quota* $\left(\frac{N}{C}\right)$, directly reflects the direct uncoupling between carbon and nutrient pathways.

Further on, *biomass nutrient quota* $\left(\frac{N}{C}\right)_B$ buffers the diel variability of the pool nutrient quota due to the intrinsic environmental variability. We shall present a deeper analysis of this behavior in the results part. Anyway, it is worthwhile to remark that biomass nutrient quota accounts for amino-nitrogen, mainly in the form of proteins and catabolic compounds, while pool quota does account for *free* nitrogen, whether nitrate or ammonia.

The biological model is driven by five ordinary differential equations. The system equations (expressed in fluxes of matter) are

$$\frac{dN_{EXT}}{dt} = N_{INFLOW} - N_{UPTAKE} \tag{6.1}$$

$$\frac{dC_P}{dt} = C_{FIXATION} - C_{GROWTH} \quad (6.2)$$

$$\frac{dN_P}{dt} = N_{UPTAKE} - N_{GROWTH} \quad (6.3)$$

$$\frac{dC_B}{dt} = C_{GROWTH} - C_{OUT} \quad (6.4)$$

$$\frac{dN_B}{dt} = N_{GROWTH} - N_{OUT} \quad (6.5)$$

C_B and N_B express the concentration of organisms in the fluid in terms of carbon and nitrogen, respectively. C_B is the only biological state variable which is passed to the physical model. However, vertical fluxes of N_B may always be obtained whenever necessary by multiplying C_B by the internal biomass nitrogen quota $\left(\frac{N}{C}\right)_B$, which is updated by the model every time step.

6.2.2 Fluxes of Matter

Carbon Fixation

Cullen (1990) and Cullen *et al.* (1992) state that nutrient limitation does not significatively affect carbon fixation except in the case of strong nutrient limiting conditions. This statement implicitly assumes the existence of two independent processes which should be considered separately. In consequence, we have split growth in two different processes: *carbon fixation* $C_{FIXATION}$, and *growth* C_{GROWTH}, in order to deal with them independently.

Carbon fixation $C_{FIXATION}$ is accounted in the model by an estimation of the photosynthetical rate normalized to biomass, expressed in units of carbon per unit of chlorophyll (mg C·mg Chl a^{-1}·m^{-3}·s^{-1}). Photosynthesis rate can be accurately estimated by bio-optical models as a function of light, chlorophyll and temperature (Bidigare *et al.*, 1992; *see* also Behrenfeld & Falkowski, 1997, 1997a). The biological model described here includes the bio-optical model described in Chapter 5 (Equation 5.2), as a sub-model for estimating the CO_2 fixation rate P^B; these kind of formulations assume no carbon limitation. Thus,

$$C_{FIXATION} = P^B \cdot [Chl] \quad (6.6)$$

In order to calculate the carbon flow in absolute units of mg C·m^{-3}·s^{-1} (all carbon flows have the same units), we have to multiply the normalized carbon fixation rate by the Chlorophyll *a* concentration $[Chl]$.

The Chlorophyll-to-Carbon Ratio $\frac{Chl}{C_B}$

Geider (1987) mathematically described the negative relation between $\frac{Chl}{C_B}$ and irradiance under nutrient-saturated growth. Later on, Cloern *et al.* (1995) found a new empirical relationship on nutrient-limited growth rate μ' (growth rate in nutrient-rich media), temperature and irradiance I,

$$\frac{Chl}{C_B} = 0.003 + \mu' \cdot 0.154\, e^{0.05 \cdot T}\, e^{-0.059 \cdot I}$$

$\frac{Chl}{C_B} = 0.003$ seems to be the lowest limit of chlorophyll to carbon ratio (Geider, 1987). The relationship with temperature is consistent with Eppley (1972), Yoder (1979), Verity (1981, 1982) and Geider (1987), giving higher $\frac{Chl}{C_B}$ values with increasing temperature. $\frac{Chl}{C_B}$ is also positively and linearly related to μ' (Laws & Bannister, 1980; Sakshaug *et al.*, 1989; Chalup & Laws, 1990). But this linear relationship varies as a function irradiance; Sakshaug *et al.* (1989) with *Skeletonema costatum* suggests that the slope of the relation between $\frac{Chl}{C_B}$ and μ' decreases nonlinearly with day light exposure, thus supporting their well known negative relationship. *See* also Mitchell & Holm-Hansen (1991) and Cullen *et al.* (1992) for further comments on these relations.

Bio-optical models are based on common P/I curves, so they can be calibrated with the aim of laboratory or *in situ* incubations with ^{14}C, or measuring the rate of O_2 evolution. The synthesis of new biomass C_{GROWTH} (in terms of carbon) is defined to be proportional to the internal nitrogen to carbon ratio $\frac{N}{C}$ (hereafter called *nutrient* or *nitrogen quota*), using the *Droop's* formulation (*see* page 71).

Nitrate Inflow

Dissolved nitrate enters the system by turbulent diffusion N_{INFLOW}. Nitrate and atomic nitrogen flows are both expressed in mg-at $N \cdot m^{-3} \cdot s^{-1}$. Nitrate inflow is computed according to (1.7), where the turbulent diffusion coefficients profile K_ρ is estimated according to Osborn's parameterization (3.25), and the gradient is calculated from empirical data during FRONTS-92 campaign. The nitrate concentration is updated every time step by the physical model.

Nitrate Uptake

Nitrate uptake N_{UPTAKE} is defined in this model as an independent process from carbon fixation, although it can be limited under low carbon fixation rates. Uptake is

the main limitation factor is irradiance. It can also be limited by high nitrogen quota values, according to *Droop's* formulation. This holds when internal nitrate pool is full, that follows high nutrient availability conditions. Nitrate uptake is defined as

$$N_{UPTAKE} = U_{max} \frac{N_{EXT}}{K_M + N_{EXT}} \cdot \left(1 - \frac{\left(\frac{N}{C}\right)}{\left(\frac{N}{C}\right)_{max}}\right) \cdot \left(\frac{P^B}{P^B_{max}}\right)^{\frac{1}{2}} \tag{6.7}$$

K_M is the half-saturation constant for nitrate. $\left(\frac{N}{C}\right)$ and $\left(\frac{N}{C}\right)_{max}$ are, respectively, the nitrogen quota, and the maximum nitrogen quota. Nitrogen quota is computed from the transient pools N_P and C_P. This is, according to the concentrations of carbon and nitrogen compounds available for the synthesis of biomass (growth).

Nitrogen quota is a fundamental term in the formulation of the nutrient uptake. This term deals with the nitrogen that has not been converted to biomass yet, or internal *free* nutrient that accumulates in the living cells. The nutrient quota is the term that reflects

environmental variability at a short time scale. It is computed as the ration between nitrogen and carbon pools. This two compartments buffer the external environmental fluctuations by coupling two independently driven fluxes (photosynthesis and nutrient uptake). A function proportional to this term controls the carbon and nitrogen output flows that constitute the synthesis of new biomass.

U_{max} is the maximum uptake rate, and it shows a temperature dependency

$$U_{max} = U_{max10} \cdot Q_{10}^{\left(\frac{T-10}{10}\right)} \tag{6.8}$$

where U_{max10} is the maximum uptake rate at 10°C. Q_{10} is the metabolic proportionality factor for the effect of temperature. For instance, if $Q_{10} = 2$, this means that μ equals two-fold μ_{10} when $T = 20$°C. T is temperature, in Celsius degrees.

The second and third terms[5] of equation (6.7) are controlling factors of growth and photosynthesis, respectively. Both terms decrease nutrient uptake in parallel with carbon flow rates. This prevents nutrient accumulation up to unrealistic values. Indeed, it is nonsense for uptake to go on much further than some undetermined values, specially under photosynthesis and/or growth limiting conditions. However, the system self-controls the upper limit of $\left(\frac{N}{C}\right)$.

[5] The second term mimics *Droop's* formulation (*cf.* equation 6.9), but it actually limits the pool nutrient quota up to a maximum value defined by the parameter $\left(\frac{N}{C}\right)_{max}$.

Growth

Carbon and nitrogen growth flows are defined by the same specific growth rate function μ [s^{-1}]

$$\mu = \mu_{max} \underbrace{\left(1 - \frac{\left(\frac{N}{C}\right)_{min}}{\left(\frac{N}{C}\right)}\right)}_{Droop} \tag{6.9}$$

as defined by Droop (1968, 1973) and Droop *et al.* (1982), where μ_{max} is the maximum growth rate, and $\left(\frac{N}{C}\right)_{min}$ is the minimum nutrient quota below which growth is not possible due to nutrient limitation. The growth rate μ also shows a temperature dependency, that is introduced by the Q_{10} function

$$\mu_{max} = \mu_{10} \cdot Q_{10}^{\left(\frac{T-10}{10}\right)} \tag{6.10}$$

μ_{10} is the maximum growth rate at 10°C.

Finally, the carbon and nitrogen flow rates are defined as

$$C_{GROWTH} = \mu \cdot C_P - R_A \tag{6.11}$$

and

$$N_{GROWTH} = \mu \cdot N_P \tag{6.12}$$

where R_A is the *activity* respiration term, which depends also on the carbon growth rate (*see* next).

Outflows

As far as this model does only deal with the phytoplanktonic fraction of the pelagic community it is necessary to define all the different closure terms. There are two loss terms: respiration and a global output term that accounts for grazing, excretion and mortality, and applies to carbon and nitrogen at the same rate.

Respiration Terms I split respiration into two different terms: activity respiration, depending on growth flow, and rest respiration rate, depending on the biomass. Both terms are in mg C·m^{-3}·s^{-1}.

$$R_A = r_A \cdot \mu \cdot C_P \tag{6.13}$$

where r_A is the fraction of growth in terms of carbon which is respired (non-dimensional).

$$R_R = r_R \cdot C_B \tag{6.14}$$

Rest respiration, as a biomass dependent process, is also temperature dependent; thus, the rest respiration rate r_R [s^{-1}] is defined as usual by

$$r_R = r_{R10} \cdot Q_{10}^{\left(\frac{T-10}{10}\right)} \tag{6.15}$$

and r_{R10} is the rest respiration rate at 10°C.

Closure Terms This model uses the same global output term m for both carbon and nitrogen pathways. It accounts for loses corresponding to grazing, mortality and excretion. The linear output coefficient m [s^{-1}] just multiplies the state variable

$$C_{OUT} = m \cdot C_B - R_R \tag{6.16}$$

and

$$N_{OUT} = m \cdot N_B \tag{6.17}$$

6.3 Overview of the Driving Equations

Finally, the driving equations of the biological model, previously defined in terms of matter fluxes in equations (6.1) to (6.5), can be now summarized as follows:

$$\frac{dN_{EXT}}{dt} = N_{INFLOW} - U_r\, N_{EXT} \tag{6.18}$$
$$\frac{dC_P}{dt} = C_{FIXATION} - \mu\,(1 - r_A)\, C_P \tag{6.19}$$
$$\frac{dN_P}{dt} = U_r\, N_{EXT} - \mu\, N_P \tag{6.20}$$
$$\frac{dC_B}{dt} = \mu\,(1 - r_A)\, C_P - (m - r_R)\, C_B \tag{6.21}$$
$$\frac{dN_B}{dt} = \mu\, N_P - m\, N_B \tag{6.22}$$

where U_r is the specific uptake rate [s^{-1}] for the nutrient, which is expressed as

$$U_r = U_{max}\, \frac{1}{K_M + N_{EXT}} \cdot \left(1 - \frac{\left(\frac{N}{C}\right)}{\left(\frac{N}{C}\right)_{max}}\right) \cdot \left(\frac{P^B}{P^B_{max}}\right)^{\frac{1}{2}}$$

Nutrient quota and the Monod function have not explicitly included in the equations for sake of readability and simplicity; nevertheless, all the driving equations of the biological model are non-linear, indeed, as it can be shown after substitution.

Part III

SOLVING

7. SOLUTION OF THE GOVERNING EQUATIONS

Differential equations represent the best way to mathematically describe dynamical systems. However, many systems of equation are difficult to solve analytically. Soon it becomes impossible to solve non-linear dynamical systems defined with more than two variables.

During the last decades, research on numerical methods has evolved in parallel with the development of computers. Since the fourties numerical methods have been successfully and massively applied to many fields, from physics and engineering to oceanography, atmospheric research, etc. Indeed, computers became indispensable tools a long time ago. But numerical methods are often nothing else that just a rough but necessary approach to the real solution.

Our system is defined by two partial differential equations and two state variables, as defined in equations (1.12) and (1.13). Each one of the time derivatives is determined by a first and a second order terms, and by a non-conservative term regarding the biological processes which needs a special consideration.

Our code is written in order to be able to solve independently each one of the terms of our system (namely, diffusion, advection, and the sources and sinks term), including solving just one term alone.

7.1 Discretization Schemes

Solving ordinary differential equations (ODEs) and partial differential equations (PDEs) always imply to carry on numerical errors that sometimes can be large enough to yield anomalous results, far away from the real solution.

There are different kinds of numerical errors, aside from truncation errors: namely, amplitude, phase and transport errors, as well as instabilities. Most of them occur only under specific conditions.

PDEs can be numerically solved by means of *initial value methods* and *boundary value methods*. Given that we intend to study the evolution in time of the defined state variables we will only consider here the first method.

There are two different kinds of discretizations schemes: *explicit* and *implicit*. With the first one we can calculate ρ_j^{n+1} for each j, at time $n+1$, explicitly from the values that are already known at time n. Implicit methods require to solve the quantity ρ for various j.

In terms of accuracy the discretization schemes can be of first order, second order, and so on, depending on how many terms of the Taylor series are used. Accuracy is higher the higher the order.

7.1.1 The Advection Term

The advection term defined as

$$\frac{\partial \rho}{\partial t} = w \frac{\partial \rho}{\partial z}$$

is discretized by the *upwind differencing* scheme (or simply *upwind*).

$$\frac{\rho_j^{n+1} - \rho_j^n}{\Delta t} = -w_j^n \begin{cases} \frac{\rho_j^n - \rho_{j-1}^n}{\Delta z}, & w_j^n > 0 \\ \frac{\rho_{j+1}^n - \rho_j^n}{\Delta z}, & w_j^n < 0 \end{cases} \tag{7.1}$$

Although this scheme is only of the first order, it works fine for our working conditions of relatively soft profiles. It is also a simple and fast scheme, specially suitable for long simulations.

So far until now we have been considering that computations can be made exactly, but this is not completely true. We have neglected the cumulative effect of round-off errors, which are always present in any numerical computation[1]. Eventually, round-off may lead to totally unrealistic results. Consequently, this kind of situations have to be avoided and to try to find a solution for each one of the difference methods. Sometimes it is a vane attempt, as far as there are methods in complex non-linear systems which are intrinsically unstable.

The suitable stability condition for the upwind scheme is the Courant-Friedrichs-Lewy condition, which is defined as

$$\frac{|w|\Delta t}{\Delta z} \leq 1 \tag{7.2}$$

This stability condition intuitively means that vertical vertical advection needs several time steps to advance beyond a spatial grid.

The lines of code (in C) for solving the advection term are presented next

```
void sink_advection(int stv)
{
int      box_n=cnfg_par[n_boxes];
register int i;

    for(i=1;i<=box_n;i++) {
        if(ws[i]<0)
```

[1] The usual method for studying the stability of the discretizations schemes is to construct a Fourier series of the difference equation. However, we will not go any further in this thesis regarding the numerical methods, as far as the applied methods have been widely tested and all of them are well known. In consequence, we address the reader to some specific texts like Richtmyer & Morton (1967) and Ames (1977).

```
            adv_temp_vect[i]=(stvar[i][stv]-stvar[i-1][stv])
                /cnfg_par[dz]*ws[i];
        if(ws[i]>0)
            adv_temp_vect[i]=(stvar[i+1][stv]-stvar[i][stv])
                /cnfg_par[dz]*ws[i];
    }
}
```

7.1.2 The Diffusion Term

For simple vertical constant diffusion profiles and $K_\rho \geq 0$, the diffusion term

$$\frac{\partial \rho}{\partial t} = K_\rho \frac{\partial^2 \rho}{\partial z^2} \tag{7.3}$$

can be easily differenced in a very intuitive way by

$$\frac{\rho_j^{n+1} - \rho_j^n}{\Delta t} = K_\rho \left[\frac{\rho_{j+1}^n - 2\rho_j^n + \rho_{j-1}^n}{(\Delta z)^2} \right] \tag{7.4}$$

This scheme is stable for

$$K_\rho \frac{2\Delta t}{(\Delta z)^2} > 1 \tag{7.5}$$

Nevertheless, for non-constant vertical diffusion profiles $K_\rho = K_\rho(z)$ the second order term, defined as

$$\frac{\partial \rho}{\partial t} = \frac{\partial}{\partial z} K_\rho \frac{\partial \rho}{\partial z} \tag{7.6}$$

requires more complicated schemes.

We used an implicit scheme which reduces the resulting equation to a tridiagonal form, where the upper and lower diagonal values are defined, respectively, as follow

$$U(j) = -\frac{\Delta t}{\Delta z^2} \frac{1}{2} \left(K_\rho(j) + K_\rho(j+1) \right) \tag{7.7}$$

$$L(j) = -\frac{\Delta t}{\Delta z^2} \frac{1}{2} \left(K_\rho(j) + K_\rho(j-1) \right) \tag{7.8}$$

The diagonal values are

$$D(j) = 1 + \frac{\Delta t}{\Delta z^2} \left(U(j) + L(j) \right) \tag{7.9}$$

Finally, the tridiagonal matrix is solved by the Thomas algorithm (*see* Press *et al.*, 1992; and *cf.* also the code included below these lines).

Using the implicit scheme allows us to deal with non-linear diffusion problems, satisfying the stability condition for long time steps.

The C code used for solving the diffusion term is included below

```
void diffusion(int stvr)
{
int      box_n=cnfg_par[n_boxes];
double   dtdz2,l_next,l_prev;
double   *diagonal,*lower,*upper,*alpha,*beta,*gamma;
register int i;

    diagonal=dvector(0,box_n+1);lower=dvector(0,box_n+1);
    upper=dvector(0,box_n+1);alpha=dvector(0,box_n+1);
    beta=dvector(0,box_n+1);gamma=dvector(0,box_n+1);
    dtdz2=cnfg_par[dt]/(cnfg_par[dz]*cnfg_par[dz]);
    l_next=(kz[0]+kz[1])/2.0;
    diagonal[0]=1.0+dtdz2*l_next;
    upper[0]=-dtdz2*l_next;
    l_prev=(kz[box_n]+kz[box_n-1])/2.0;
    diagonal[box_n]=1.0+dtdz2*l_prev;
    lower[box_n]=-dtdz2*l_prev;
    for(i=1;i<box_n;i++) {
        l_next=(kz[i]+kz[i+1])/2.0;
        l_prev=(kz[i]+kz[i-1])/2.0;
        lower[i]=-dtdz2*l_prev;
        upper[i]=-dtdz2*l_next;
        diagonal[i]=1.0+dtdz2*(l_prev+l_next);
    }
    alpha[0]=diagonal[0];
    gamma[0]=stvar[0][stvr];
    for(i=1;i<=box_n;i++) {
        beta[i]=lower[i]/alpha[i-1];
        alpha[i]=diagonal[i]-beta[i]*upper[i-1];
        gamma[i]=stvar[i][stvr]-beta[i]*gamma[i-1];
    }
    stvar[box_n][stvr]=gamma[box_n]/alpha[box_n];
    for(i=box_n-1;i>=0;i-)
        stvar[i][stvr]=(gamma[i]-upper[i]*stvar[i+1][stvr])/alpha[i];
    free_dvector(diagonal,0,box_n+1);free_dvector(lower,0,box_n+1);
    free_dvector(upper,0,box_n+1);free_dvector(alpha,0,box_n+1);
    free_dvector(beta,0,box_n+1);free_dvector(gamma,0,box_n+1);
}
```

7.1.3 The Biological Term

The biological term, accounting for sources and sinks, is defined by a system of ODEs (*see* chapter 6).

Solving the biological term, full of non-linear equations, requires a very flexible integration method. The Runge-Kutta with a fixed time step proved to be too slow and

inefficient. Consequently, we chose a fifth order Runge-Kutta method with an adaptive stepsize, that provided a much better performance fitting the necessary accuracy. The routines described in Press *et al.* (1992) were finally used (we do not include the code; *cf. op. cit.*).

7.2 Coupling the Biological and Physical Terms

The coupling between the biological and the physical requires some explanation, as far as the convergence conditions must be always fulfilled.

The integration schemes implemented for integrating the physical terms use a fixed time time step whilst the biological model uses an adaptive time step scheme. In order to sincronize the solving of the governing equations (1.12) and (1.13) and keeping both the convergence for the physical and the biological terms, we first solve the biological equations for a period of time equal to the given time step, allowing the routine to freely vary the time step (or stepsize) within the starting and ending time, until accuracy fits the demanded value (usually, 10^{-5}). Afterwards, we solve the physical terms, using a given fixed time step. Then, the program goes on again with the solving of the biological equations.

The concentrations calculated by the biological model are then transported (by diffusion and/or advection and sedimentation) over the next time step (in any case, only phytoplankton can sediment but not the dissolved nutrients).

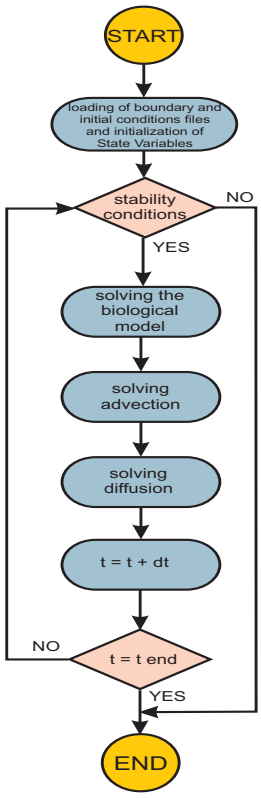

Fig. 7.1: Flow diagram of the run-time execution process of the coupled physical-biological numerical simulations.

7.2.1 Convergence Criteria

To consider the results of the coupled physical-biological model more formally we must be aware of the fulfillment of the *convergence criteria* by the solutions provided by the model.

In general, we consider that the numerical simulations give a convergent solution if

$$|e_{n+1}| < |e_n| \tag{7.10}$$

where e_{n+1} and e_n are the error at times $n+1$ and n, respectively, given an iteration formula of the type

$$x_{n+1} = f_{(x_n)} \tag{7.11}$$

and where S denotes the solution, and e_n the error, e.g.

$$e_n = x_n - S \tag{7.12}$$

We also address the reader to the text by de Vahl Davis (1986) for an deeper introduction to the convergence criteria.

Simulations of the coupled physical-biological model under constant forcing proved to converge to the same constant value. As far as the maximum time step is fixed by the model, and the time steps attained by the biological model can only be equal or smaller than the time step fixed for the physical process, we consider that the general solution of the overall model safely fulfills convergence criteria.

Part IV

RESULTS

8. DYNAMICS OF THE BIOLOGICAL SYSTEM: *ONE-BOX* SIMULATIONS

The complex non-linear dynamics of the biological model requires a preliminary analysis. In order to go deeper into the dynamical analysis of the eco-physiological processes considered in the biological model, we shall first present a short five-days simulation in *one-box*. Therefore, the biological model has been run alone; this means, without vertical transport. Next, we shall present a longer seasonal simulation as representative of the long-term dynamics.

Eco-physiological processes like nutrient uptake are extremely fast compared with phytoplankton growth rates. In principle, this makes internal (pool) nutrient concentrations to vary in a very short time, and pool nutrient quota to show a daily oscillation, as well. However, all the flows considered in the biological model are calibrated according to mean values described in the literature. This is a first remark.

As the shortest characteristic time scale of the turbulence, defined by the Kolmogorov scale (or, equivalently, by the Batchelor scale; *see* Chapter 2), fall within the range of seconds, the biological model must be able to resolve the most relevant processes at such time scales in order to explicitly consider its influence. Hence, the largest time step of the coupled physical biological model is set to one minute, and the adaptive time step scheme used in the integration of the biological model often goes further down to a few tenths of seconds. At such small scales experimental evidences becomes extremely difficult to achieve. This is an important second remark.

8.1 Photosynthetical Parameters

We have used in all the simulations parameter values representative for pelagic conditions of oligotrophic waters, suitable for the Northwestern Mediterranean Sea. Standard parameter values common for all the simulations are shown in appendix B. Simulations computed with different values will be indicated, as they are discussed.

8.1.1 α^B, β^B and P^B_{max} Parameter Values

The values of initial slope α^B, the photoinhibition slope β^B (*in* mg C mg Chl a^{-1}m^{-3} h^{-1}/(μE m^{-2}s^{-1})), and the photosynthetical capacity P^B_{max} (expressed *in* mg C mg Chl a^{-1}h^{-1}) were measured during FRONTS'92 campaign at two different depths (10 and 50 m). All the incubations were carried out on-board at surface temperature.

St.	$\overline{\alpha^B}$	$\overline{\beta^B}$	P^B_{max}			$P^B_{max}10$	
			10m	50m	50m (corr.)	10m	50m
14	0.015	0.003	4.8	1.2	0.74	2.21	0.55
45	0.015	0.002	3.4	1.5	1.13	1.65	0.73
61	0.012	0.002	1.72	1.02	0.65	0.83	0.49
65	0.022	0.001	4.08	1.08	0.75	2.07	0.55
76	0.024	0.001	3.02	0.24	0.16	1.50	0.12
86	0.049	0.004	2.88	1.84	1.44	1.60	1.02

Tab. 8.1: Measured values of the initial slope α^B, photoinhibition slope β^B, and the photosynthetical capacity P^B_{max} at 10 and 50 meters, including also the values at 50 meters *corrected* for the temperature, using $Q_{10} = 2.3$. In the two far-right columns $P^B_{max}10$ indicates the calculated values at 10°C. *See* text for the units and additional explanations.

Measured values of P^B_{max} at 50 m have been corrected for the temperature at this depth, using equation (5.4) (*see* Table 8.1).

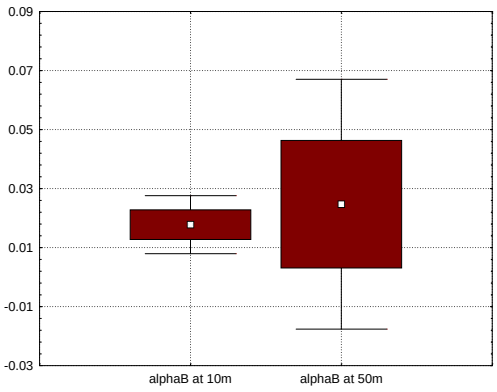

Fig. 8.1: Means and standard deviations (filled boxes) of the initial slope α^B at 10 and 50 meters, during FRONTS'92 cruise. *t*-test (p=0.351672).

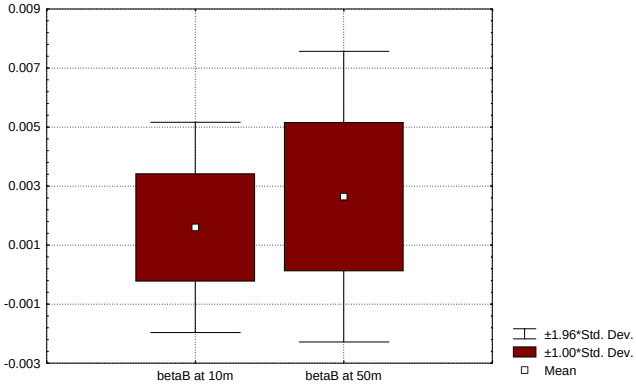

Fig. 8.2: The same plot for the photoinhibition slope β^B. Means at 10 and 50 meters. *t*-test (p=0.470896).

$\overline{\alpha^B}$ and $\overline{\beta^B}$ values from 10 meters show a rather small standard deviation in contrast with the values from 50 meters. However, the means are not significatively different at $p<0.05$. ANOVA also determines no differences between both sets of the two parameters. Consequently, we take in both cases the mean values calculated from the two values of each station, respectively, as representatives of the whole water column (Table 8.1).

The mean initial slope $\overline{\alpha^B}$ shows a rather high linear correlation with surface temperature (r=0.91, $p<0.05$; Figure 8.1), despite $\overline{\alpha^B}$ *vs.* temperature is rather weakly correlated (r=0.22). The photoinhibition slope also yields similar results as the initial slope

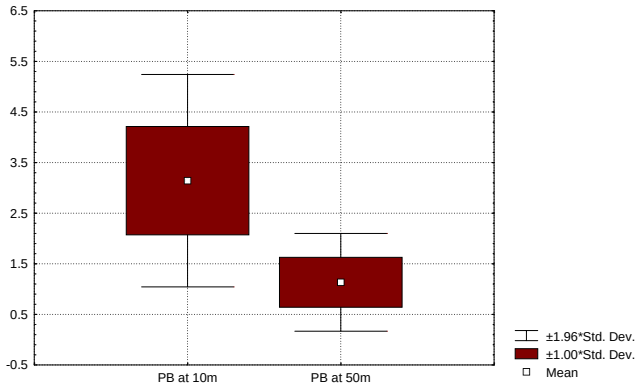

Fig. 8.3: Means and standard deviations of the photosynthetical capacity P^B_{max} at 10 and 50 meters. Student *t*-test (p=0.003369).

(Figure 8.2).

In the case of P^B_{max}, means are significatively different at $p < 0.05$ (Figure 8.3). Thus, in order to compute the photosynthetical rate at each depth we consider P^B_{max} values at 10 meters to be representative of the water mass from the surface down to the depth of the thermocline, and the values measured at 50 meters as representative from the thermocline to 100 meters.

8.2 Initial Values

- Nitrate concentration N_{EXT} is initialized with value measured at the surface.
- Carbon biomass C_B and the internal carbon pool C_P are initialized with the same value, using the chlorophyll *a* concentration near the surface, and converted to carbon using $\frac{Chl}{C_P}$, $\frac{Chl}{C_B} = 0.04$.
- Nitrogen biomass N_B and the nitrogen pool N_P are set proportionally to carbon concentrations, according to Redfield.

The values are taken from the biological station 86.1, during FRONTS'92 campaign (October–November, 1992).

8.3 Boundary Conditions and Forcing

8.3.1 Diffusion Transport of Nutrients

Simulations dealing only with the biological model are run with a constant nutrient inflow under surface irradiance.

As we have seen in section 1.1.2 (page 17), nutrient transport by molecular diffusion can be neglected from the model equations. This statement can be also empirically evidenced by comparing nutrient inflow driven by molecular diffusion (D=1.65$\times 10^{-9}$ m^{2}s^{-1}; Li & Gregory, 1974) and carbon fixation rate, assuming that the organism can take up all the incoming nitrogen. Upflux rate is assumed to be maximum taking the largest nitrate gradient found at the nitracline ($\sim$0.0057 mg-at N m^{-4}s^{-1}, at station 86.1).

Results show that the upper limit of nitrate uptake is seven orders of magnitude lower than the lowest carbon fixation rate, giving a nutrient quota five orders of magnitude lower than Redfield, which is unrealistically low even for nutrient limited populations. Simulations show a monotonically decreasing trend of the nutrient quota down to unrealistic values (that would lead to the death of the organisms), just after two or three sunny days (starting with summer nitrate concentrations in water). Consequently, such low upwelling transport rates can not support the measured phytoplankton concentration for the given conditions.

8.3.2 Temperature

The first simulation is run under constant temperature (17°C). Temperature exerts a clear effect on biological processes, like carbon fixation (Li *et al.*, 1984), so far. We will show a set of simulations within a temperature range between 13 and 25°C in order to explore such influence.

8.3.3 Irradiance Series

Simulation in *one-box* are run for a period longer than the FRONTS'92 cruise to show the forcing effect of irradiance on carbon and nutrient fluxes within the organism.

Longer series of irradiance are not available in magnetic media during 1992. In order to present longer series of results, we take data beginning at the first of May of 1996, which is the first available data series. The irradiance time series used come from the Meteorological Service of the Servei de Medi Ambient (Generalitat de Catalunya), sixty kilometers far to the south of the French border. The measurements are taken in the northern catalan coast (Roses, Girona). The series have three gaps, the longest one lasting for 6 days. During these lacking periods the gaps are filled in with measurements from another station, Lloret de Mar (Girona), at nearly eighty kilometers southward from Roses. Irradiance values during night are set to 0.1 μE m^2 s^{-1} ($\sim$ 0.05 W m^{-2}), which is near the value of full moon irradiance under clear sky. The full series used is 210 days long, beginning the 10^{th} of May and lasting until December, the 6^{th}.

8.4 Results

We first begin with a short five days simulation, in November the 1^{st}. The used P/I parameter values for $\overline{\alpha^B}$ and P^B_{max} are taken from station 86. For the rest of the parameter values *see* appendix B. The water temperature is set constant at 17°C.

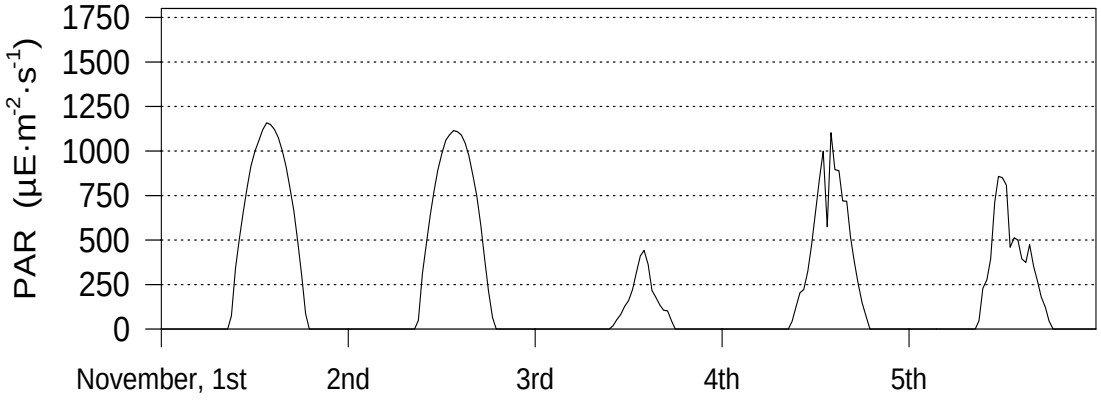

Fig. 8.4: Photosynthetically Active Radiation (PAR) at Roses (Girona, Spain) in 1996. Values averaged every 30 minutes.

The short five days long PAR series (Figure 8.4) shows two first sunny days, followed by a covered one, and then by two more cloudy days. The main feature we must point out is the low amount of PAR energy received by the phytoplankton during the third day, which is reflected in all the matter fluxes, as it will be shown next.

8.4.1 Carbon Dynamics

Carbon flows are represented by the carbon assimilation (photosynthesis) $C_{FIXATION}$, and the synthesis of biomass, or carbon growth C_{GROWTH}.

As stated above, all *one-box* simulations are run under full PAR at the sea surface. Consequently, carbon fixation shows a reduction around noon due to a photoinhibiting effect, except during the third day, under covered sky due to the lower irradiance (Figure 8.5).

Growth rate, in terms of carbon C_{GROWTH}, reaches a daily maximum at nearly the sunset, reflecting a cumulative effect during the day-light period. The carbon pool compartment partially buffers the diel variability, as well as non-periodic environmental fluctuations (Figures 8.6 and 8.7). Carbon biomass C_B also reflects the effect of nutrient availability, respiration and mortality loses. On the other hand, dependency of C_{GROWTH} on C_P concentration is clearly shown by their closely syncronized daily oscillation.

Carbon flows are, evidently, correlated with PAR irradiance (Figure 8.4) because they are functionally related (Equation 5.2). But $C_{FIXATION}$ does not appear to be fully correlated with PAR, as far as photosynthesis is not linearly related with irradiance (Figure

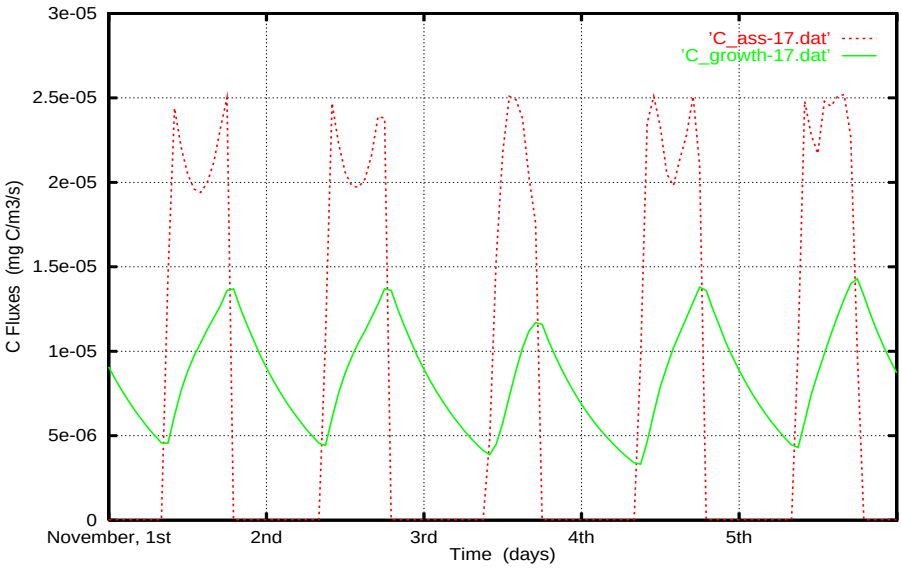

Fig. 8.5: Five days simulation of the two main internal carbon flows: carbon assimilation 'C_ass-17', and synthesis of biomass 'C_growth-17'. Both in carbon concentration units. Depressions on carbon assimilation around noon are due to the photoinhibiting effect.

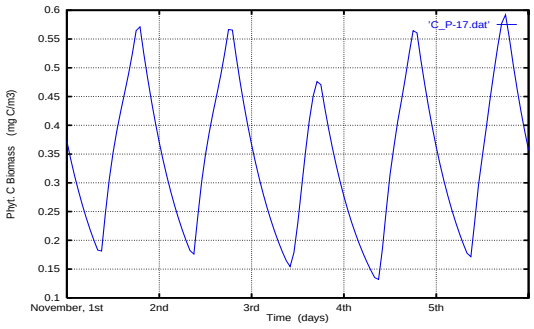

Fig. 8.6: The carbon pool compartment C_P closely follows PAR series.

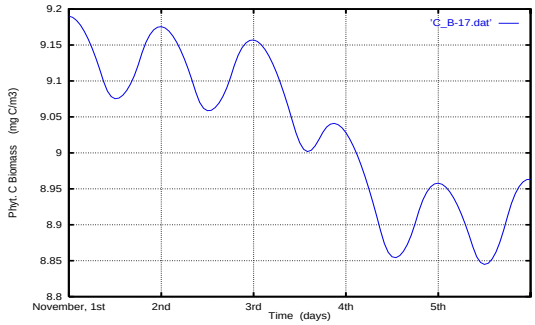

Fig. 8.7: Carbon biomass C_B shows a time integrated balance of input C_{GROWTH} and output C_{OUT} fluxes.

5.1). On the other side, as we have indicated above, simulations are run under full surface irradiance; this means that in clear days, high irradiance values pushes photosynthesis up to levels at which photoinhibition reduces the efficiency of the carbon fixation process.

Present simulations show that the maximum carbon growth rates take place several hours after noon time (between 18:00 and 20:00 hours GMT). Simulations reflect at this level too the slower carbon flow rate in comparison with the nutrient flow rate (*see* next section). Results show a phase show a phase shift of $\sim$2–4 hours.

The model shows that carbon flows reflect total daily integrated PAR irradiance closer than short period irradiance fluctuations. This agrees with expectation from ex-

perimental studies (Platt *et al.*, 1980; Gallegos & Platt, 1981); total daily PAR accounts for the input of energy which is finally invested in the fixation of carbon by the photosynthesis. Consequently, irregularities in the PAR irradiance series are carried on to the upcoming days. Thus, the effect of a cloudy day (3^{rd} of November) is not reflected at the same day on C_B, but during the next day (*see* Figure 8.7). The model shows that the carbon growth flux is reduced the day after a covered one because the carbon pool compartment C_P keeps a lower amount of transient carbon compounds; the recovery takes a longer time. On the other hand, the carbon pool compartment closely mimics PAR series (Figure 8.6).

Because of the non-linear dynamics of the biological processes, several low irradiance days may carry on a negative growth cumulatively for some days, depending on the total PAR energy received by the phytoplankton.

8.4.2 Nutrient Dynamics

Nutrient dynamics is much faster than carbon dynamics; nutrient uptake rates show the highest values around the sunrise time (Figure 8.8), but they are immediately turned down as soon as the internal nutrient pool compartment is filled or, equivalently, the nutrient quota reaches the maximum value.

Nutrient uptake is quickly reduced after reaching the maximum storage level because the utilization rate N_{GROWTH} does not encompass C_{GROWTH} by a factor near the Redfield ratio, and nutrient storage necessarily has to be limited, or nutrient excretion taken into account (Lomas & Glibert, 1999).

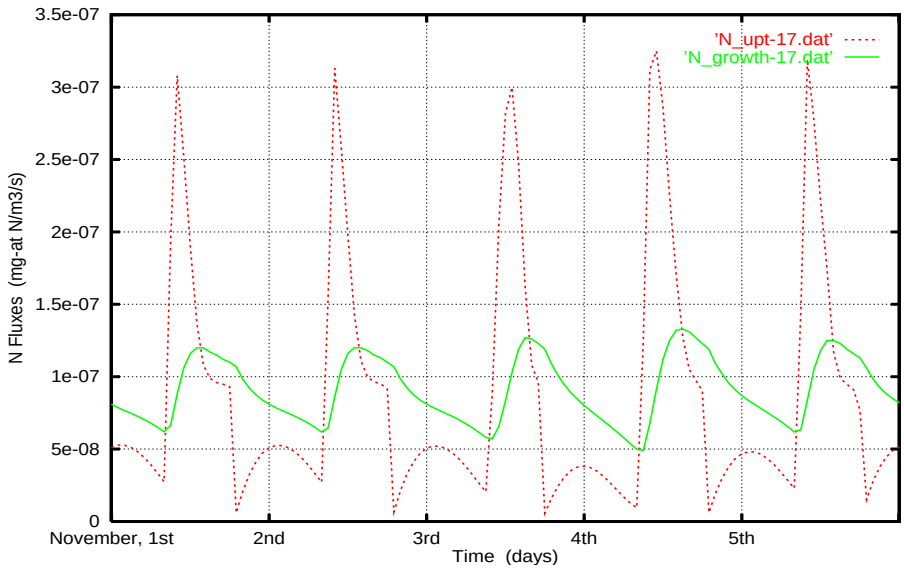

Fig. 8.8: Internal flows of nitrogen where 'N_upt-17' and 'N_growth-17' account for the uptake of nitrate, and the synthesis of biomass in terms of nitrogen, respectively.

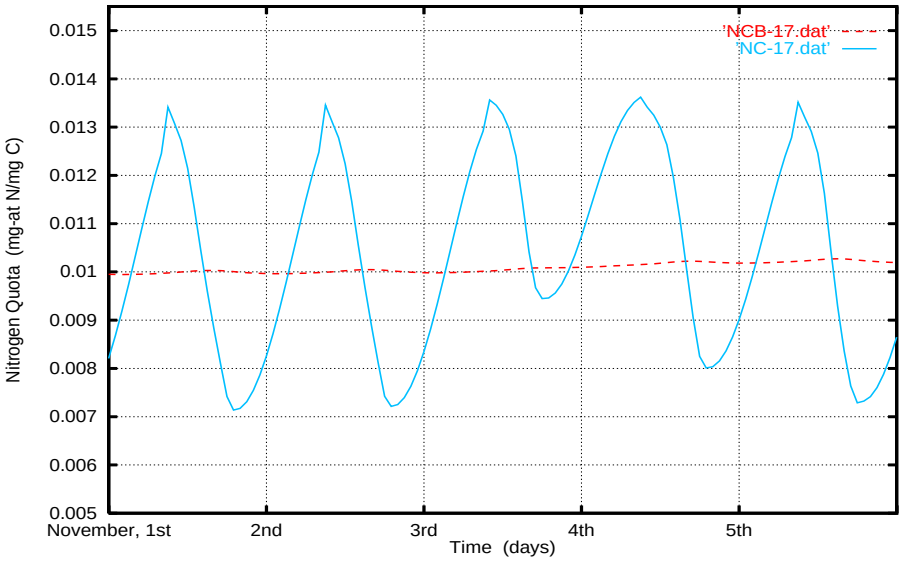

Fig. 8.9: Pool and biomass nitrogen quotas, 'NC-17' and 'NCB-17', respectively, for a five-days simulation.

The fast nutrient dynamics of the phytoplankton has strong ecological and physiological implications. Phytoplankton aggregates seem to be able to take advantage of the fast characteristic intermitency of the turbulent transport mechanisms, in such a way that phytoplankton can quickly and efficiently take up the small quantities of nutrients carried on by turbulent flows.

A close analysis of the nutrient flows shows that the synthesis of biomass in terms of nitrogen takes approximately 4 hours after it has been absorbed by the organism. The maximum fixation rate takes place at noon in clear days, whilst it is delayed in more than one hour during covered days.

8.4.3 The Nutritional Status of the Phytoplankton

Biomass nutrient quota may be regarded as an indicator of the *nutritional status* of the phytoplankton. The optimal reference value is determined by the Redfield ratio (=0.0126 mg-at N mg C^{-1}). Below this value we can presume that the phytoplankton suffers from nutrient limitation. It is also assumed that biomass nutrient quota can not vary within a large range without functional efficiency loss, or damage.

On the contrary, pool nutrient quota may show a very large variability, as far as it deals with nutrients accumulated in vacuoles and short carbohydrates, and both directly reflect the intrinsic environmental variability.

During this short five-days simulation biomass nutrient quota (Figure 8.10) shows values 20% lower than the Redfield reference value. This feature supports the hypothesis of nutrient limitation. As a matter of fact, nutrient limitation is expected near the surface before winter mixing, as a consequence of the low nitrate concentration values observed

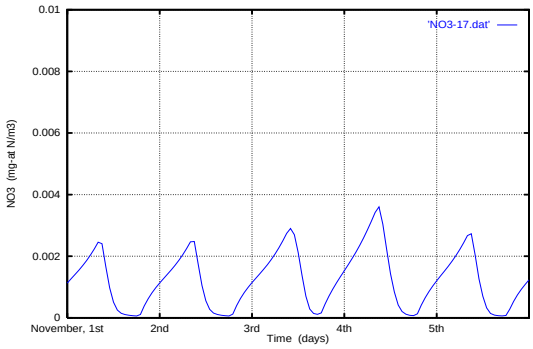

Fig. 8.10: Simulation of the nitrate concentration for the period November, 1^{st}–5^{th}.

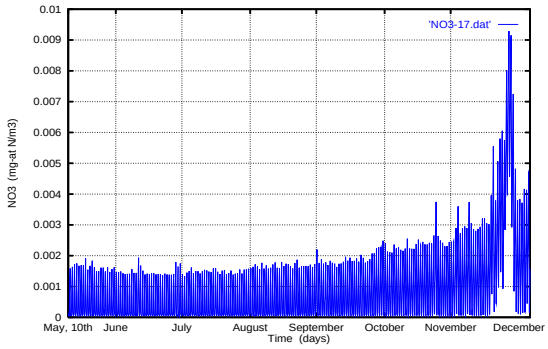

Fig. 8.11: Nitrate concentration evolution during the full simulation.

just below the surface. Indeed, simulations have been forced with a very low and constant nutrient inflow, estimated for station 86 ($\sim 7.8\times10^{-3}$ mg-at N $m^{-2}day^{-1}$). However, an extended simulation (Figure 8.13) shows a smooth full recovery of the biomass nutrient quota up to near Redfield values after a period of six cloudy days (reflected by a period of highly constant values of the pool nitrogen quotas), during the second half of November (Figure 8.14). This recovery trend is not due to an increase of the nutrient inflow, as we keep it constant. Nevertheless, we did not consider an expected effect of temperature on the overall dynamics; as we shall see in the next section, temperature plays also an important role on determining the nutritional status of the phytoplankton.

Longer simulations show additional information about phytoplankton nutrient dynamics; and variable weather conditions evidenced in the PAR irradiance series (Figures 8.12 and 8.13), allow us to point out several new features.

For the given conditions set up for these simulations, and leaving constant both temperature (17°C) and nutrient inflow, the internal nutrient dynamics, in terms of biomass nutrient quota, shows a smooth trend driven only by the total amount of PAR energy. Short-term PAR variability is hardly buffered, but the smoothed long-term variability is reflected by the organisms in the biomass nutrient quota and biomass concentration that change within a plausible range of variability.

The long term recovery of the biomass nutrient quota at the end of the simulation, is attained by the model without the effect of either temperature nor hydrodynamical mechanisms; this is an important remark. Indeed, real PAR series is the only forcing factor considered in our simulations up to now.

Nevertheless, we can observe in Figures 8.10 and 8.11 that nitrate concentration does not reaches the measured values, but resting in a very low level. As we stated in the previous paragraphs, we have not considered yet mixing at this stage yet, as far as nutrient inflow has been set to a constant value as representative of permanently nutrient limiting conditions.

8.4.4 Day & Night Balanced Matter Flows.

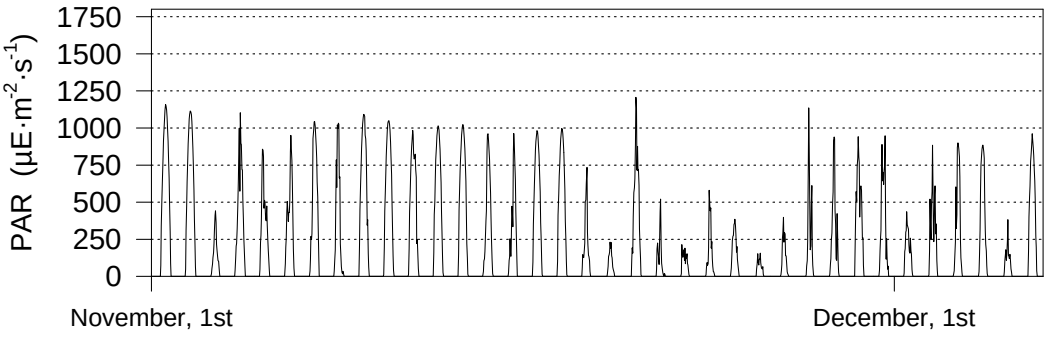

Fig. 8.12: Thirty-six days PAR hourly values series since November, 1^{st} till December, 6^{th} (1996), at Roses (Girona, Spain).

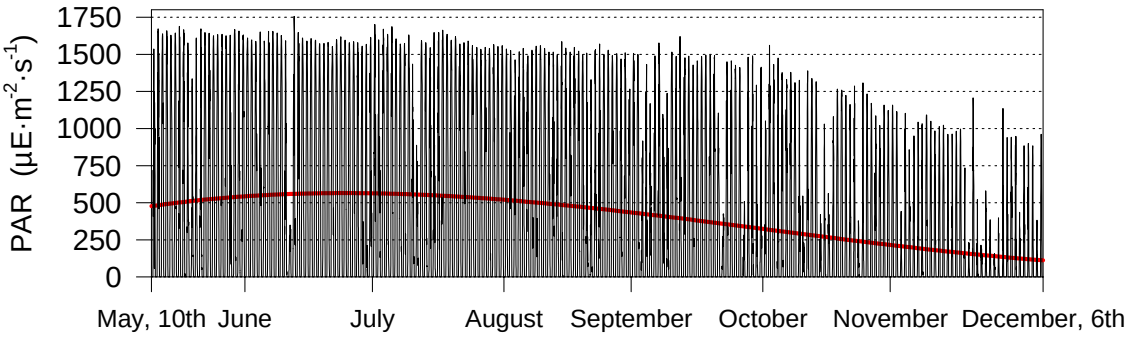

Fig. 8.13: Second half of 1996 of PAR series at the same site (hourly values). The thick red line shows a polynomial fitting.

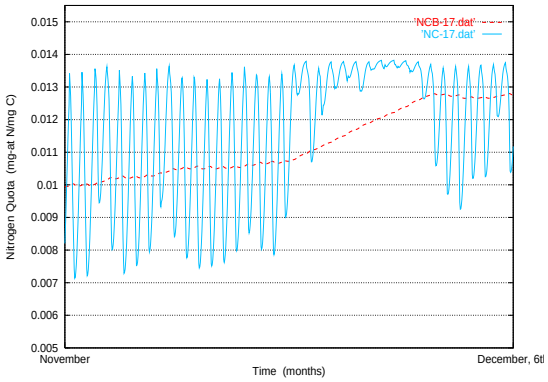

Fig. 8.14: Pool and biomass nitrogen quotas, 'NC-17' and 'NCB-17', respectively, for a thirty-six days simulation forced by PAR series plotted in Figure 8.12.

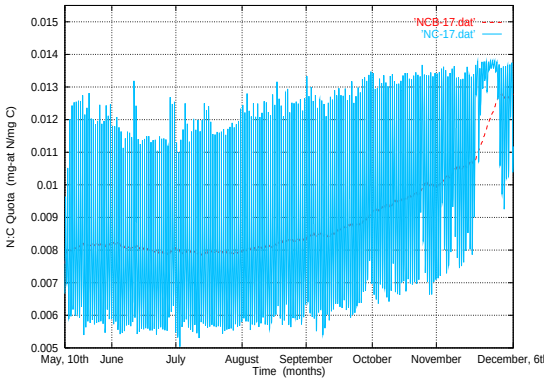

Fig. 8.15: Same nitrogen quotas for a long seasonal half-year simulation corresponding to Figure 8.13.

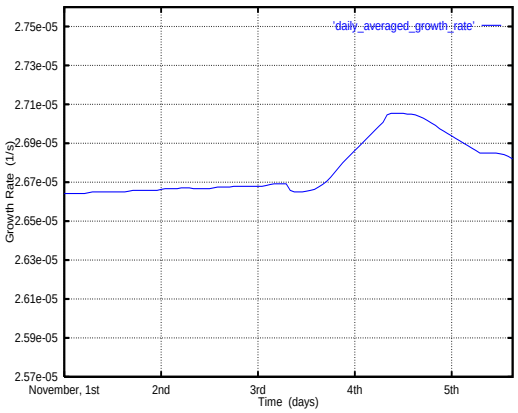

Fig. 8.16: Daily averaged growth rate $\overline{\mu}$ (s^{-1}), during the short five-days simulation. This plot is a close-up of Figure 8.17 (right).

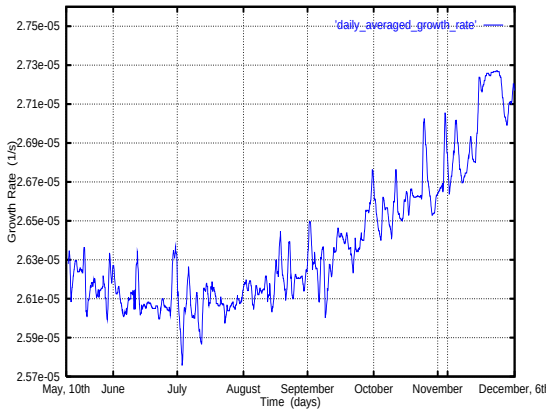

Fig. 8.17: Full series of the daily averaged growth rate.

An Overall Analysis of the Biological Model

The biological model solves the driving equations at very short time steps, thus a significant insight of the model can be gained after looking at the balanced flows of matter at a daily scale, and specially focusing to day and night periods.

The calculated photosynthetical rate normalized to biomass (in terms of chlorophyll *a*) P^B, multiplied by the measured chlorophyll *a* concentration, gives the carbon growth rate ($C_{FIXATION}$). For clear day, at noon, e.g., PAR = 1149 μE m^2 s^{-1}, $C_{FIXATION}$ yields 1.68 mg C m^{-3} day^{-1}, at 17°C. The model shows that during the light-hours 54% of the carbon fixation rate is converted to biomass (C_{GROWTH}), and the resting 46% accumulates in the carbon pool C_P. At night, the carbon pool empties partially, reaching the lowest value just before sunrise time, while its maximum is attained before the sunset. C_P decreases nearly 75% of the maximum daily value at night (Figure 9.23).

As it has been defined in Chapter 6, carbon growth is directly proportional to the specific growth rate μ, which is in addition proportional to the Droop's term (6.9). The value that the nutrient quota takes around noon allows a 95% of the maximum specific growth rate μ_{max}; the specific growth rate varies proportionally to the nutrient quota.

Consequently, in order to compute the number of duplications *per day* of the phytoplankton aggregate μ_D, we take the daily average of the growth rate $\overline{\mu}$, instead of the instantaneous value μ, therefore

$$\mu_D \equiv \frac{1}{86400 \cdot \overline{\mu}} \tag{8.1}$$

The significative increase of the averaged growth rate observed during the 4^{th} of November occurs after the accumulation of nitrogen in N_P, which returns in a higher nutrient quota value (Figure 8.16).

We point out once again that also in this case the growth rate series only reflects sun irradiance variability, and that the concurrent temperature and hydrodynamical conditions are not considered in *one-box* simulations (the effect of temperature over the phytoplankton dynamics is studied in the next section).

Under the conditions set up for these simulations specific growth rate closely follows nitrate concentration (*cf.* Figures 8.17 and 8.11), which is the most limiting resource under full irradiance. However, as the nutrient inflow is kept constant and limiting during the whole simulation, nitrate concentrations becomes function of irradiance: nitrate concentration increases as lower PAR enables lower photosynthetical rates.

A closer analysis of the simulated values of the daily averaged growth rate $\overline{\mu}$ shows a cumulative effect of different factors not directly related with the forcing series. Indeed, the averaged growth rate series does not mimic a daily pattern, as light driven factors do. The characteristic scale of $\overline{\mu}$ seems to be longer than one day, pointing out to a more complex dynamics.

The degree of dispersion of the daily averaged values can be related with buffer capacity of the nutrient and carbon pools: in other words, the variability of the averaged growth rates can be related with reservoir capacity of both pools, but specially with the capacity of the nutrient pool, as it may be inferred according to these results. Although the carbon and nutrient pools are allowed to freely vary in the model, this can not be the case of the living organisms, as far as they can not obviously show an unlimited cumulative capacity. Nevertheless, the results obtained show a buffer capacity of the pools of around 4–5% of the total biomass. Such values are small enough to fall into biologically plausible expectations.

On the other hand, the seasonal variation of the specific growth rates are very small: growth rates vary only a 6% during the whole period since May to December. This can be explained because the present simulations are run under fixed environmental conditions of temperature, but specially because of the fixed nutrient inflow, which is evidenced as the main limiting growth factor. This prevents phytoplankton to react to the intrinsic, but also large variability of the turbulent events which enter nutrients to the euphotic layer from the rich deeper layers. Therefore, simulation results show that the 6% of variability of the daily averaged specific growth rates $\overline{\mu}$ is explained only by the seasonal PAR forcing (Figure 8.18).

C_{GROWTH} is the most relevant flow in the biological model. It expresses the rate at which biomass is changing; as far as C_{GROWTH} accounts for the net rate of change, there is always a fraction in the carbon flow that is respired, as *activity* respiration. However, the major role in controlling this carbon flow belongs to the growth rate μ, and μ has been modeled as a function of the *Droop* term, and further on, as a function of the pool nutrient quota.

From an eco-physiological perspective, C_{GROWTH} has been modeled as a function of the nutritional status of the cells. The optimal reference value is close or a little above the Redfield ratio $(\frac{N}{C})_{Redfield} = 0.0126$ mg-at N mg C^{-1}, corresponding to C:N (106:16).

Figure 8.19 shows how sensitive C_{GROWTH} formulation's flow is against the limit set by the minimum nutrient quota. Let us take an hypothetical organism which is able to resist nutrient limiting conditions down to 100^{th} part of the Redfield ratio. In that case we

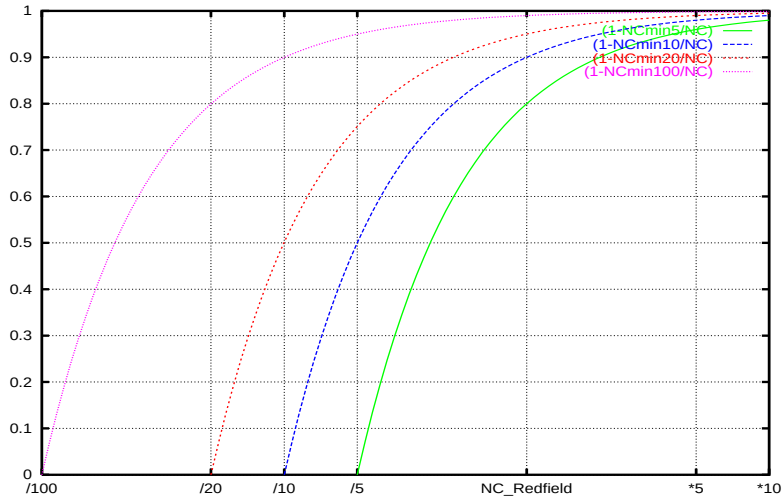

Fig. 8.18: The four plotted functions show the assimptotic behavior of the *Droop* term for four different values of the minimum nutrient quota (*see* equation 6.9), from the hundredth, twentieth, tenth and fifth of the Redfield ratio. Abcisa log-axis ticks are labeled proportionally to Redfield: '/100' indicates the 100^{th} part of $(\frac{N}{C})_{Redfield}$, '/20' the 20^{th} part, and so on. '$*5$' and '$*10$' indicate five and ten-fold of $(\frac{N}{C})_{Redfield}$, respectively.

observe that for a nutrient quota equal to Redfield's the organism attains the 99% of the maximum growth rate μ_{max} for the given temperature, but only 80% for an organism with a minimum nutrient quota set to a fifth part of the Redfield ratio. This point needs further research.

The main differences between day and night values (Figures 8.20 and 8.21) are principally derived from the carbon pathway. At night, photosynthesis is null, but the synthesis of biomass decreases only 20.8% after a sunny day.

The nitrogen pathway shows insignificant differences between day and night, but a reduction of the nutrient uptake (*see* Figure 8.19). We observe that nutrients does not significatively accumulate under nutrient limiting conditions, whether day or night (Figure 8.20), other than the short-term (diel) variability. Nutrients are quickly taken up after sunrise in order to fill the nitrogen pool up to its maximum capacity. However, the absorption efficiency (which is related with both, the efficiency for capturing and carrying the molecules of nutrient inside of the organism, and the number or concentration of carriers) is not limited in the model. In consequence, phytoplankton may reduce external nitrate concentration down to very low values.

The buffering capacity carried on by the pool compartments, however shows a fine but significant behavior, aside of the overall light-driven synchrony (Figure 8.21). Minimum values occur nearly at the sunrise in both carbon and nitrogen pools. But three main differences can be observed in the series: (1) the sharper carbon daily maxima against the smoother nitrogen ones, (2) the shifting, with a synchronic maximum during the cloudy

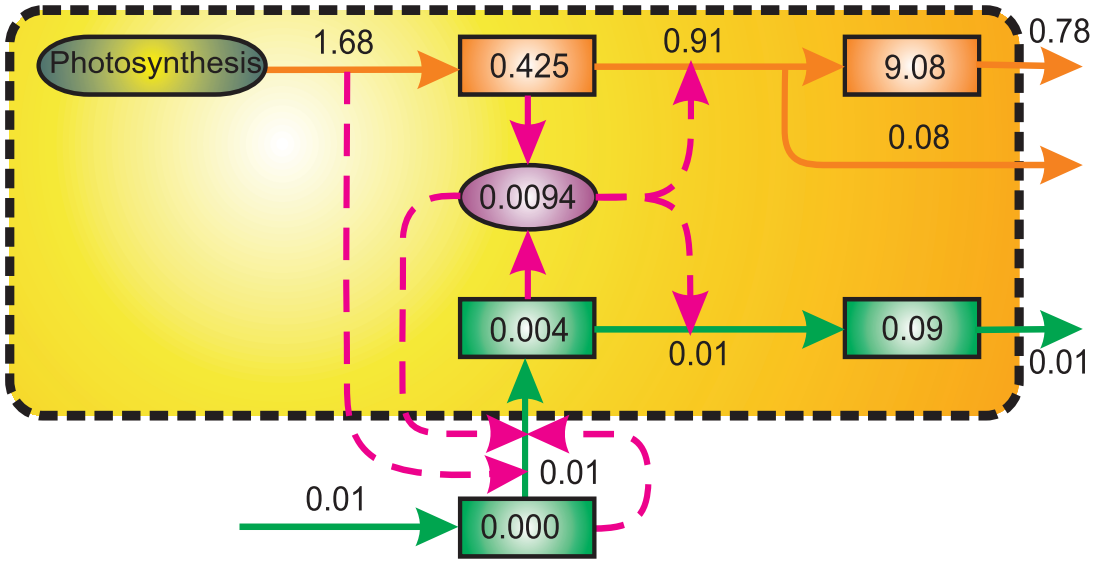

Fig. 8.19: Day-light balanced results of matter flows (continuous lines) and standing stocks (squared boxes) for the first of November, at noon (12:00 GMT). Carbon flows (red) are in mg $C\,m^{-3}\,day^{-1}$, and nitrogen flows (green) are in mg-at $N\,m^{-3}\,day^{-1}$. The carbon and nitrogen standing stocks are in mg $C\,m^{-3}$ and mg-at $N\,m^{-3}$ units, respectively. Temperature: 17°C.

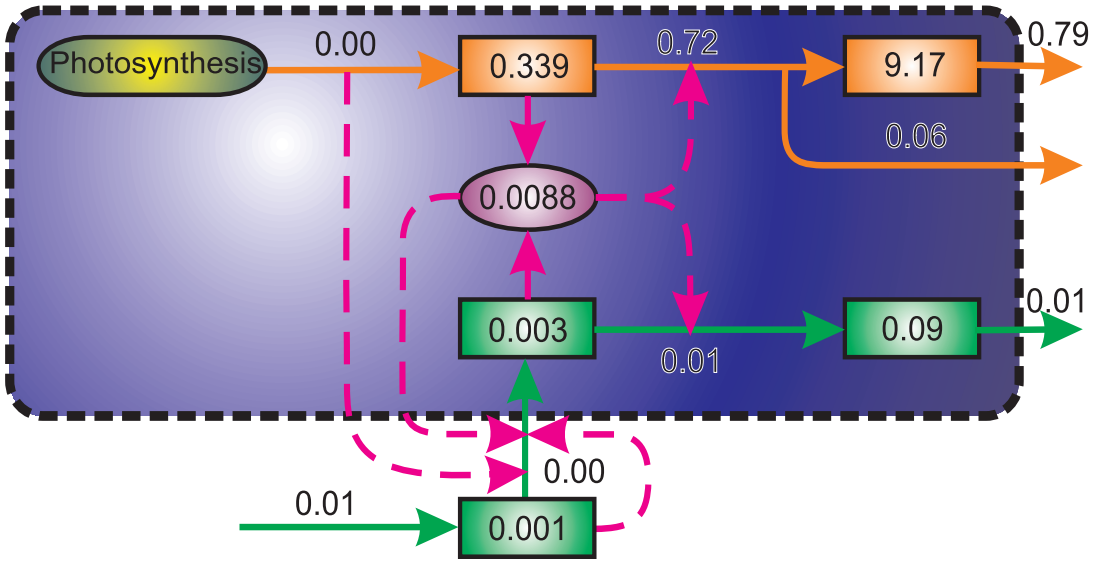

Fig. 8.20: Balanced results for the following mid-night period, at 23:00 GMT.

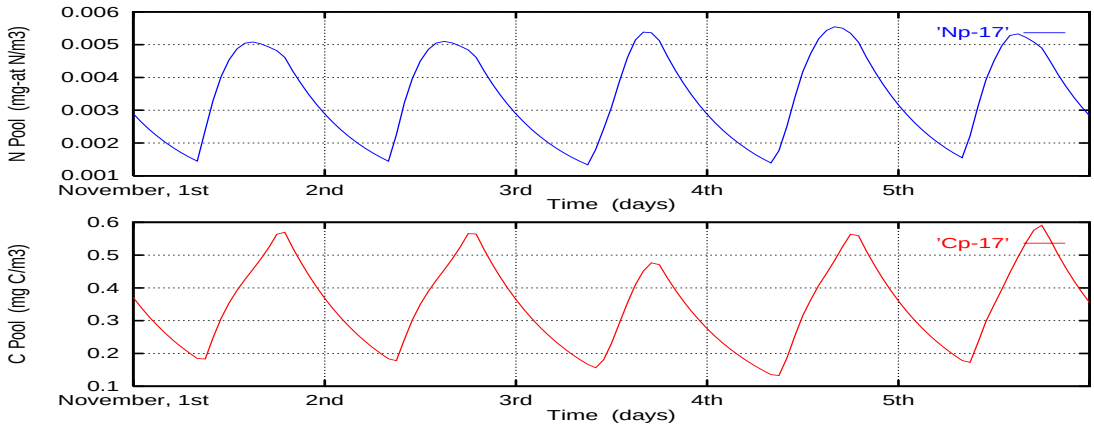

Fig. 8.21: Minor but significative differences may be evidenced in nitrogen (top) and carbon (bottom) pool dynamics regarding amplitude, shape and shifting.

November, 3^{rd} day, and, (3) the opposite trend during the cloudy day compared with the apparent direct light-driven relationship between both pools.

8.4.5 Temperature Regulation of Carbon and Nitrogen Flows

Carbon Flows

Temperature exerts a strong non-linear effects on the biological model. A clear effect is the exponential increase of metabolic processes like carbon fixation due to the Q_{10} term; in the case of carbon fixation it can be easily deduced upon the analysis of the equation resulting after the substitution of equation (5.4) into (5.2): Figure 9.17 shows an exponential vertical displacement that evidently closely fits Q_{10} increase rate.

But the most outstanding effect of temperature in the carbon pathway, which may be evidenced by the model, is the reduction of the photoinhibition with the raise of temperature on the carbon fixation flow (Figure 9.17). This effect seems to be in good agreement with the experimental results reported for short-term incubations by Gallegos & Platt (1981), Glibert *et al.* (1985) and Lomas & Glibert (1999).

In nature, photoinhibition under low temperatures has been hypothesized to be due to temperature limitation of the enzymes in the dark reactions of photosynthesis (Kirk, 1983). As far as the biochemical reactions have not been included in the model, the effect which is reflected in the results can only be introduced by its effect on P^B_{max}. Consequently, the rate how photoinhibition is effected by temperature depends on two parameters: the Q_{10} itself, assumed as constant for all the temperature related processes, and β.

Carbon growth shows a much regular influence of temperature (Figure 8.23): it mainly shows an expected exponential trend due to the Q_{10} term. It is also remarkable the small influence of temperature at the lowest carbon growth rates, this is, before the sunrise time, when the carbon pool gets the lowest values.

Contrary to photosynthesis (but in parallel with the carbon growth flow), the time-evolution of the phytoplankton carbon biomass C_B shows a higher sensibility against diel oscillation with the raise of temperature (Figure 8.24). This means that because of the

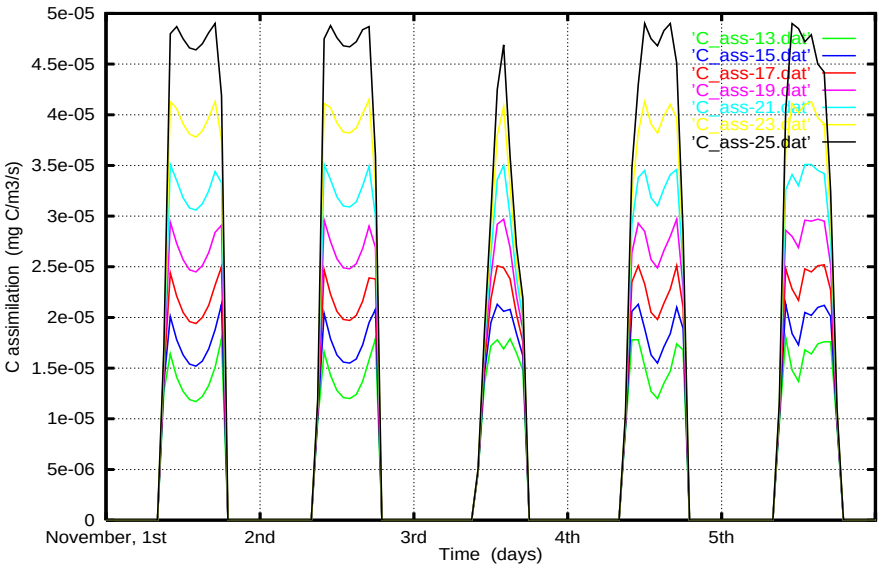

Fig. 8.22: Carbon fixation (photosynthesis) flow during the five-days simulation at different temperatures, ranging from 13 to 25°C.

non-linearity of the equations due to the Q_{10} term, the forcing introduced by the variation of irradiance (both, daily and seasonal variation) introduces a stronger effect at higher temperatures. On the other hand, the exponential effect of temperature still remains: biomass is exponentially higher as temperature increases, and proportional to the Q_{10} function.

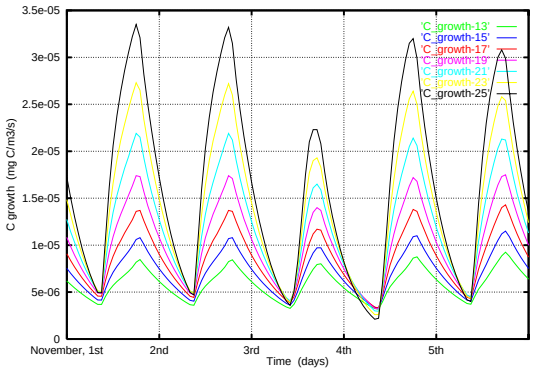

Fig. 8.23: Variation of carbon growth at temperatures within the range from 13 to 25°C, during the same period.

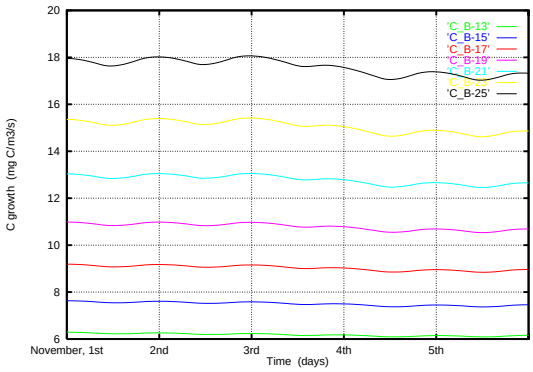

Fig. 8.24: Variation of the carbon biomass at the same range of temperatures.

Nutrient Flows

According to the model, phytoplankton nutrient uptake shows in parallel with carbon fixation, a strong non-linear effect of temperature. However, in the case of nutrient uptake, the changes due to the effect of temperature, evidenced within the range from 13 to 25°C, introduce a non-linear qualitative effect, as well. Photoinhibition is clearly limiting the uptake of nitrate at the lowest temperature (13°C) around noon; and it is still somehow evident at 15°C during the 4^{th} and 5^{th} days, but its effect completely disappears at temperatures greater than 15°C (Figure 9.20).

Under moderate PAR values ($\sim$500 μE m^2 s^{-1}), nutrient uptake is maximum at noon for temperatures near 13°C. As temperature increases maximum nutrient uptake rates quickly move towards the sunrise time (at temperatures greater than 19°C maximum uptake values are found nearly at the sunrise). For PAR values large enough to produce photoinhibition, maximum nutrient values are found at the sunrise time for temperatures as low as 15°C.

In any case, when maximum uptake rates are found during the early hours, the results also show a rapid decrease to a minimum value which is attained when the nutrient pool compartment is filled. Such minimum value is reached a few hours after the sunrise. Thus, we may conclude that the temperature globally increases the uptake rates of nutrient.

As far as the synthesis of biomass (which is also effected positively by temperature) takes place also during the night hours, nutrients are taken up at night, as well; in this case, however, the non-linear effect of temperature shows a negative exponential trend that saturates around 25°C.

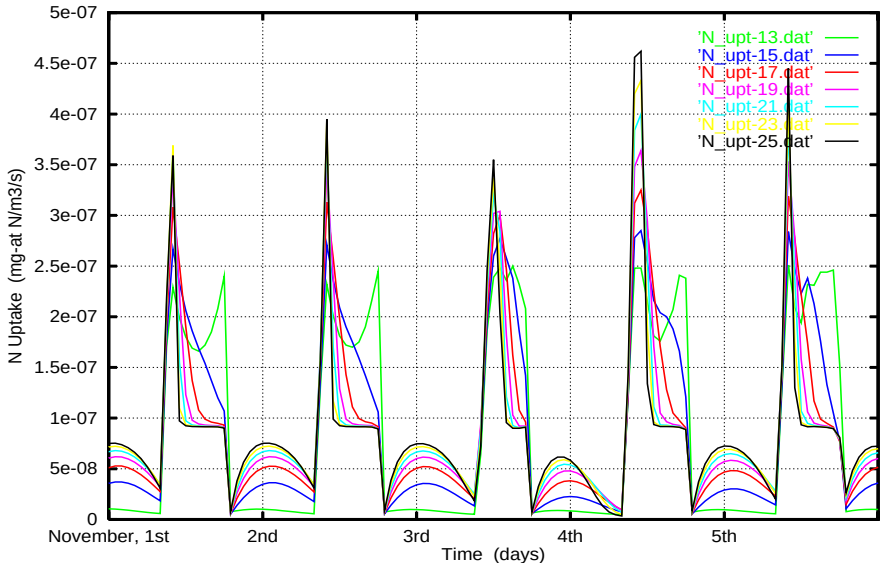

Fig. 8.25: Variation of the nutrient uptake flow rates within the same range.

8.4.6 Temperature and the Nutritional Status

Both pool and biomass nutrient quotas are very sensitive parameters in the biological model, developing a very rich dynamics (Figures 8.26 and 8.27). They both show a global decreasing trend with temperature, presenting maximum values near the sunrise and minimum values at the sunset. However, diel oscillation is more strongly smoothed at lower temperatures; at 13°C the variability is very much reduced. This may be interpreted as a reduced sensibility of the phytoplankton aggregate, in terms of its nutritional status, against external forcing (light) at lower temperatures. As far as photosynthesis is limited at lower temperatures, the nutrient demand becomes also reduced in that case.

In spite of the nutrient inflow has been kept constant during the whole simulation, we can also deduce a higher sensitivity of the phytoplankton nutritional status *vs.* intrinsic variability of the nutrient inputs at higher temperatures.

In agreement with the buffering role of the poll compartments, pool nutrient quota shows a much higher variability than biomass'. Pool nutrient quota also presents an assimptotic decreasing trend, negatively correlated ($r = -0.9918$) with the $f_{(Q_{10})}$ function[1], this is, with the metabolic effect of temperature (*see* Chapter 6).

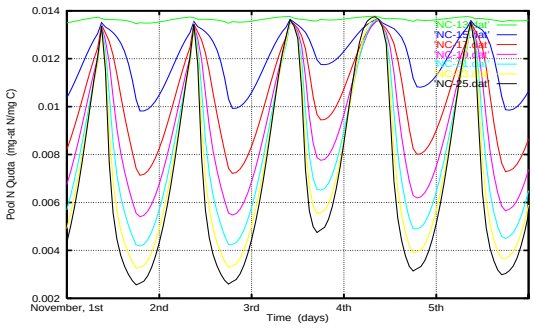

Fig. 8.26: Variation of the pool nutrient quota for the temperatures, ranging from 13 to 25°C, during the five-days period.

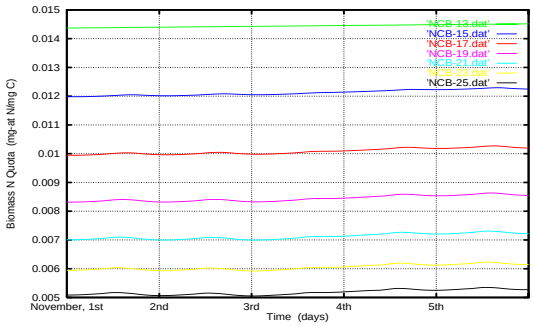

Fig. 8.27: Variation of the biomass nutrient quota during the same range of temperatures and simulation period.

[1] $f_{(Q_{10})} = Q_{10}^{\frac{T-10}{10}}$, where T is temperature, in Celsius degrees.

9. MASS TRANSPORT WITHIN *DIFFUSIVE BOUNDARY LAYERS* IN PHYTOPLANKTONIC ORGANISMS

The size range of phytoplanktonic species, from individual cells to colonial organisms, covers several orders of magnitude: from around a micron, or less, up to a few millimeters. Although most species size falls far below Kolmogorov length scale the largest organisms can be larger than Kolmogorov's. The effect of turbulence on the organisms, which depicts a different scenario depending on the size of the organisms, can be evidenced throughout the effect over the transport of mass within the DBLs.

All the exchanges of mass between a living organism and the bulk fluid occur within the surrounding DBL. At the same time, the thickness of the DBL also depends on the environmental flow characteristics; the intensity of turbulence and the sinking velocity may significatively modify δ_{eff} (*see* Ploug *et al.*, 1999b; for an experimental evidence), and organisms may also vary C_0 due to variable uptake rates. However, because diffusion transport of carbon and nutrients finally depends on different molecular diffusion coefficients, the resulting DBL thickness δ^{max} of each one of the chemical species must also vary and, thus, be differently affected by the hydrodynamics.

Mass transport computations of CO_2 described by equation (4.22), and the nutrients NO_3^- and PO_4^{3-} (4.6), allow us to evaluate a mean flux ratio C:N:P through the DBL. Though environmental variability and nutrient limitating conditions may introduce quite large deviations from the mean values, for a non-limiting situation the optimal mean flux ratio (considering respiration losses) should approach theoretically to Redfield composition 106:16:1.

9.1 Transport of Carbon

Carbon enters the photosynthetical reaction as CO_2. Nonetheless, a number of phytoplanktonic species are able to take up HCO_3^- and concentrate it intracellularly in the cytosol where it is converted to CO_2 by the carbonic anhydrase (CA) (Colman & Gehl, 1983; Dixon *et al.*, 1987), maintaining a steady state flux of CO_2 to ribulose 1,5-bisphosphate carboxylase/oxygenase (RubisCO) (Nimer *et al.*, 1997). Other species show an extracellular CA activity catalyzing the $HCO_3^- \rightarrow CO_2$ conversion at the plasma membrane (Burns & Beardall, 1987; Tsuzuki & Miyachi, 1989; Dionisio-Sese & Miyachi, 1992). In marine phytoplankton the extracellular CA activity may be regulated by environmental parameters; Merrett *et al.* (1993) evidenced such a control in cultures of *Emiliana huxleyi*

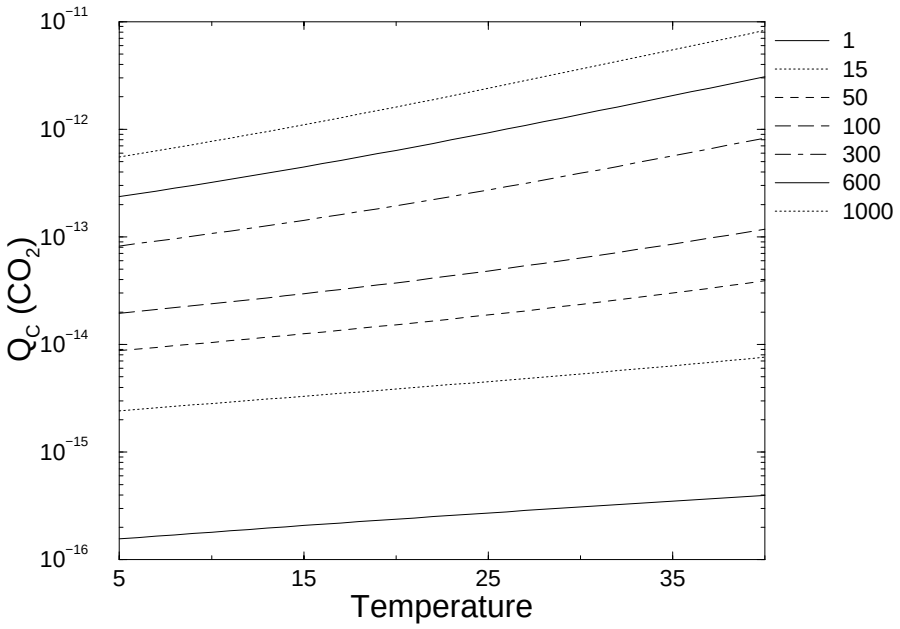

Fig. 9.1: Total transport rates of CO_2 (Q_C, in $\mathrm{Mol\,C\,s^{-1}}$) *vs.* temperature for different organism radii (in μm).

under total external DIC limiting conditions. In addition, organisms showing a functional extracellular CA activity can generate a pH drift resulting from the external production of OH^- by the catalytic release of CO_2 from HCO_3^- (Nimer *et al.*, 1996), which can also have an additional effect over the CO_2 transport through the DBL (*see* next).

An initial approach by Riebesell *et al.* (1993) in a stagnant fluid environment obtained a flux ratio C:N:P of about 28:38:1, which would indicate a severe carbon limitating flux, up to CO_2 concentrations of 10–15 μM. However, they considered CO_2 as the only possible carbon source, thus without taking into account HCO_3^- direct uptake, or surface $HCO_3^- \rightarrow CO_2$ conversion by means of CA activity. Experimental evidences (Raven *et al.*, 1993; Tortell *et al.*, 1997; Nimer *et al.*, 1997) have shown that CO_2 is often not the *only* inorganic carbon source for phytoplankton growth. Therefore, carbon limitation can not be stated upon this hypothesis unless it is proved that other carbon sources are not used. We think that is also necessary to outline the range of the physical environmental conditions which could yield to a carbon limitation, though regarding bicarbonate as a possible inorganic source, as well.

9.2 Transport of Nitrogen and Phosphorus

Considering CO_2 as the unique inorganic source of carbon for the photosynthesis the relative transport ratios shows a clear carbon limitation trend within a wide range of organism sizes (Figures 9.4 and 9.5). But it is interesting to note that the highest temperatures in-

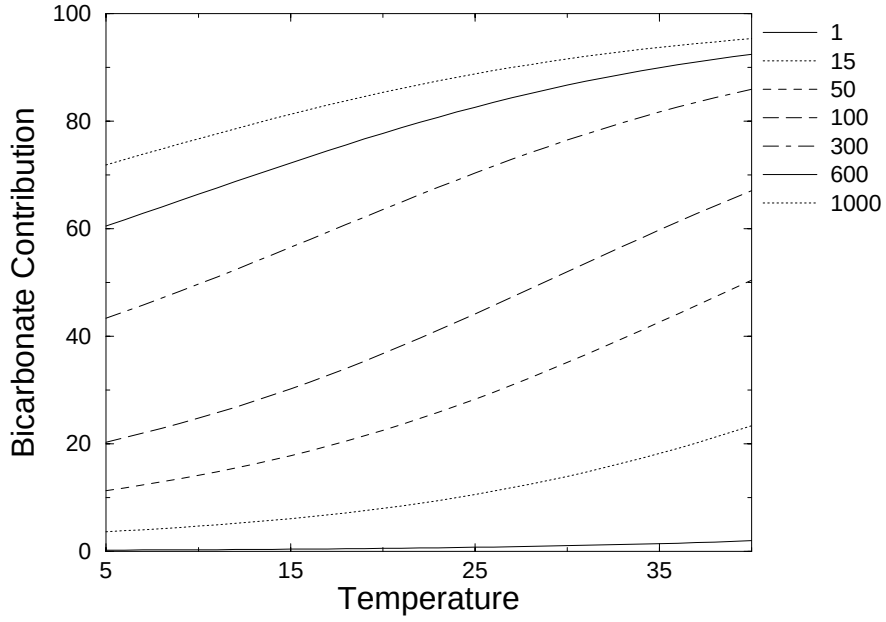

Fig. 9.2: Percentual HCO_3^- contribution by spontaneous $HCO_3^- \rightarrow CO_2$ conversion to the total CO_2 transport within the DBL against temperature for different sizes (same legend as for Figure 9.1).

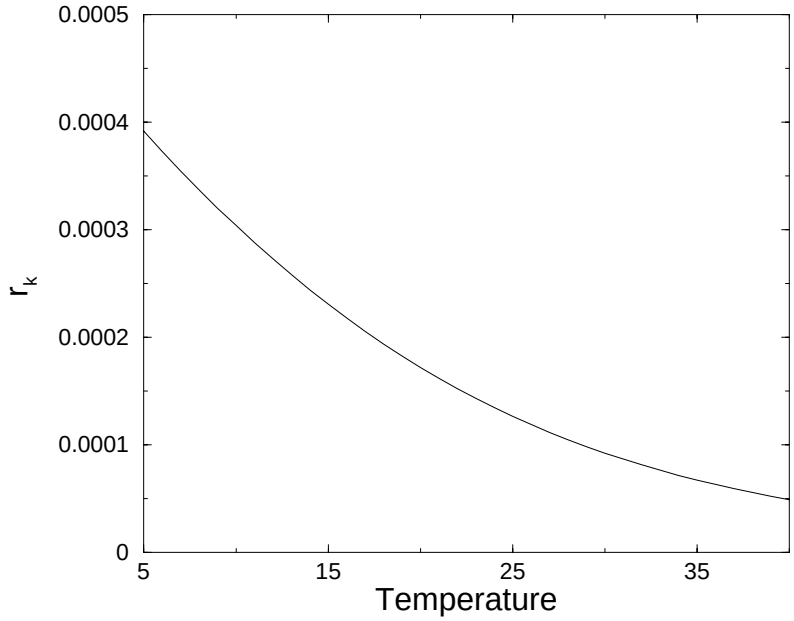

Fig. 9.3: Variation of the reacto-diffusive length r_k (meters) against temperature.

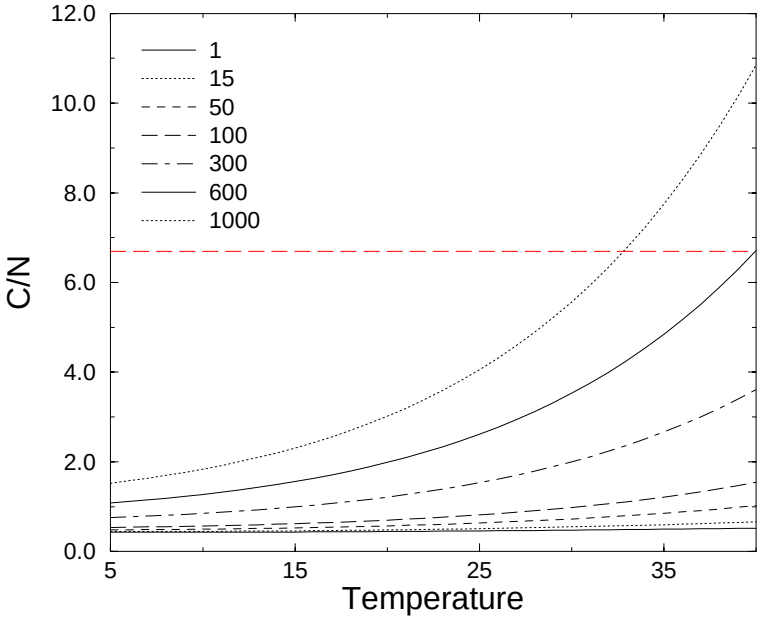

Fig. 9.4: Carbon to nitrogen flux ratios within the DBL for different organism sizes (legend values are in μm). The horizontal dashed line refers to Redfield C/N=106/16.

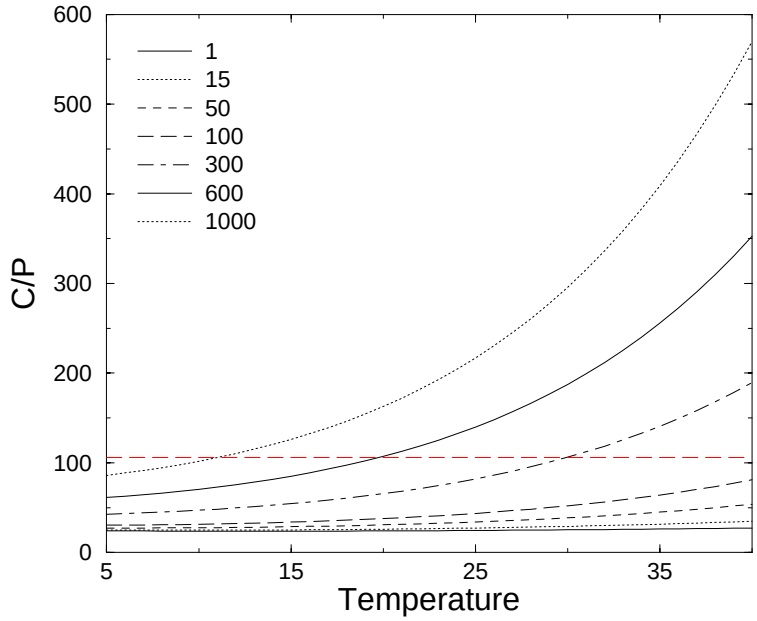

Fig. 9.5: Carbon to phosphorus flux ratios for different organism sizes. The horizontal dashed line refers to Redfield C/P=106/1.

troduce a lower constraint to the CO_2 transport, specially for the case of large organisms. However, the model predicts a clear carbon limitation status within the whole usual range of temperatures.

According to these formulations, temperature affects little the N/P ratio because it only enters the model throughout the influence on the molecular diffusion coefficients, and slope estimates differ just around 5–8%. In any case, the model predicts N/P flux values higher than Redfield composition ratio ($\sim$55) within a wide range of size and temperatures. This means that the N/P flux ratio is 3.3–3.6 time higher than Redfield ratio for the usual temperature range (5–30°C).

The main common degree of freedom of the model for the three elemental components C, N and P is the concentration gradient within the DBL. There is still quite a big uncertainty about carbon and nutrient concentrations at the organism surface. C_0 depends on the efficiency transfer rate, areal density of transmembrane transporters, the energetic status and nutrient requirements, so far CO_2 transport across membranes by lipid solution may only occur if it goes into favor of concentration.

Obviously, environmental variability and nutrient requirements do not necessarily match, at least for time periods longer than a few minutes. Anyway, in order to set up a necessary comparison basis we can initially regard phytoplanktonic organisms as perfect osmotrophs (Karp-Boss *et al.*, 1996).

The variability of the concentration ratio C_0/C_∞ within a reasonable range does not introduce big changes on the flux estimates, but it has a fundamental effect over the C/N and C/P ratios. Consequently, C_0=0, for CO_2 , nitrate and phosphate surface concentrations, seems to be a safe initial approach. Further information on efficiency and kinetics of transmembrane transport will enable a significative advance towards more realistic approaches.

Regarding the carbon transport through the DBL the model has an additional degree of freedom which is the relative contribution to the overall CO_2 transport rate by spontaneous extracellular conversion. It enters the model by means of the reacto-diffusive length r_k.

9.3 Overall Mass Transport within Phytoplanktonic DBLs

The relative contribution of HCO_3^- to the total CO_2 available at the surface of the organism also changes non-linearly with size (Figure 9.2). For a small phytoplankter (r_0=1μm) bicarbonate contribution just varies from 0.25–1.3% within the common ocean's temperature range of 5–35°C (Salinity=35 p.s.u.). For organisms or colonies larger than $\sim$400 μm (at 5°C), and $\sim$200 μm (at 17°C), bicarbonate contribution dominates ($\geq$50%) total diffusive CO_2 transport. The relatively low influence of temperature over the bicarbonate contribution in large organisms is due to the lower impact of the reacto-diffusive length r_k, which is not a scale dependent phenomenon (Figure 9.3). This means that temperature exerts a major influence over the small organisms than over the large ones. Thus, large phytoplankters are less sensitive to the temperature changes regarding the total CO_2 transport than small ones.

The model successfully points out to the sensitive C/N ratio, that shows quite a large variability for temperature and, specially the size of the organism.

Size	T_C=5°C	T_C=25°C	T_C=30°C
Small (15 μm)	0.45	0.57	0.64
Large (600 μm)	1.43	5.02	7.20

Tab. 9.1: Predicted values of C/N flux (molar) ratios per organism, at three different temperatures. Sizes are in μm. The model predicts large organisms (r_0=600 μm) C/N flux ratios equal Redfield (=6.63) at T_C=29°C.

Small organisms (size=15 μm) show a permanent C/N limitation status within a wide range of temperatures. However, table 9.1 depicts two completely different scenarios with strong ecological implications for large phytoplankton species of about 600 μm. In this case, low temperatures play a physical environmental limitation role over CO_2 transport regarding nitrate flux, with C/N values far below Redfield. But temperatures nearly 29°Cwould allow large organisms, under optimal light and nutrient conditions, to potentially fulfill growth carbon demands (pH=8.2).

On the other hand, at pH=8.2 HCO_3^- concentrations are 140–245 times CO_2 concentration (5–30°C). Consequently, the larger concentration of bicarbonate could possibly lead smaller phytoplanktonic species to preferently exploit the abundant bicarbonate pool by exclusion by the large species that would be ecologically favored for the CO_2 uptake.

In any case, the apparent C/N limitation of small phytoplankton would strongly limitate growth. Empirical evidences (Tortell *et al.*, 1997) and numerous laboratory studies (*see* Kerby & Raven, 1985; Raven *et al.*, 1993; Nimer *et al.*, 1997) question the doubtful hypothesis of carbon limitation in the open ocean, unless (e.g.) zinc availability impairs CO_2 uptake and fixation by phytoplankton (Morel *et al.*, 1994). Theoretically, we may infer that bicarbonate is probably the best alternative for the small phytoplankton under the conditions determined by high pH values.

Aside of whether CA is found at the external side of the plasmatic membrane (Rotatore *et al.*, 1995), or HCO_3^- is first actively transported into the cell (Dixon & Merret, 1988; Coleman & Rotatore, 1995).

The model shows that the diffusive transport of CO_2 +HCO_3^-would yield a C/N ratio far above Redfield, which under optimal growth conditions would definitely fulfill carbon requirements of small phytoplankton from the minimum pH=7.4 and temperatures as cold as 5°C (Figure 9.6).

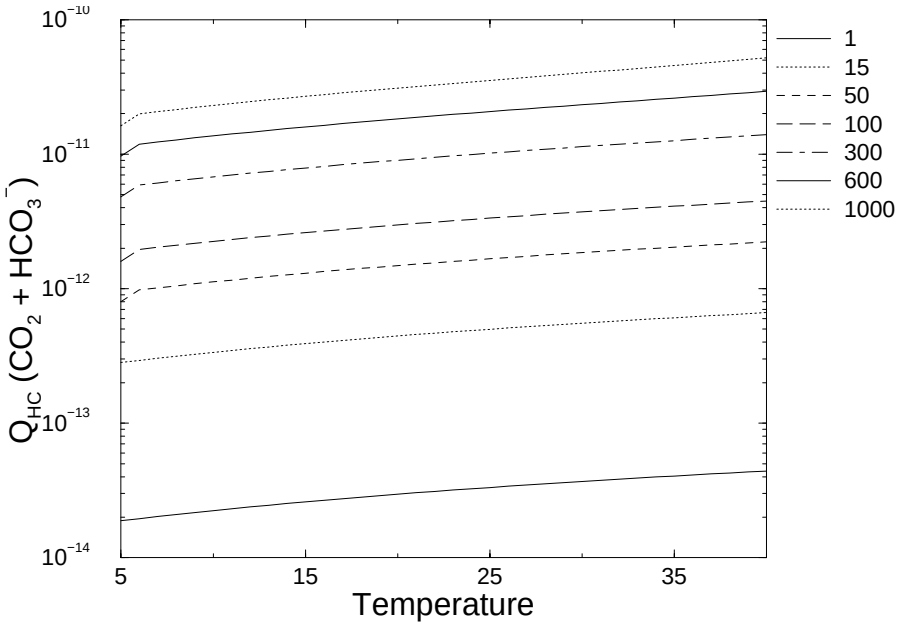

Fig. 9.6: Total CO_2 + HCO_3^- transport rates (Q_C, in $\mathrm{Mol\,C\,s^{-1}}$) *vs.* temperature for different organism radii (in μm).

10. DYNAMICS OF THE COUPLED PHYSICAL-BIOLOGICAL SYSTEM IN THE WATER COLUMN

This chapter deals with the overall effect of small-scale turbulence and phytoplankton activity, in terms of turbulent transport of nitrate and carbon fixation, respectively, within the ocean euphotic layer.

The main objective presented in this chapter was studying the effect of nitrate upwelling over the vertical fluxes of carbon and nitrogen in the open ocean. A very close coupling between the vertical transport of nitrogen from deeper layers and phytoplankton carbon fixation can be theoretically expected in steady-state conditions. Nevertheless, small variance of nitrate transport rates near the nitracline may not show a clear effect over the carbon fixation rates: non-linear dynamics of the primary production process requires a careful analysis and modeling approach. In addition nitrogen upwelling is taken as the main nitrogen resource for new production, though atmospheric deposition may be relevant in coastal areas.

In order to minimize coastal influences like horizontal nutrient inputs or bottom effect, only the farest and deepest stations of FRONTS'92 campaign have been selected, located around 38–48 nautical miles offshore between Barcelona and northern Mallorca coast, at the NW Mediterranean Sea (Fig. 10.1). FRONTS'92 campaign was chosen for data availability, but also because stratified and non-stratified hydrodynamical conditions were both present in the same cruise.

Aware of the methodological complexity for calibrating the extremely fast biological processes like nutrient uptake, explicitly regarded in the model, we used the *on-board* measurements of the photosynthetical parameters α^B and P^B for calibrating the phytoplankton carbon fixation process which rules the internal carbon pathway, thus letting the internal nitrogen pool to freely vary according to external nutrient availability and nitrogen requirements (Redfield) for the synthesis of biomass.

The regions where phytoplankton dynamics does reflect smaller or greater influence of small-scale turbulence over the vertical transport of nitrate will be also critically discussed at the end of this Chapter.

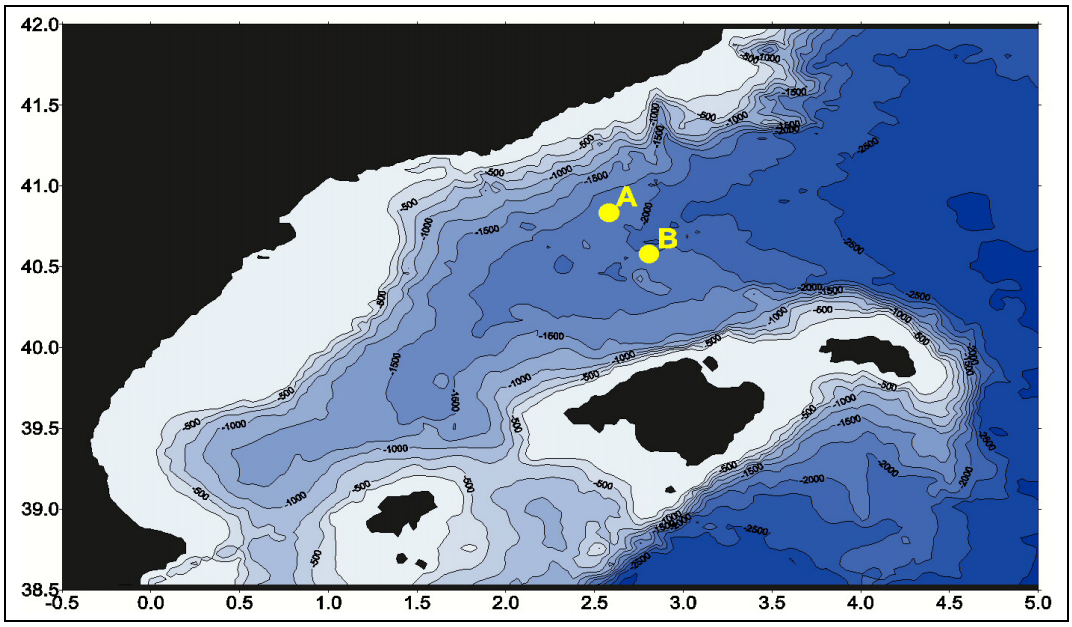

Fig. 10.1: View of the Northwestern Mediterranean Sea area, and FRONTS'92 study sites A (stations 14, 61 and 76) and B (stations 45, 65 and 86).

10.1 Environmental Setup

As reflected in Chapter 8 temperature plays a relevant role in the biological processes by controlling fundamental metabolical rates; the temperature dependency on parameters like the maximum photosynthetical rate P^B, and the maximum growth rate μ_{max}, as well as in transport parameters (maximum nutrient uptake rate, U_{max}), is explicitly considered in the whole simulated profiles.

Temperature profiles in FRONTS'92 cruise were taken between the fifteenth and thirtieth of October 1992, being stations 14 and 86, the most and less stratified stations, respectively, and other stations ranging in between. Stations 14 and 86 also show the largest differences in temperature at the surface ($\sim$3°C). The mixed layer can be observed in all cases below 25 meters, although station 86 only shows a weak stratification. Below 80 meters depth, temperature approximates to 13.3°C in all stations (Figs. A.7–A.12; all FRONTS'92 vertical profiles are reported in Appendix A).

Six stations were initially selected according to the availability of measurements of the photosynthetical parameters: 14, 45, 61, 65, 76 and 86. Later on, station 65 was rejected because measuring errors were suspected.

Nitrate profiles show a depleted upper layer down to 50 meters (Figs. A.19–A.24). The depth of the nutricline at the most stratified site 14, is nearly 10 meters above than at station 86, although the maximum chlorophyll concentration at station 14 appears 10 meters below than station 86.

10.1.1 The Biological State Variables

The state variables defined is the biological model (C_B, N_B, C_P and N_P; *see* page 66) are initialized with balanced values obtained after running the biological model alone. The values were selected from the simulation described in Chapter 8. Initial values at each one of the study sites were computed according to the next protocol:

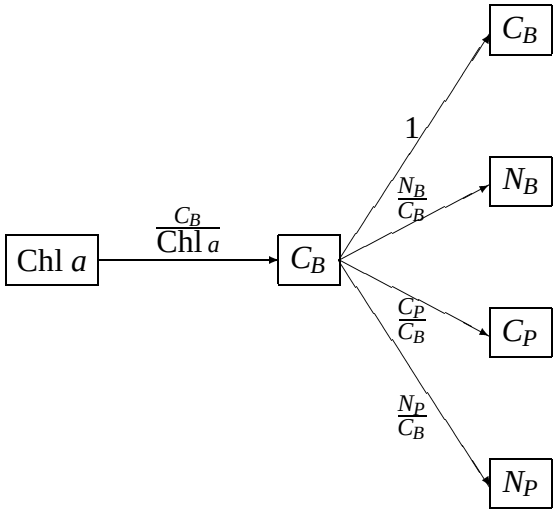

Chlorophyll *a* concentration was converted to phytoplankton carbon biomass C_B according to the fixed ratio $\frac{C_B}{\text{Chl } a} = 25$. Afterwards, C_P, N_B and N_P profiles were estimated according to balanced fixed ratios obtained in *one-box* simulation at the reference temperature (17°C): $\frac{N_B}{C_B} = 0.009949$, $\frac{C_P}{C_B} = 0.040482$ and $\frac{N_P}{C_B} = 0.000333$.

10.1.2 Parameter Field

The parameter values used in the 1-D simulations were the same as for the *one-box* simulation and they are all summarized in Appendix B.

10.2 Forcing

The coupled physical-biological 1-D model is forced with onboard hourly time series of irradiance that only applies to the photosynthetical process, as far as just the photosynthetical available spectrum of sun irradiance (400–700 nm) is taken into account.

Second, during the whole simulation time the 1-D model is forced with a constant profile of vertical turbulent diffusion coefficients. However, because long series of CTD profiles were not available in the NW Mediterranean for a specific location, simulations were restricted to one day, assuming that hydrodynamical conditions at the most sensitive

intermediate layers within the euphotic zone do not significatively change during this short period of time.

10.2.1 Light Field

Sun irradiance was measured in $\mathrm{W\,m^{-2}}$, and then converted to $\mu\mathrm{E\,m^{-2}\,s^{-1}}$ by using the factor 4.599696 ($\approx 4.6\ \mu\mathrm{E\,m^{-2}\,s^{-1}}/[\mathrm{W\,m^{-2}}]$; Morel & Smith, 1974). Finally, the PAR fraction is taken as 0.46% of the total sun irradiance (Baker & Frouin, 1987).

The light field (PAR transmitancy) was measured at each station with a radiometer. The vertical attenuation coefficients profiles have been computed according to equation (5.12), taking the chlorophyll absorption coefficient $k_c = 0.015\ \mathrm{m^2\ mg\ Chl}\ a^{-1}$ as an averaged *apparent* mean value of oligotrophic ocean waters (*see* Appendix C, for a comprehensive list of published values of the chlorophyll absorption coefficients of both *apparent* and *inherent* absorption coefficients [page 59]; *see* also Mobley, 1994).

Vertical chlorophyll concentration profile changes during the simulation time. Consequently, it is necessary to split the overall attenuation coefficient in order to determine the fraction of light which is absorbed by the phytoplankton, but leaving constant the attenuation due to non-phytoplanktonic conditions does not significatively change during the (short) simulation time.

Therefore, we have specifically discriminated between the irradiance absorbed by the phytoplankton, defined as K_{PH}, and the fraction absorbed by other dissolved substances or particulated matter, namely, *non-phytoplanktonic* with its attenuation coefficient defined as k_{np}. Finally, the vertical k_{np} average was taken for the whole column

Calibration of the Carbon Assimilation Process

The bio-optical models presented in Chapter 5 are powerful tools for the estimation of phytoplankton primary production in marine as well as in freshwater environments. The later, has been over the time logistically more available than open seas. Therefore, long and dense time series of the most relevant biological parameters from Middle-Europe lakes are often available.

Taking advantage of the long datasets available for Lake Constance (Germany) we can show for a sampling period not longer than a week (in winter), the prediction power of the bio-optical models for modeling both vertically resolved and integrated phytoplankton primary production by comparing simulation and measurements for a complete 1987 cycle (Fig. 10.2).

The model closely follows the blooming events and production rates during the all the seasons. Indeed, the largest disagreements between simulated and measured results occur in winter, when temperature strongly limits phytoplankton growth.

10.2.2 Vertical Turbulent Diffusion Transport

In order to estimate the vertical turbulent diffusion coefficients at each depth according to Osborn's parameterization (equations 3.25 and 3.36), as previously described in Chap-

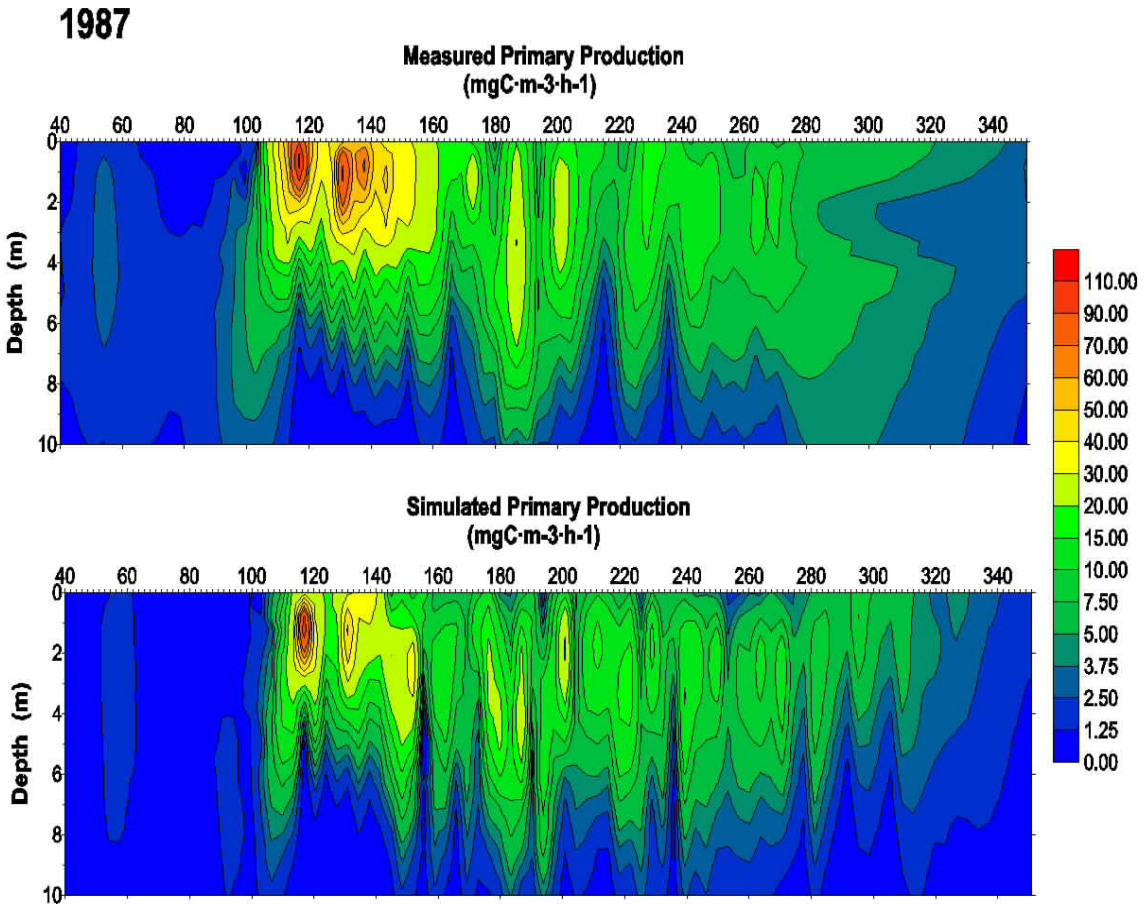

Fig. 10.2: Simulated *vs.* measured phytoplankton primary production in Lake Constance during 1987.

ter 3.

Density was calculated according to the seawater state's equation by Millero & Poisson (1981) (Figs. 10.2.2–10.2.2 show all the density profiles taken at each site during the sampling day; *see* page 138 for additional information). Density gradient profiles were necessary to be calculated as well (Figs. 10.4–10.8), and they give us a direct information about the stratification of the water column.

Kinetic energy dissipation profiles were computed with onboard U_{10} measurements (values were about 3.1–3.7 $\mathrm{m\,s^{-1}}$). Finally, the resulting profiles were smoothed by using a Savitzky-Golay filter (n_L, n_R=4, M=4; *see* Press *et al.*, 1992).

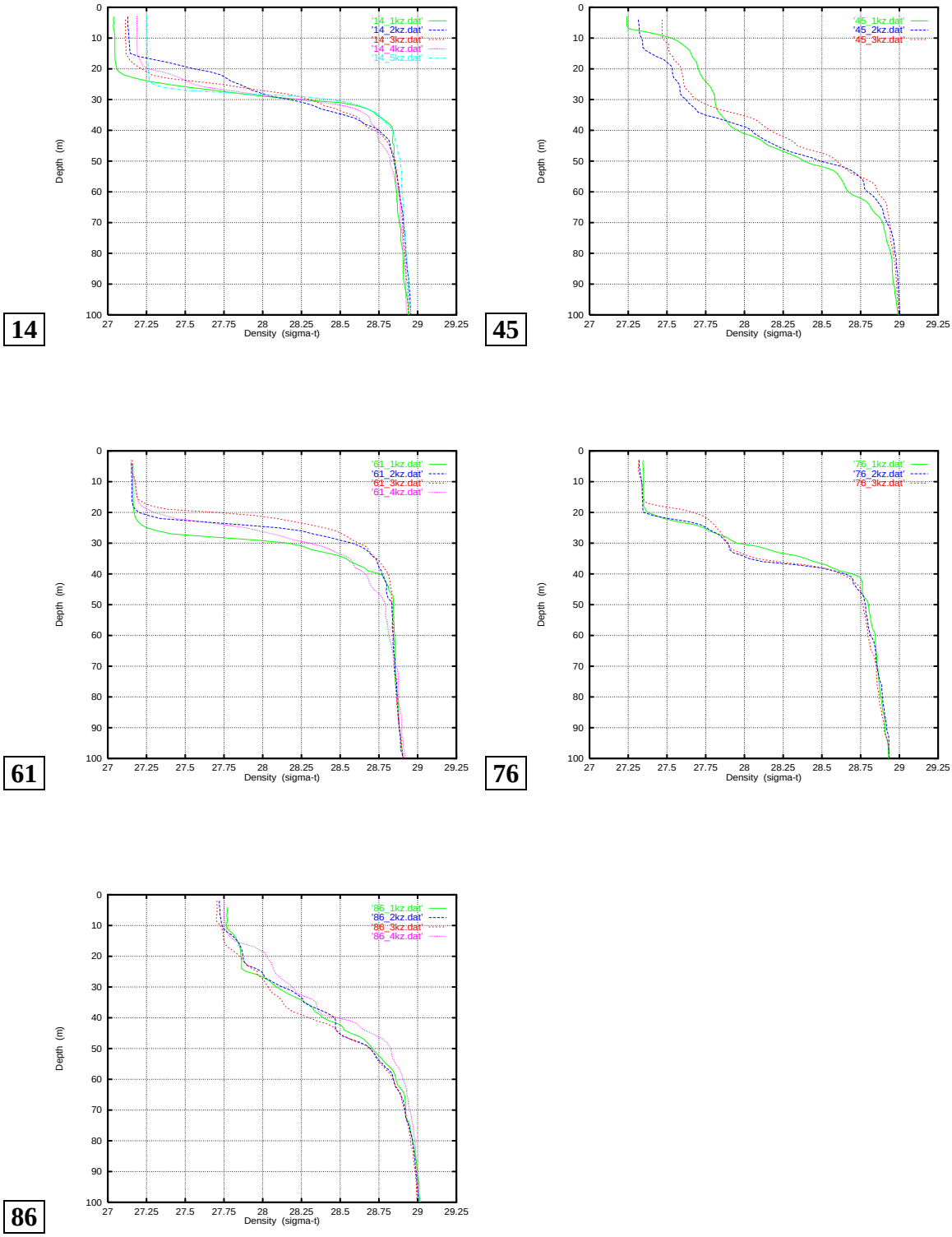

Fig. 10.3: Density profiles at the FRONTS'92 biological stations.

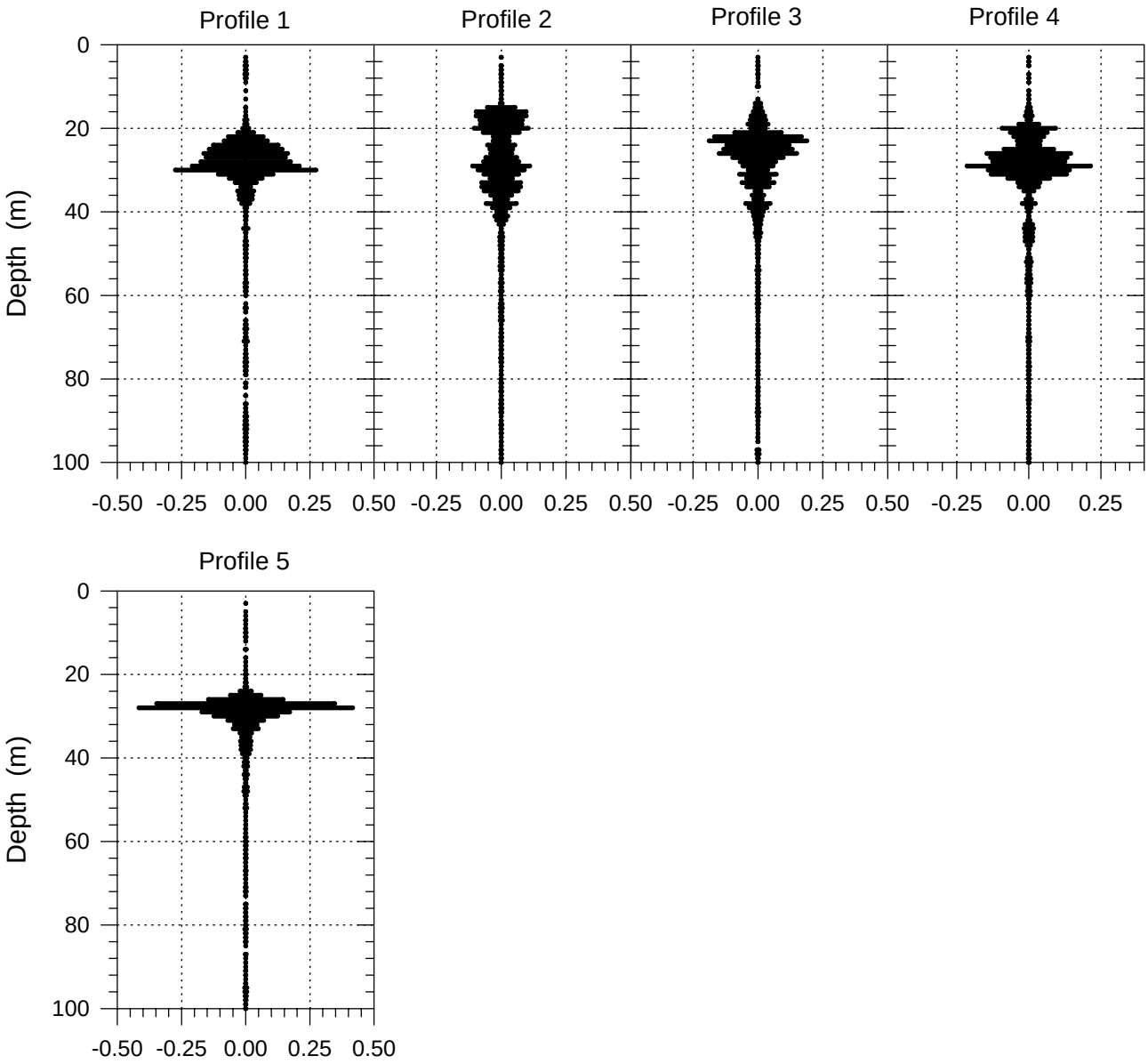

Fig. 10.4: r.m.s. density gradient profiles at station 14.

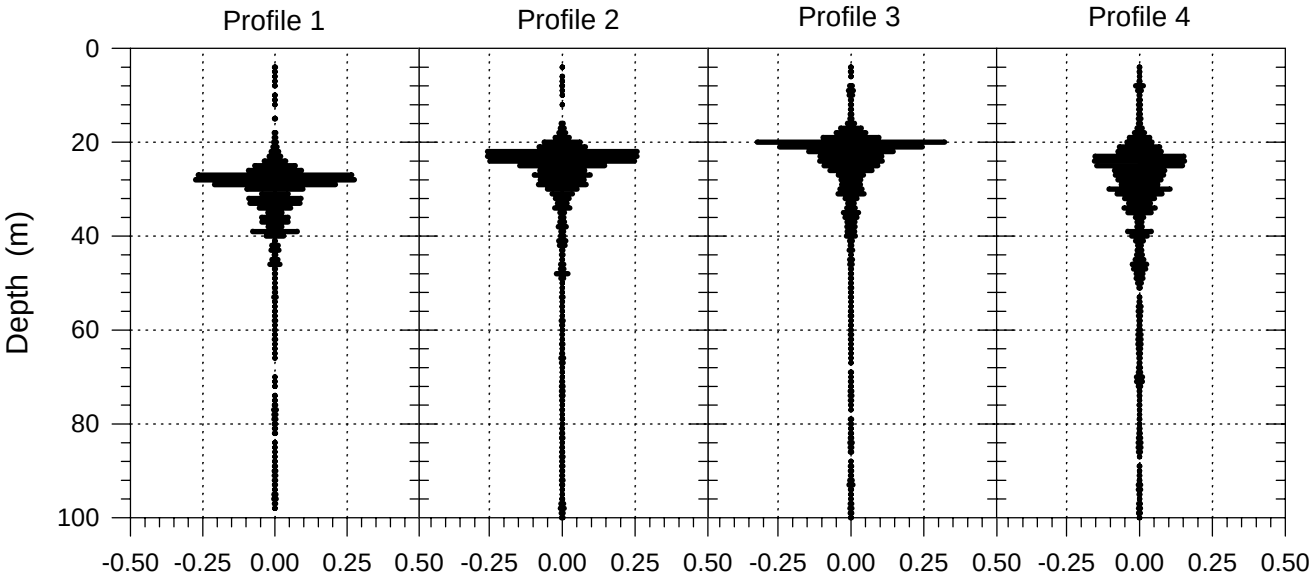

Fig. 10.5: r.m.s. density gradient profiles at station 61.

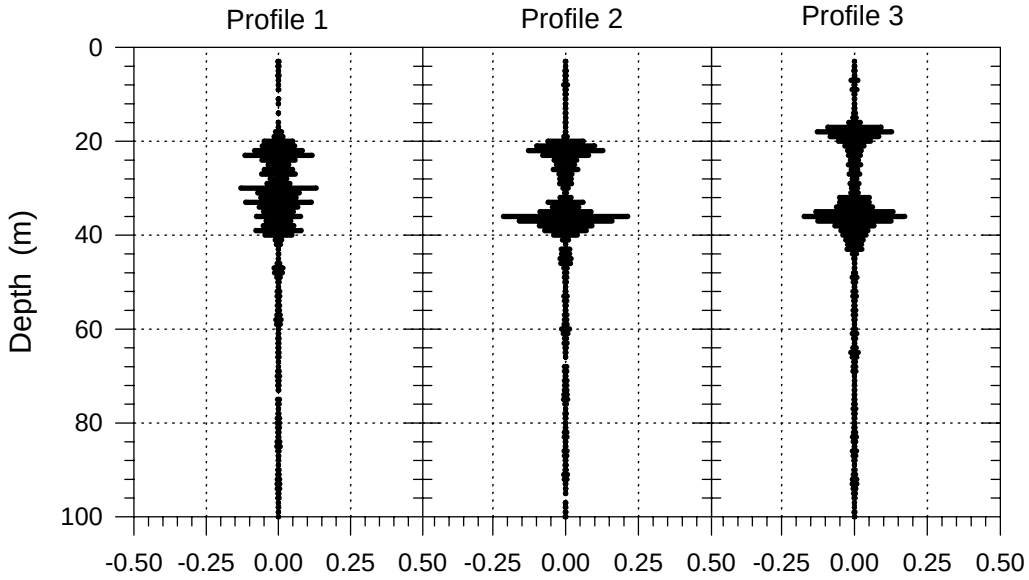

Fig. 10.6: r.m.s. density gradient profiles at station 76.

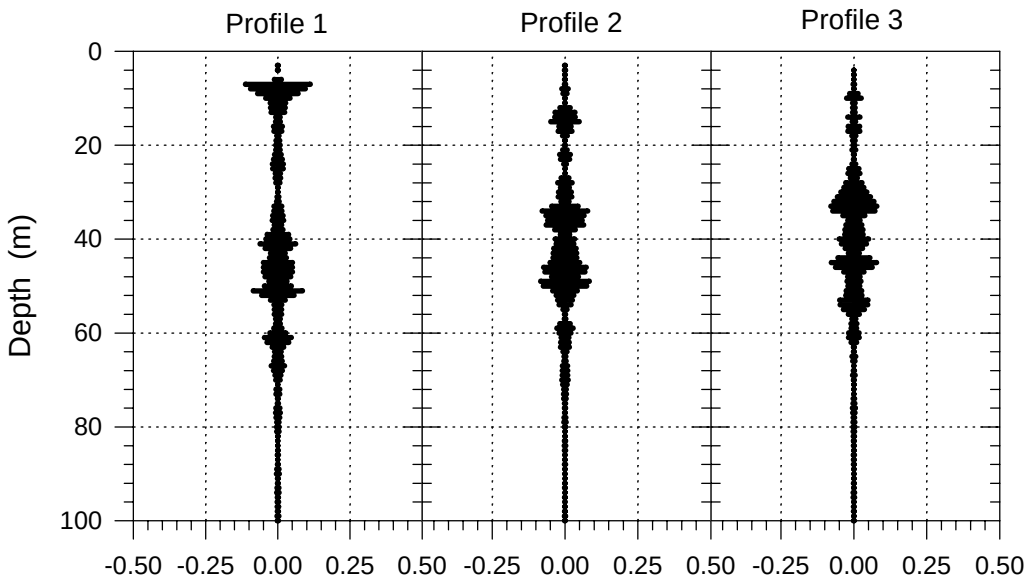

Fig. 10.7: r.m.s. density gradient profiles at station 45.

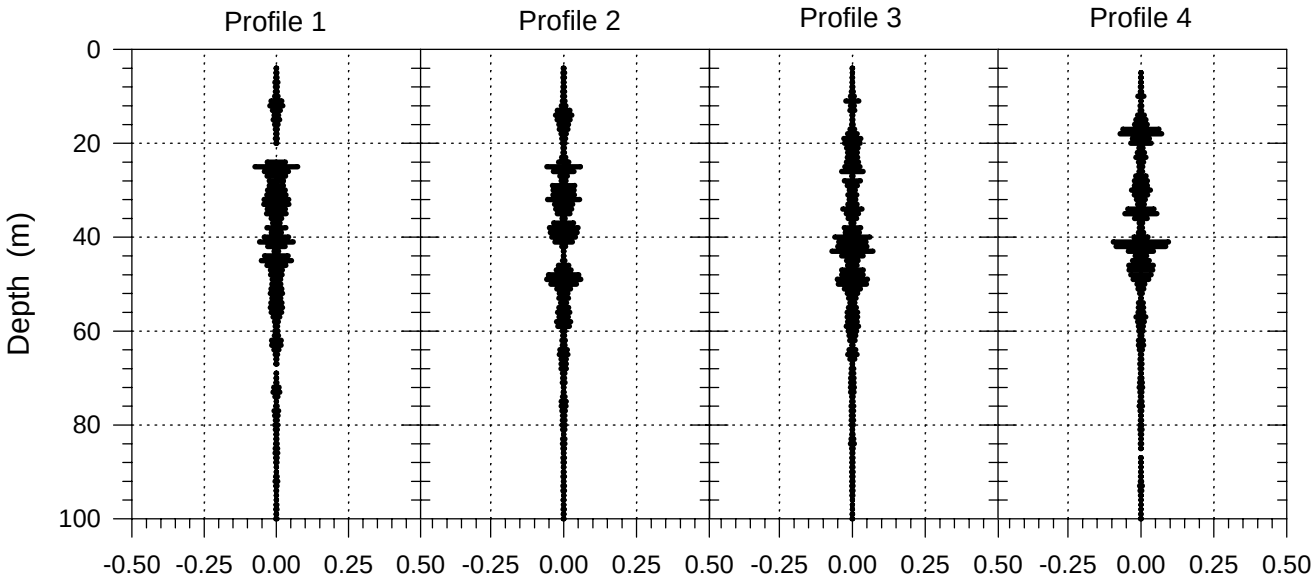

Fig. 10.8: r.m.s. density gradient profiles at station 86.

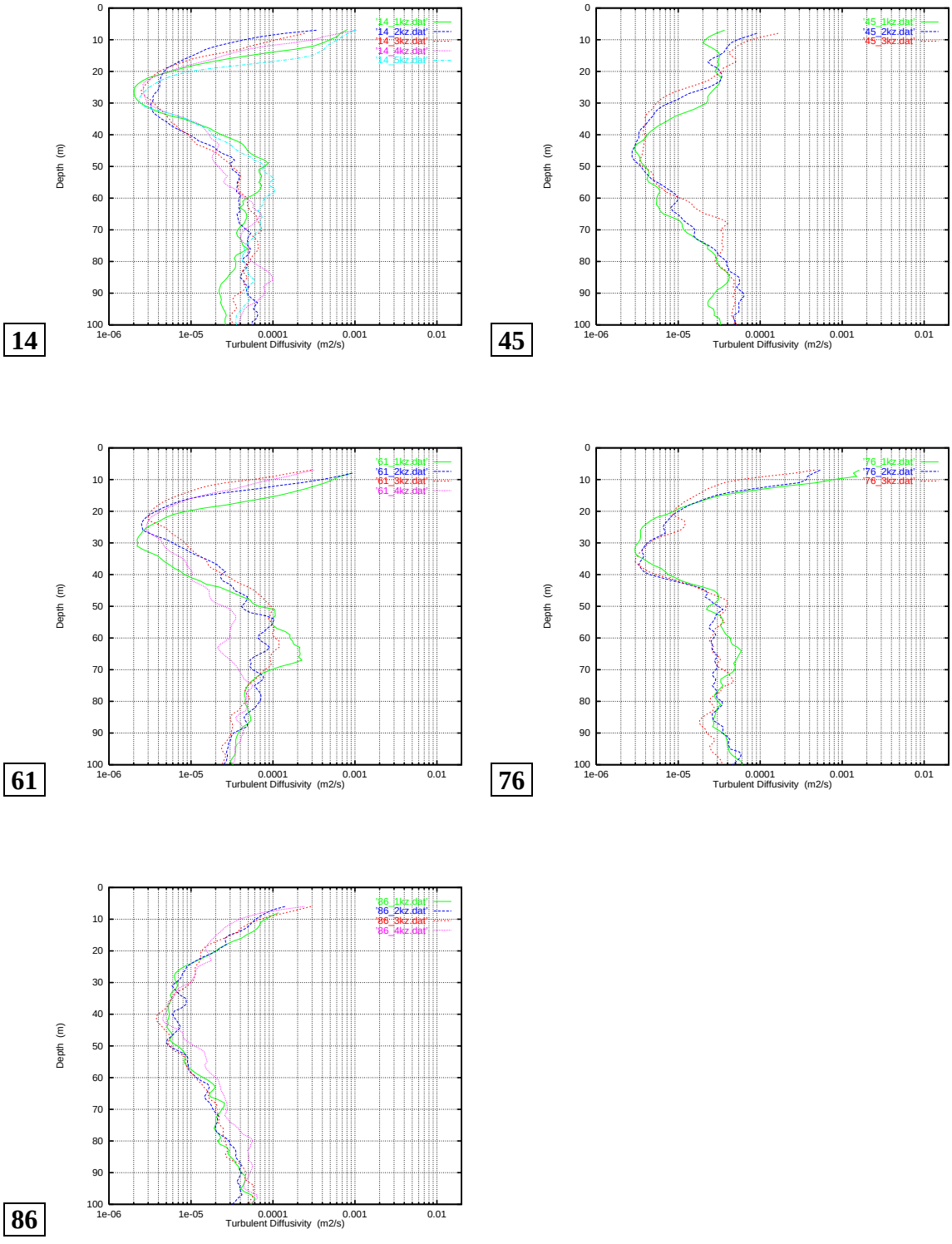

Fig. 10.9: Vertical profiles of vertical turbulent transport coefficients $K\rho$ estimated at the FRONTS'92 biological stations.

10.3 Results

In order to properly analyze the coupling between carbon and nitrogen vertical fluxes in phytoplankton dynamics we shall first describe the amount of CO_2 that is fixed in the water column at each study site, according to the hourly irradiance time series and environmental conditions.

Although, phytoplankton population can grow very fast during spring blooming periods, once the uppermost layers of the water column become nutrient depleted and phytoplankton populations have to grow deeper and deeper. However, the greater is the depth were phytoplankton is forced to develop, less radiative energy is available for growth; therefore, lower specific growth rates can be attained, in spite of the higher nutrient concentrations.

Our simulations in the NW Mediterranean Sea focus on the uppermost 100 meters of the water column, thus taking the whole euphotic layer (Figs. A.26–A.27). Results will be, however, compared and contrasted with usual discrete measurements of the biological parameters.

However, because the time scale of the pelagic phytoplanktonic system in late October (in terms of specific growth rates) is usually longer than one day, it can not be expected that both light and nutrient availability could optimal for giving the maximum growth rates.

In order to evaluate the photosynthetical process during the simulation period we shall also evaluate the quantum yield efficiency, this is, how much radiative energy (how many quanta) is necessary for fixing a given amount of CO_2 . All together, light and nutrient availability, and phytoplankton biomass will provide us with some necessary information for the evaluation of the dynamics of the coupled physical-biological system.

10.3.1 Carbon Fixation

Comparing daily vertically integrated CO_2 fixation results with the *on board* primary production measurements one may observe an acceptably good agreement, though the differences do not seen to follow a clear trend (r=0.7744; this correlation is, however, significative at just about 88%).

St.	Carbon Fixation ($mg\,C\,m^{-2}\,day^{-1}$)	
	Measured	Simulated
14	19.04	17.48
45	7.45	10.31
61	6.81	5.72
76	9.56	12.87
86	12.45	19.63

Tab. 10.1: Simulated *vs.* measured daily integrated carbon fixation rates.

Vertical profiles of carbon fixation (Fig. 10.12) show more clearly the nature of some disagreements between simulations and measurements. Comparisons are not straightforward, as the measured primary production values (Fig. 10.14) are vertically integrated every ten meters (five, at the sea surface); thus, the measured have to be divided by layer's height.

The largest differences in the integrated values appear in the less stratified profiles, 86 and 45; also the weakly bi-stratified profile 76, show quite a large disagreement between measured and simulated values. The most stratified profiles, 14 and 61, show reasonably low disagreements: 8 and 16% of variability, respectively, although the simulation at station 14, however, largely overestimates carbon fixation near the surface.

Time evolution of the carbon fixation rate (Fig. 10.10) gives a direct estimate of the vertically integrated rates during the simulation time.

On the other hand, phytoplankton biomass shows a very low variation during the short period of simulation, thus measurements and simulations do not arise as a significative source of variability. In addition, attention has put devoted to fairly reproduce the underwater light field. Therefore, we may infer from our simulations that the source of variability may come from the effect of the vertical overturning, by means of the turbulent mixing processes, over the photosynthetical adaptation mechanisms. There is still quite a large uncertainty about the modeling of phytoplankton photo-adaptation mechanisms indeed, and such a type of eco-physiological processes are not yet explicitly considered in bio-optical models.

Simulations at stations 45 and 61, however, show a good resemblance to the measured profiles, though the well mixed profile 86 gives the highest differences on reproducing the most productive layer.

A possible explanation for the evidenced differences between simulations and measurements, in spite of the fact that the photosynthetical parameters has been calibrated with measurements, is that the model starts far from a *steady-state* status. Indeed, the model also lacks of a previous light history. Nevertheless, with the empirical data which is available to us it was not possible to extend the simulation time under controlled environmental conditions.

10.3.2 Operational Quantum Yield

The quantum yield, describes the efficiency of the photosynthetical process. It provide us with a valuable information on the efficiency of the carbon fixation process. Here, the *operational* quantum yield $\phi' = C_{FIXATION}/I_{PAR(z)}$ is defined by using PAR instead of absorbed photosynthetical radiation (PUR).

Although these values can not be directly compared to empirical estimates of phytoplankton quantum yield, they can be used as a raw estimate of carbon fixation efficiency in our simulations; (e.g.) the major production rate in station 14 (Fig. 10.13) does not reflect a greater production efficiency (Fig. 10.12), but just a greater daily irradiance.

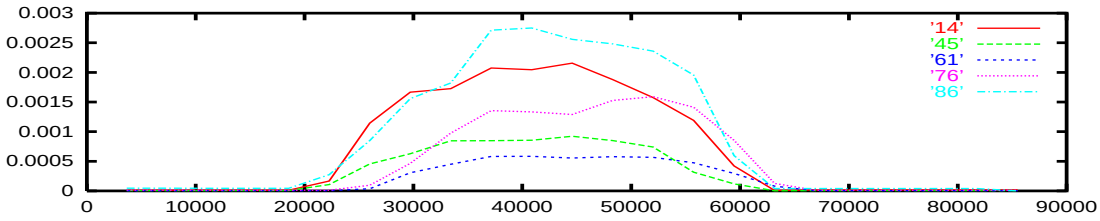

Fig. 10.10: Vertically integrated carbon assimilation $C_{FIXATION}$ ($\mathrm{mg\,C\,m^{-2}\,h^{-1}}$). Simulation time in abcisa (in seconds).

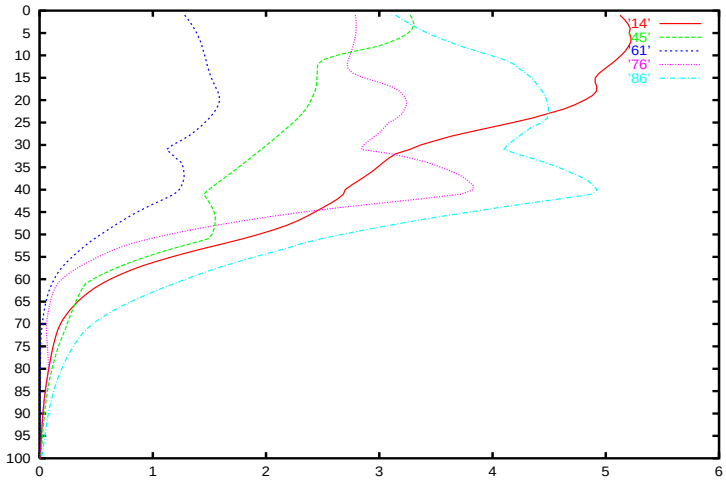

Fig. 10.11: Simulated daily integrated carbon assimilation $C_{FIXATION}$ ($\mathrm{mg\,C\,m^{-3}\,day^{-1}}$) at noon, for the FRONTS'92 biological stations 14, 45, 61, 76 and 86.

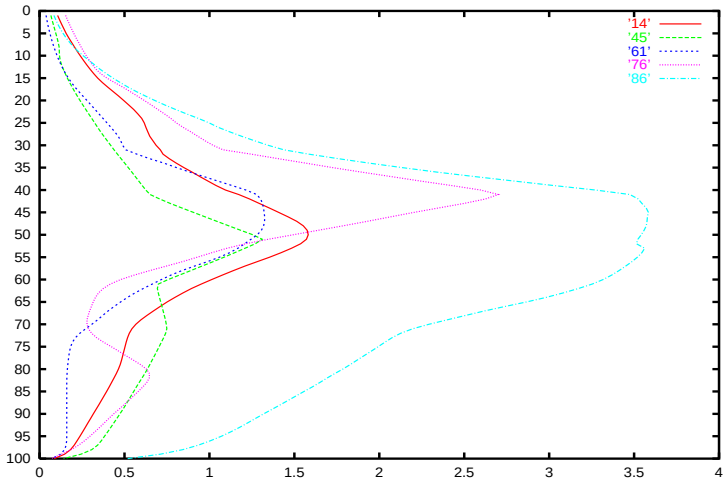

Fig. 10.12: Operational quantum yield ϕ', at noon ($\mathrm{mg\,C\cdot E^{-1}}$).

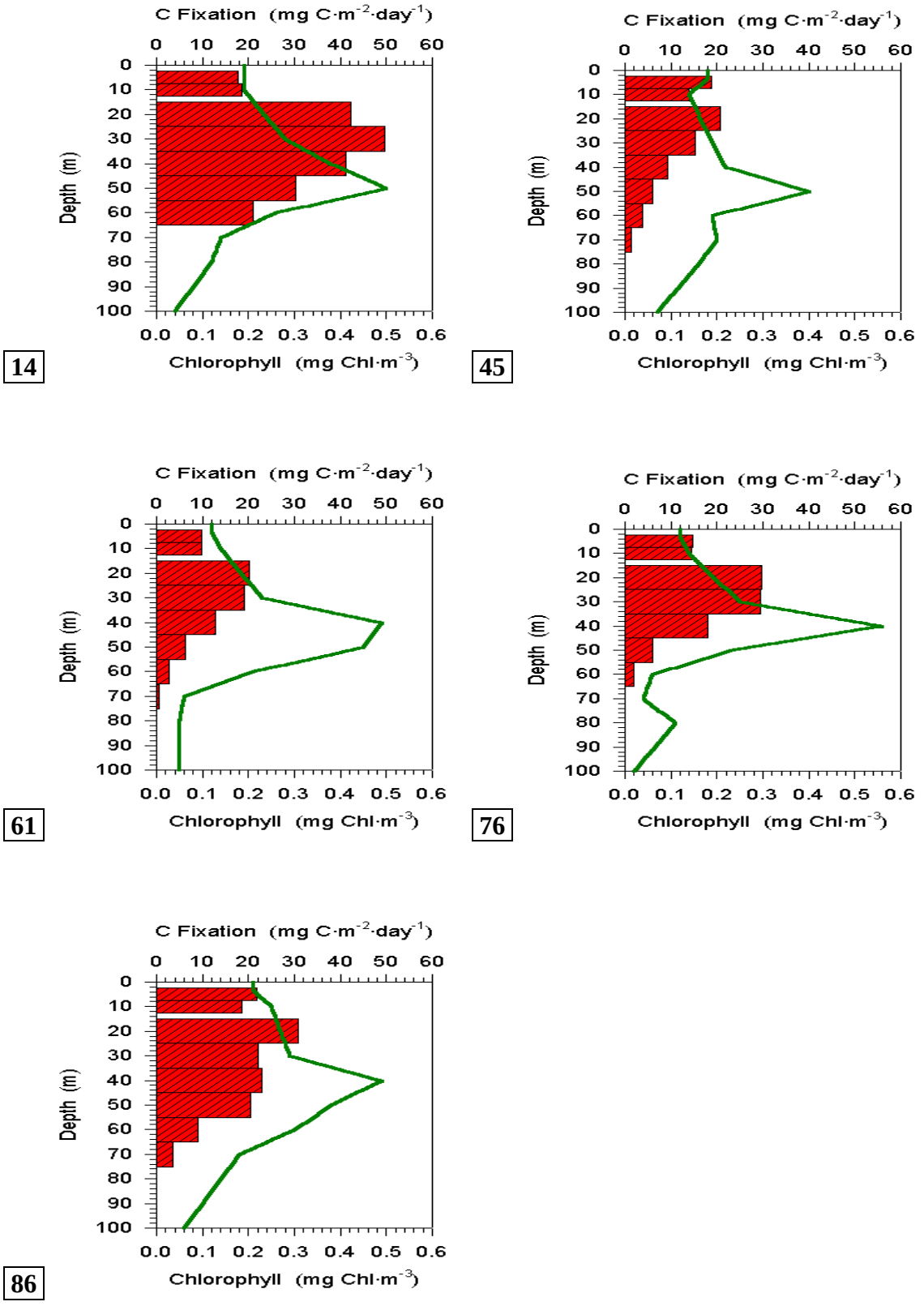

Fig. 10.13: Measured phytoplankton primary production (bars), and Chlorophyll *a* (line).

On the other side, the model gives lower efficiency values for the most stratified profiles than for the less stratified ones. Nevertheless, only five profile analysis we do not feel confident for taking this efficiency-stratification relationship as a rule, but just to note it as a reference output.

10.3.3 State Variables

Simulations for the two main state variables, nitrate N_{EXT} and phytoplankton biomass C_B are shown in plots (10.14) and (10.15). As it could be expected after only one day of simulation time, both profiles did not significatively change but just a slight smoothing according to the diffusion coefficients.

A preliminary evaluation of the simulation results compared with initial values, shows that nutrient profiles in the open ocean are probably the resource which is closest to near *steady-state* conditions. The peak at 70 m in profile 76 (Fig. 10.14), that was probably overestimated in the original nitrate profile, would be quickly smoothed out after a few days of simulation by turbulent diffusion; therefore, it can be safely ignored from our analysis as far as it does not apparently reflect any hydrodynamical singularity.

However, there is one exception for the most stratified case 14, where we observe an unrealistic growth from the surface down to 20 meters. Such a fast increase of biomass is directly related with the large subsurface carbon fixation rate (Fig. 10.11); we will reject further results on profile 14 because (only in this case) the model fails in giving reasonable results on nutrient quota (*see* next).

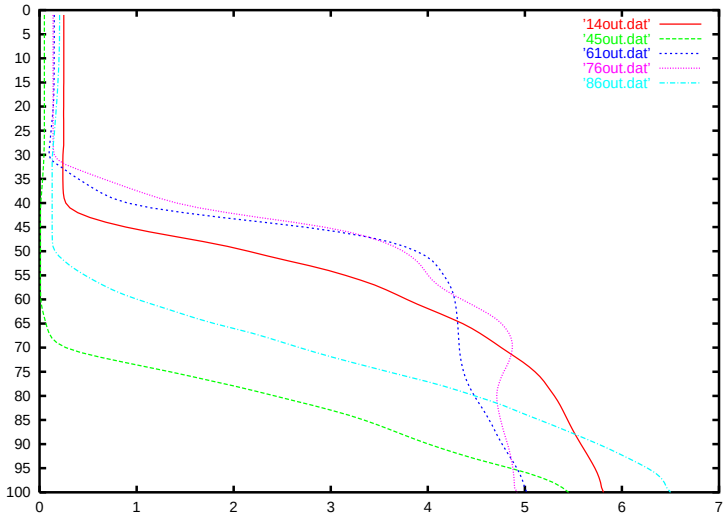

Fig. 10.14: Simulated vertical profiles of nitrate (mg-at N m^{-3}), after 24 hours of simulation time, for the FRONTS'92 biological stations 14, 45, 61, 76 and 86.

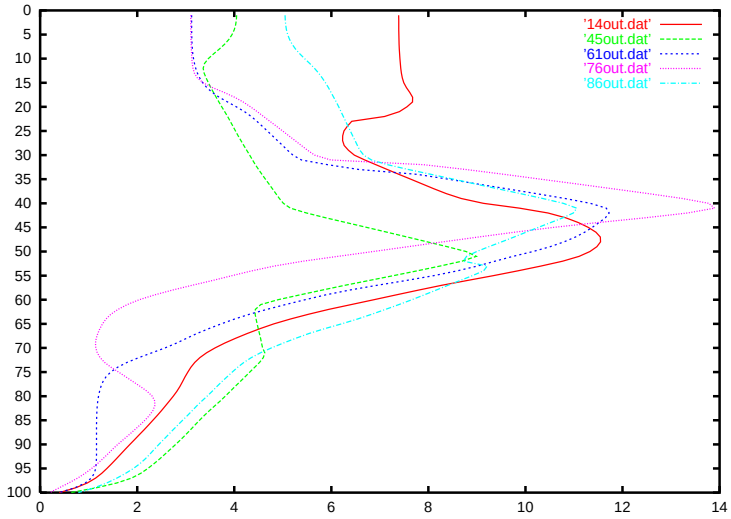

Fig. 10.15: Simulated vertical profiles of phytoplankton biomass (mg-at C m^{-3}), after 24 hours of simulation time.

Pool state variables C_P and N_P show a higher temporal and spatial variability, than biomass state variables, as it could be expected. However, a final synthesis is better summarized by the biomass nutrient quota, which reflects in a longer time scale the variability of the pool quota.

The main objective of the intermediate pool state variables is to buffer environmental variability, and to encompass the different time scales of both the carbon and nitrogen pathways, in order to provide a smooth and continuous flux of carbon and nitrogen to the synthesis processes of biomass.

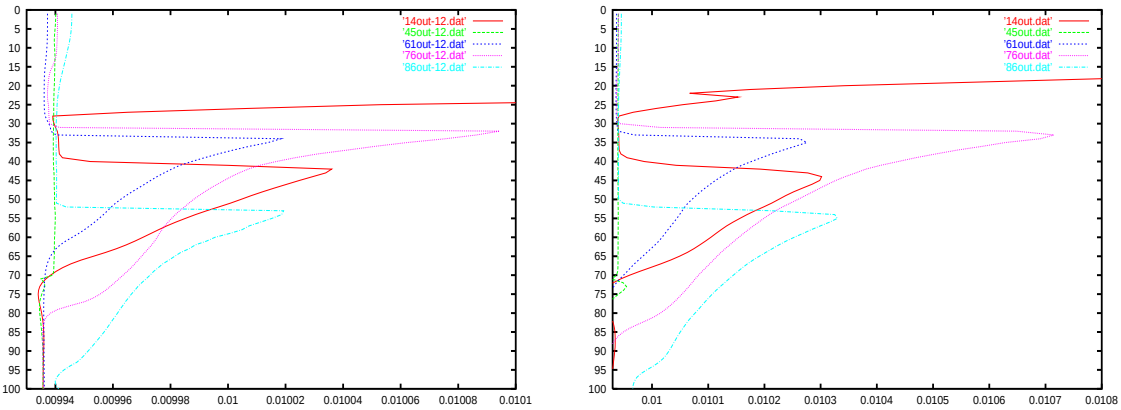

Fig. 10.16: Simulated profiles of $(N:C)_B$ ratios, at noon (left), after 12 hours of simulation time, and midnight (right) t=24 hours.

St.	∇NO_3^- (mg-at N m^{-4})	N Depth (m)	K_ρ ($m^2\,s^{-1}$)	NO_3^- Vert. Transp. (mg-at N $m^2\,day^{-1}$)
14	0.2835	52	6.84×10^{-5}	1.6755
45	0.2237	74	1.97×10^{-5}	0.3808
61	0.3750	44	2.27×10^{-5}	0.0736
76	0.3038	43	1.47×10^{-5}	0.3858
86	0.1850	66	1.71×10^{-5}	0.2733

Tab. 10.2: Vertical turbulent transport rates of nitrate computed at the nitracline depth.

10.3.4 Vertical C:N Flux Ratios

Biomass nutrient quotas (or ratios) is probably the parameter that better describes the fundamental approach and achievement of this model. It summarizes the full interaction between vertical nutrient transport and phytoplankton growth, in terms of CO_2 fixation; thus, it drives its specific growth rate.

The model describes better growth conditions, this is, higher quota values, just below the deep chlorophyll maximum, though the absolute values of the present runs remain always below Redfield reference values, and show a small vertical variability, indeed.

Table (10.2) shows the estimated net vertical fluxes of nitrate through the nitracline, which is expected to be directly related with the phytoplankton growth. As it has been pointed out at the beginning of this chapter, it has been estimated that the study sites are far enough to get a significative nitrogen input by atmospheric deposition. Therefore, we have taken nutrient upwelling as the main nutrient source for growth.

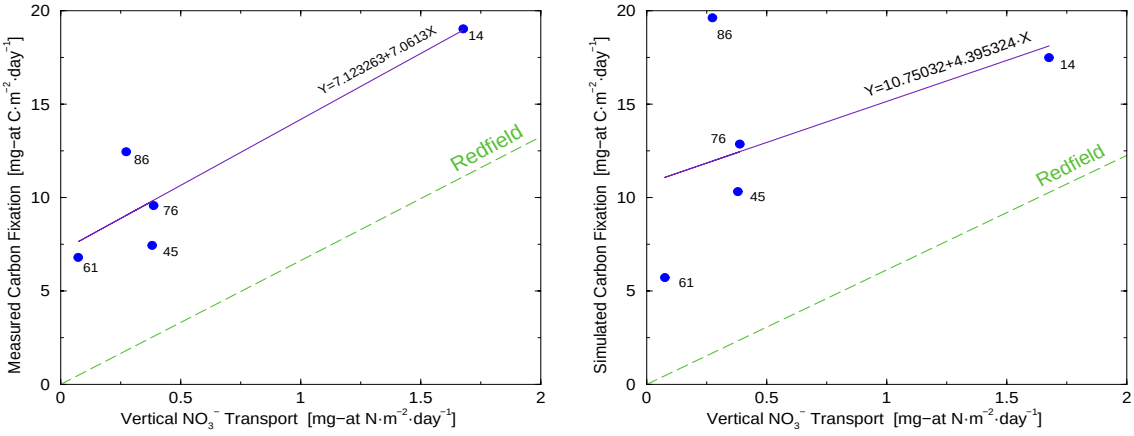

Fig. 10.17: Vertical nitrogen to carbon measured (left) and simulated (right) carbon fixation rates.

The relationship between measured carbon fixation and the estimated vertical nutrient transport has been evaluated, yielding a correlation index r=0.9050, statistically significative ($p<0.05$). The relationship with the simulated values reflects, however, a lower correlation index (r=0.5031). The correlation index is bad enough, taking into account the pulling effect of the result for station 14. However, despite this small correlation trend, measured and simulated carbon fixation rates (Table 10.1) show a reasonably agreement, regarding the number of mechanisms (both, physical and biological) involved at the different levels of the water column, and the oversimplification which results from any modeling exercise.

The small number of values provided this study do not allow to show a close relationship between phytoplankton carbon fixation and nitrogen upwelling. In any case, the methodological approach that has been developed for this study will enable a future insight in order to finally evaluate the strength of such relationship.

Experimental and theoretical evidences address further studies towards the relationship between turbulent mixing and phytoplankton growth in order to quantify first, the coupling between carbon and nutrient vertical fluxes and, second, the control of phytoplankton growth and blooming events by strictly hydrodynamical conditions.

Part V

FINAL DISCUSSION
&
CONCLUSIONS

FINAL DISCUSSION AND CONCLUSIONS

Physical processes occurring in the ocean cover extremely wide spatial and temporal ranges, but the effect of each one of the physical environmental processes over the phytoplankton dynamics depends somehow on their characteristic temporal and spatial scales.

At this stage the spatio-temporal evolution of a single particle of fluid can not be yet fully determined by the driving equations, mainly because of their chaotic component behaviour. However, under the circumstances defined by the classic work by Kolmogorov in 1941, the fundamental characteristics of the so-called *small-scale turbulence* (SST) can be statistically but also rigorously determined, so far. Therefore, one may expect to achieve a statistically evidence of the effect of SST over the most sensitive elements of the pelagic ecosystem.

However, the overall effect of SST over the spatio-temporal phytoplankton dynamics can not be studied with a single experimental approach, or by just a single theoretical scheme. Usually, every processes, determined by its characteristic spatial and temporal scales, require a different methodology. For instance, SST is the main physical processes responsible for the mixing mechanism in the ocean. But at the same time, SST also plays a fundamental role by modifying the fluxes of matter around the small planktonic organisms. Both play an effective role over the marine or freshwater ecosystems, but each one require a different approach in order to quantitatively evaluate their relative contribution or effect.

In nature many different physical environmental processes may occur at the same time and in the same area, although their relative contribution may vary from time to time, and place to place. Indeed, it should be possible to identify the spectral signature of the most relevant physical environmental conditions. However, we are still far from having a full picture of just the most important aspects of SST that may play a role over the phytoplankton dynamics.

In consequence, the study of phytoplankton dynamics in natural condition can not be disregarded from the study of the most relevant physical environmental processes; among them, SST exerts a very strong influence. As it has been shown in the previous chapters, SST plays an essential role in the productivity of aquatic ecosystems. Its influence is specially evident at lowest trophic levels as a typical *bottom-up* effect; this is, by driving

the vertical upwelling of nutrients from the deeper layers. In terms of mixing SST can be also identified as the responsible mechanism which drives the spatial re-distribution of the phytoplankton patches, as well.

On the other side SST plays also an important role by affecting the transport of matter within the fluid *Diffusive Boundary Layers* (DBLs) around every single phytoplanktonic organism. Indeed, a big attention has been devoted to this issue during the last years. This is mainly because at such small scale we are mainly dealing only with molecular diffusive transport, thus leaving aside the direct effect of turbulent phenomena. Such circumstances allow us to simplify relatively our analysis for small water parcels. Thus, turbulence is not directly affecting mass transport within DBLs but just indirectly; this is, by modifying the concentrations gradients around the organisms.

The biological model developed in this thesis provides two fundamental advances. First, uncoupling nutrient uptake from the photosynthetical process (by means of the Droop's formulation) makes nutrient uptake to react during short periods of time independently from sun irradiance. For instance, the model successfully reproduce the fast nutrient uptake rates around sunrise time. On the other hand, nutrient uptake is able to quickly react against sudden changes of the external nutrient concentration. The accumulation of N and C inside of the organism in terms of functionally isolated pools represents a very useful modeling advance. This is because these internal pools behave like shock absorbers against the intrinsic environmental variability. They damp or smooth the variability of the different independent resource inputs (N, C) and irradiance, thus providing more constant fluxes to the rigid metabolic synthesis requirements. Secondly, uncoupling photosynthesis (or carbon fixation) from the synthesis of biomass makes possible to maintain synthesis of biomass during night time.

Additionally, the experimental and empirical evidences about the impact of nutrient limitation on phytoplankton growth suggest that such limiting effect is not generally exerted over the whole autotrophic metabolism, but just on the final synthesis of biomass. It has been demonstrated the nutrient limitation does not significatively affect the photosynthetical process, unless very strong limitating condition occurs. Such a behaviour has been also successfully reproduced by the formulations presented in this thesis.

Increasing the time resolution of the biological key-processes explicitly considered in our model (this is, not just decreasing the simulation time step) was a necessary condition in this thesis in order to be able to reproduce the effect of SST over the phytoplankton dynamics. In this respect, the adimensional number T_B^* provides a useful analysis tool for the relationship between the physical environmental factors and the relevant biological processes related with phytoplankton productivity in the water column.

On the other hand, carbon has not been regarded as a potential limiting resource in the biological model described in Chapter 6, although carbon limitation has been introduced as a key hypothesis in the small-scale mass transport within DBLs (Chapters 4 and 9). On the contrary, it has been fundamentally stressed the limiting role dissolved nutrients. Indeed, the model accounts for the *state-of-the-art* in oceanography for both the modeling of phytoplankton biology and the most relevant vertical physical processes, but most of the formulations published up to now (ours included) do not reflect yet some

fundamental exchange fluxes between the ocean and the atmosphere.

The parameterizations used in this thesis dealt well with a wide range of stability conditions of the water column, from summer stratification to strong mixing conditions. Nevertheless, the turbulent diffusion coefficients in the uppermost layer ($\sim$2–3 meters) often can not be calculated due to the difficulties introduced by wave movements. Such limitation does not represent a big constraint or introduce a strong influence in our simulations, but it could introduce a significative uncertainty source when considering atmosphere-ocean exchanges (e.g., atmospheric deposition, etc.).

The model takes into account stratification and turbulent diffusivity. About the biological processes, the model takes into account the effect of photoinhibition and temperature and nutrient limitation. The physical processes like nutrient upwelling and stratification are finely reproduced in the model.

Finally, we must point out that the physical and biological parameters take the values measured from the literature for two reasons. Both, modeling and numerical simulations require a big effort in terms of development and computer skills. This thesis was planned mainly as a synthetical approach to the combined physical-biological modeling of phytoplankton dynamics. Therefore, experimental work felled initially beyond the scope of this study. The second reason is that open ocean research often lacks of the logistical benefits of proximity to the coast, which reverts on the benefits of a larger body information available. In addition, it is often difficult to cope with all the physical and biological parameters necessary for the calibration of the present model for the same location, or even for the same cruise. Then, modeling in oceanography may not be just a useful and successful approach, but sometimes a necessary one.

The physical-biological model presented in this thesis may be useful in field work to asses whether the measured profiles at single stations are representative of transient states, or the observed physical-biological conditions have nearly reached a steady state. This may be investigated further by running the model with the measured profiles, and observing their evolution in time.

Finally, this model may provide the researcher, or the environmental manager, with forecastings on different setup hypothesis.

Part VI

APPENDIXES

APPENDIX

A. DATASET AND FORCING TIME SERIES

In this thesis we have worked with a subset of the open ocean data of FRONTS-1992 cruise, carried out the in October-November 1992. Most of the oceanographic data (nutrients, chlorophyll, etc.) are reported in *Datos Informativos*, number 27, by Masó & Grupo Varimed (1995). We choose FRONTS-1992 cruise for two main reasons. Because we find different stability conditions during a short period in a small area: well stratified conditions (stations 14 and 61; Figures 10.2.2 and 10.2.2), transient staggered conditions (station 76; Figure 10.2.2) and onset breaking conditions (stations 45 and 86; Figures 10.2.2 and 10.2.2). The second reason is availability.

The stations considered here are shown in Table 7.1. All stations are located between Barcelona and Mallorca (Balearic islands), in the Northwestern Mediterranean Sea (Figure 10.1); there are two main areas defined by stations 14, 61 and 76 (site A), and 45, 65 and 86 (site B). The position of the vessel was not constant. It drifted some miles at every station. Consequently, there are slight differences in T-S diagrams (Figures A.1 to A.6).

We may assume that in all these stations there is no direct coastal influence, like river outflow or coastal runoff, which is a necessary condition for assuming horizontal homogeneity. On the other hand, we also assume no influence of the bottom. However, we may not completely neglect the possible influence of southwards currents along the continental shelf, although they mainly occur at deeper layers than what we are considering in this study (Margalef & Estrada, 1987).

A.1 Temperature, Salinity and Density

Temperature is a forcing function for the biological model (Figures A.7 to A.12). It directly influences metabolic processes according to the Q_{10} factor. Temperature profiles come from CTD casts. Temperature and salinity are used for computing density profiles according to the equation of state (Millero & Poison, 1981). Stability conditions of the water column derived from density profiles will be further used for computing turbulent diffusion fluxes. Salinity is not used anywhere else in the calculations.

Station	Obs	Date	Time GMT	Situation	Max Depth
14.1	B	18/10/92	6:11	40 40.5 N 2 49.9 E	2000m
14.2		18/10/92	10:00	40 41.1 N 2 49.7 E	2002m
14.3		18/10/92	14:00	40 41.7 N 2 50.1 E	2004m
14.4		18/10/92	18:17	40 40.6 N 2 50.5 E	2015m
14.5		18/10/92	21:32	40 40.6 N 2 52.2 E	2058m
45.1	B	22/10/92	4:52	40 56.5 N 2 34.4 E	1700m
45.2		22/10/92	9:57	40 56.3 N 2 33.3 E	1680m
45.3		22/10/92	15:00	40 54.9 N 2 35.4 E	1745m
61.1	B	26/10/92	5:48	40 40.5 N 2 50.1 E	2000m
61.2		26/10/92	8:54	40 40.4 N 2 50.1 E	2020m
61.3		26/10/92	11:49	40 39.8 N 2 52.4 E	2240m
61.4		26/10/92	14:50	40 40.3 N 2 50.3 E	2020m
65.1	B	27/10/92	4:56	40 56.0 N 2 34.6 E	1700m
65.2		27/10/92	7:37	40 55.7 N 2 33.5 E	1700m
65.3		27/10/92	11:08	40 56.4 N 2 33.7 E	1680m
65.4		27/10/92	13:33	40 40.5 N 2 50.1 E	1698m
65.5	*	27/10/92	15:49	40 56.6 N 2 34.3 E	1684m
65.6	*	27/10/92	18:00	40 58.0 N 2 34.4 E	1647m
65.7	*	27/10/92	21:33	40 55.8 N 2 34.3 E	1705m
65.8	**	28/10/92	0:16	40 40.5 N 2 50.1 E	1711m
76.1	B	29/10/92	9:39	40 40.1 N 2 50.9 E	2038m
76.2		29/10/92	14:15	40 40.5 N 2 51.0 E	2026m
76.3		29/10/92	16:55	40 39.2 N 2 52.4 E	2293m
86.1	B	30/10/92	6:29	40 56.4 N 2 34.3 E	1690 m
86.2		30/10/92	9:35	40 56.5 N 2 34.5 E	1689 m
86.3		30/10/92	11:23	40 56.6 N 2 34.8 E	1690 m
86.4		30/10/92	15:12	40 55.5 N 2 31.6 E	1717 m

Tab. A.1: Stations considered in the present study belonging to FRONTS-1992 cruise. * Indicates malfunction in the salinity sensor. ** Not available. B, Biological stations with available chlorophyll *a*, nitrate, irradiance and additional measurements.

Station	Chl *a*
14	22.93
45	19.06
61	19.44
65	19.12
76	17.12
86	25.22

Tab. A.2: Vertically integrated Chlorophyll *a* in mg Chl $a \cdot m^{-2}$, linearly interpolated from discrete measurements.

Station	NO_3^-
14	236.875
45	92.70
61	251.905
65	238.07
76	269.83
86	177.18

Tab. A.3: Vertically integrated values of nitrate in mg-at $N \cdot m^{-2}$, linearly interpolated from discrete measurements.

A.2 Chlorophyll a

Chlorophyll *a*, measured by a standard method from water samples (Yentsch & Menzel, 1963), is only available for the first profiles in each station (Figuers A.13 to A.18). Chlorophyll *a* is often considered as a direct estimation of phytoplankton biomass, despite of the relatively high variability of the $\frac{Chl}{C_B}$ ratio that is used as a conversion factor (section 6.2.2). Chlorophyll is linearly interpolated every meter before entering the model (converted to carbon units) as initial conditions profiles. It is also directly used for calculating the vertical attenuation of light due to phytoplankton (*See* section A.4).

The total chlorophyll *a* from 0 to 100 m, that we take as a raw estimation of the phytoplankton biomass, indicate different growth conditions. We observe that in similar low stability conditions (stations 45 and 86) station 45 shows a definitely lower biomass than in station 86. Station 86 was sampled one week later nearly at the same site. Stratification is thus not the unique factor which promotes phytoplankton growth.

A.3 Nitrate

Nitrate is the only limiting nutrient resource considered in this model. It is also sampled at discrete depths during the oceanographic campaigns.

Like chlorophyll *a*, nitrate is linearly interpolated every meter in order to properly deliver the initial conditions file for the numerical simulation.

A.4 Irradiance

Bio-optical models need the vertical light profiles for estimating the carbon fixation rate in the water column. To this purpose, the underwater light field can be measured or estimated by different parameterizations. Hourly irradiance time series during the sampling day are shown in Figure A.25.

A.4.1 Calibration of the Underwater Light Field

The characteristics of the underwater light field are usually different for oceanic and coastal waters, as well as for inland waters. In the figures A.26 and A.27 we observe how PAR is attenuated in depth. In these plots we also realize that it is not possible to get a good estimation using a simple exponential function. The profiles can be improved by adding an additional attenuation term for chlorophyll $K_{PH} = k_c + [chl]$ (in mg Chl $a \cdot \mathrm{m}^{-3}$) to the previous function, and a *non-phytoplanktonic* attenuation term k_{np} (*see* equation 5.8). We take the apparent chlorophyll absorption coefficient as $k_c = 0.016$, in $\mathrm{m}^2 \cdot$ mg Chl a^{-1}. We observe the highest k_{np} values near the surface except of station 14.

Riley (1956) introduced another direct estimation of the underwater light profiles, also including the chlorophyll attenuation $K_D = 0.04 + 0.0088 \cdot [Chl] + 0.054 \cdot [Chl]^{2/3}$, where $[Chl]$ is the chlorophyll *a* concentration in mg Chl $a \cdot \mathrm{m}^{-3}$, at each depth. We rejected the later because it does not properly fit to our data.

A.5 Turbulent Diffusion Coefficients

Our main concern in this thesis is to achieve a careful estimation of the stability conditions of the water column. The density profiles computed upon CTD data is then used for estimating the vertical turbulent diffusion coefficients profiles; they have been computed according to equation (3.25). Results plotted in Figures 10.2.2 to 10.2.2, are smoothed using a Savitzky-Golay filter ($n_L = 4$, $n_R = 4$, $M = 4$; Press *et al.*, 1992).

A.6 Dataset (Plots)

[Next pages.]

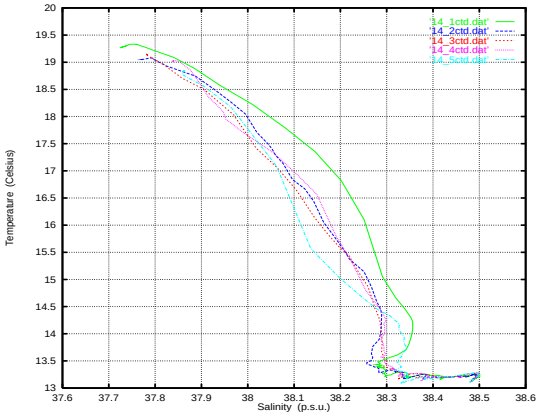

Fig. A.1: T-S diagram at Station 14.

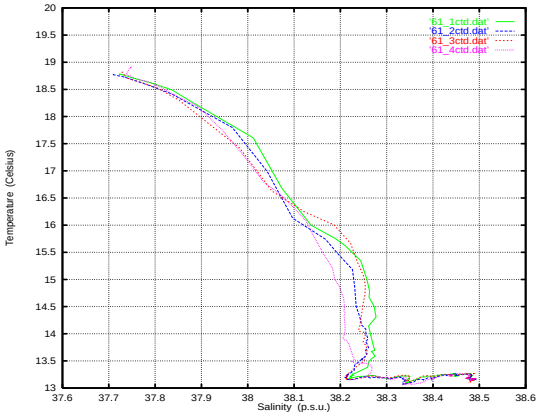

Fig. A.2: T-S diagram at Station 61.

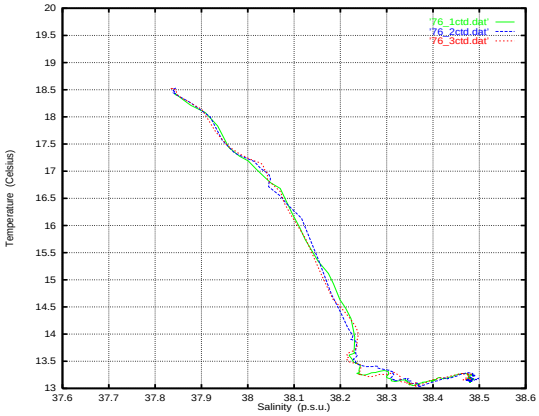

Fig. A.3: T-S diagram at Station 76.

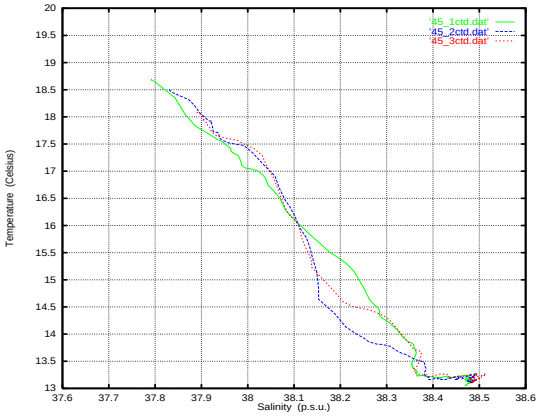

Fig. A.4: T-S diagram at Station 45.

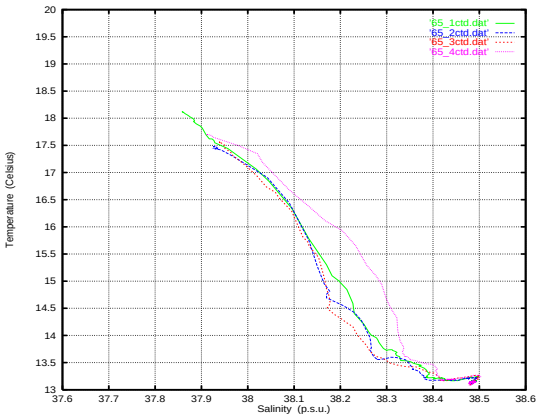

Fig. A.5: T-S diagram at Station 65.

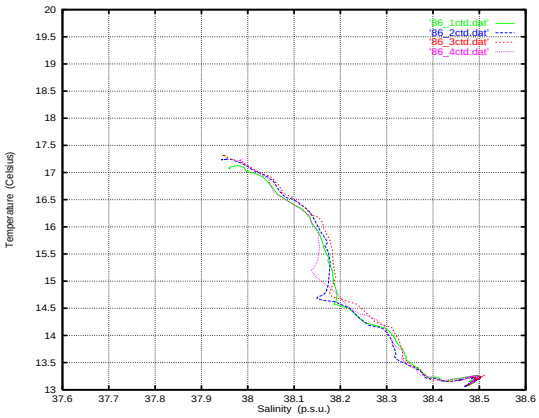

Fig. A.6: T-S diagram at Station 86.

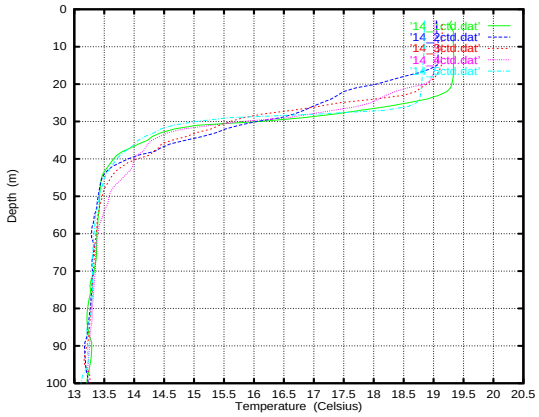

Fig. A.7: Temperature at Station 14.

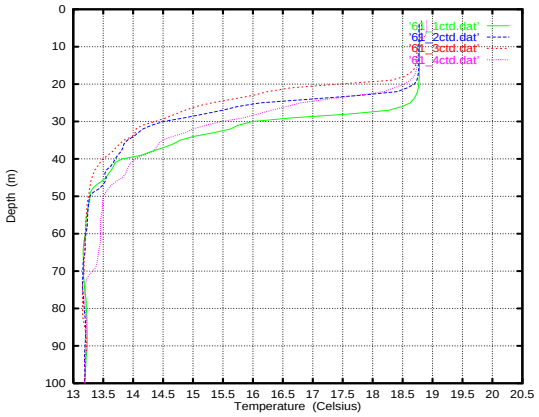

Fig. A.8: Temperature at Station 61.

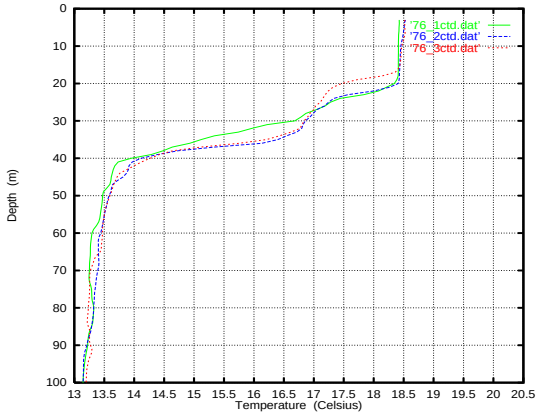

Fig. A.9: Temperature at Station 76.

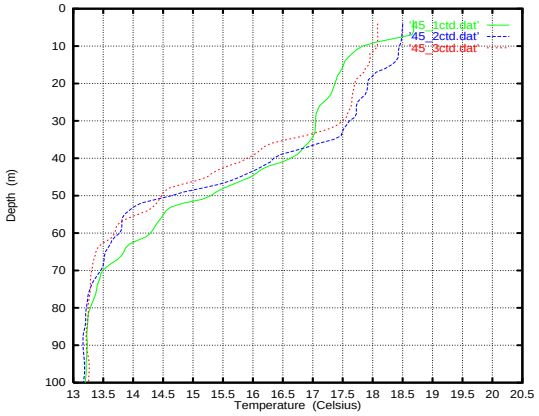

Fig. A.10: Temperature at Station 45.

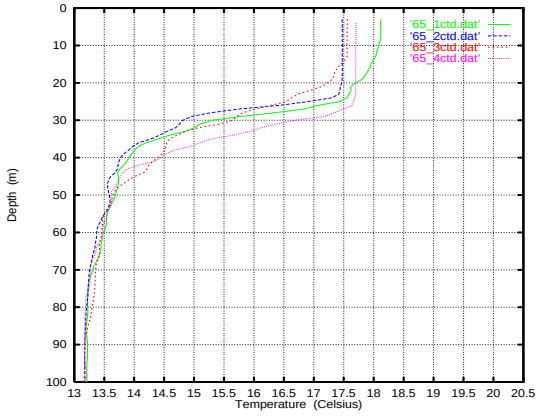

Fig. A.11: Temperature at Station 65.

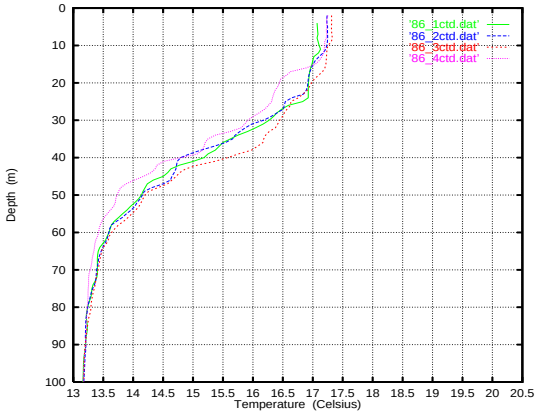

Fig. A.12: Temperature at Station 86.

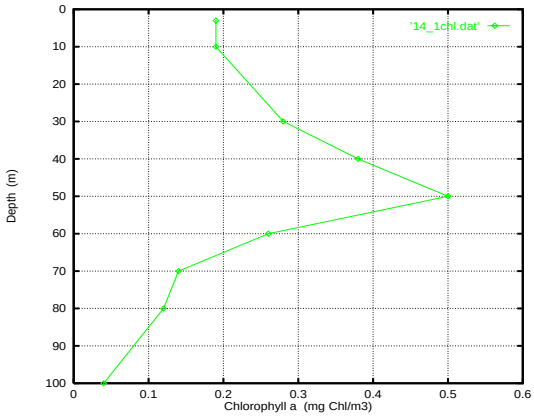

Fig. A.13: Chlorophyll *a* at Station 14.1.

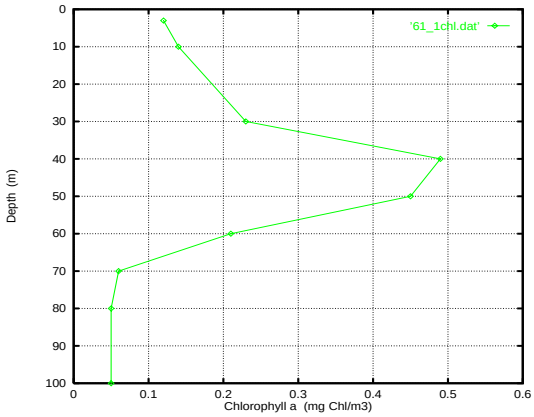

Fig. A.14: Chlorophyll *a* at Station 61.1.

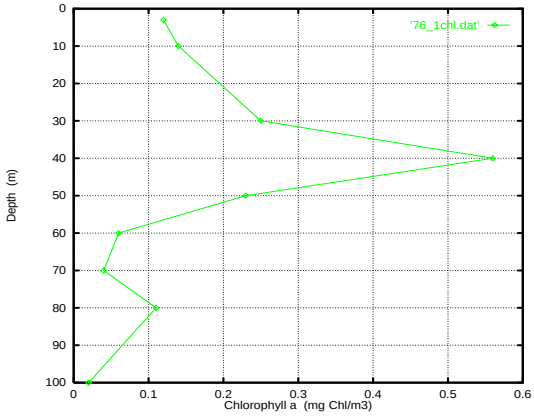

Fig. A.15: Chlorophyll *a* at Station 76.1.

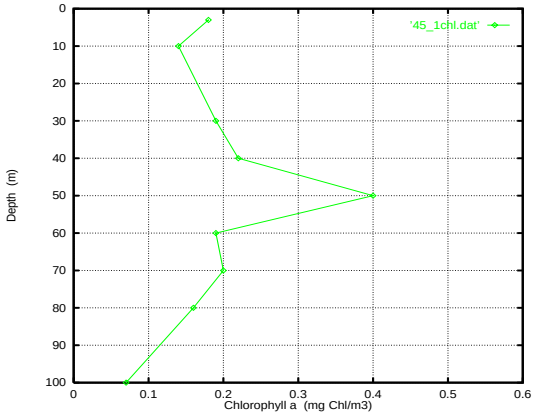

Fig. A.16: Chlorophyll *a* at Station 45.1.

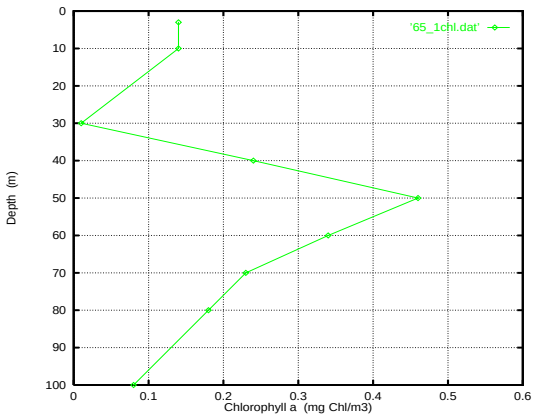

Fig. A.17: Chlorophyll *a* at Station 65.1.

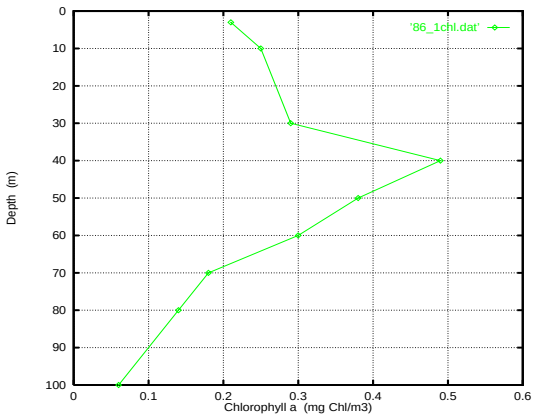

Fig. A.18: Chlorophyll *a* at Station 86.1.

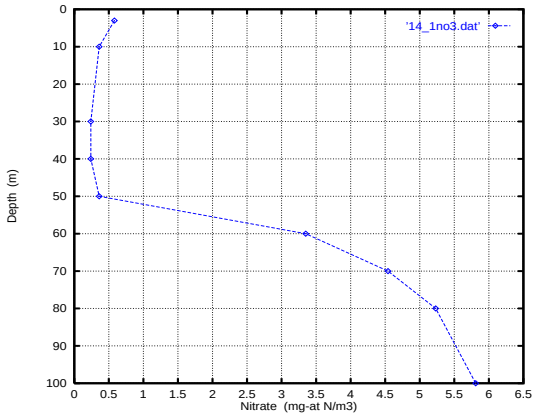

Fig. A.19: Nitrate at Station 14.1.

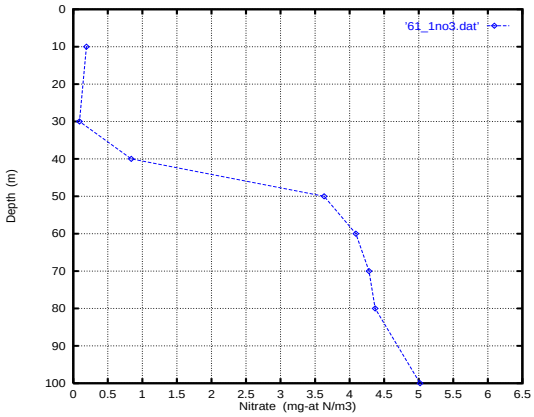

Fig. A.20: Nitrate at Station 61.1.

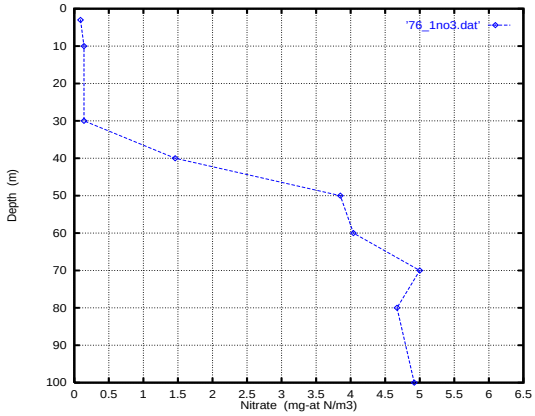

Fig. A.21: Nitrate at Station 76.1.

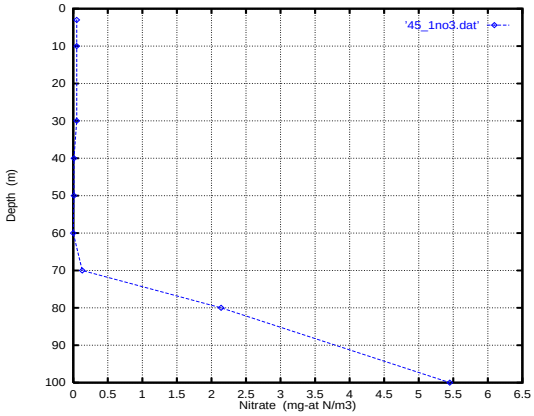

Fig. A.22: Nitrate at Station 45.1.

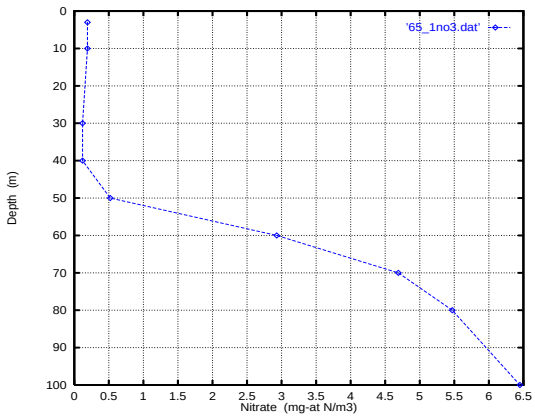

Fig. A.23: Nitrate at Station 65.1.

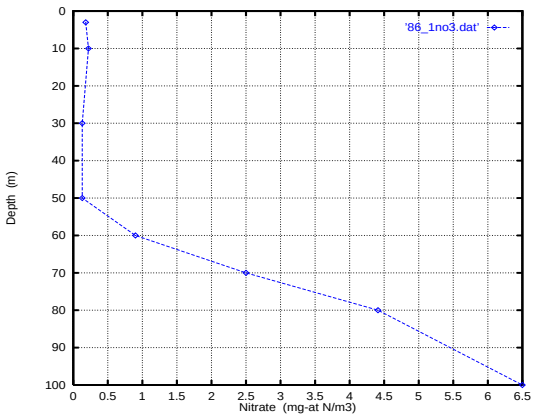

Fig. A.24: Nitrate at Station 86.1.

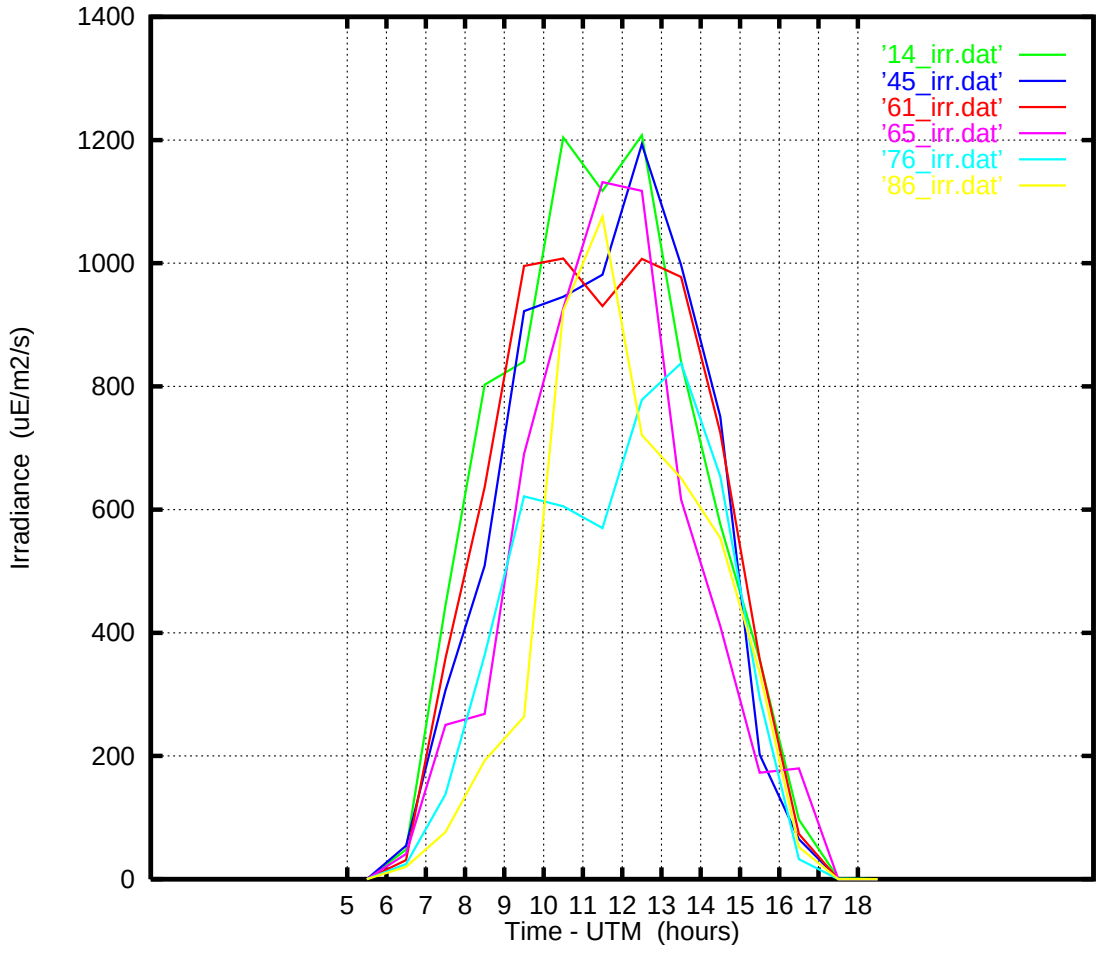

Fig. A.25: On board hourly irradiance measurements for the six considered sampling stations. Dates are, respectively, 18/10/1992, 22/10/1992, 26/10/1992, 27/10/1992, 29/10/1992 and 30/10/1992, for stations 14, 45, 61, 65, 76 and 86.

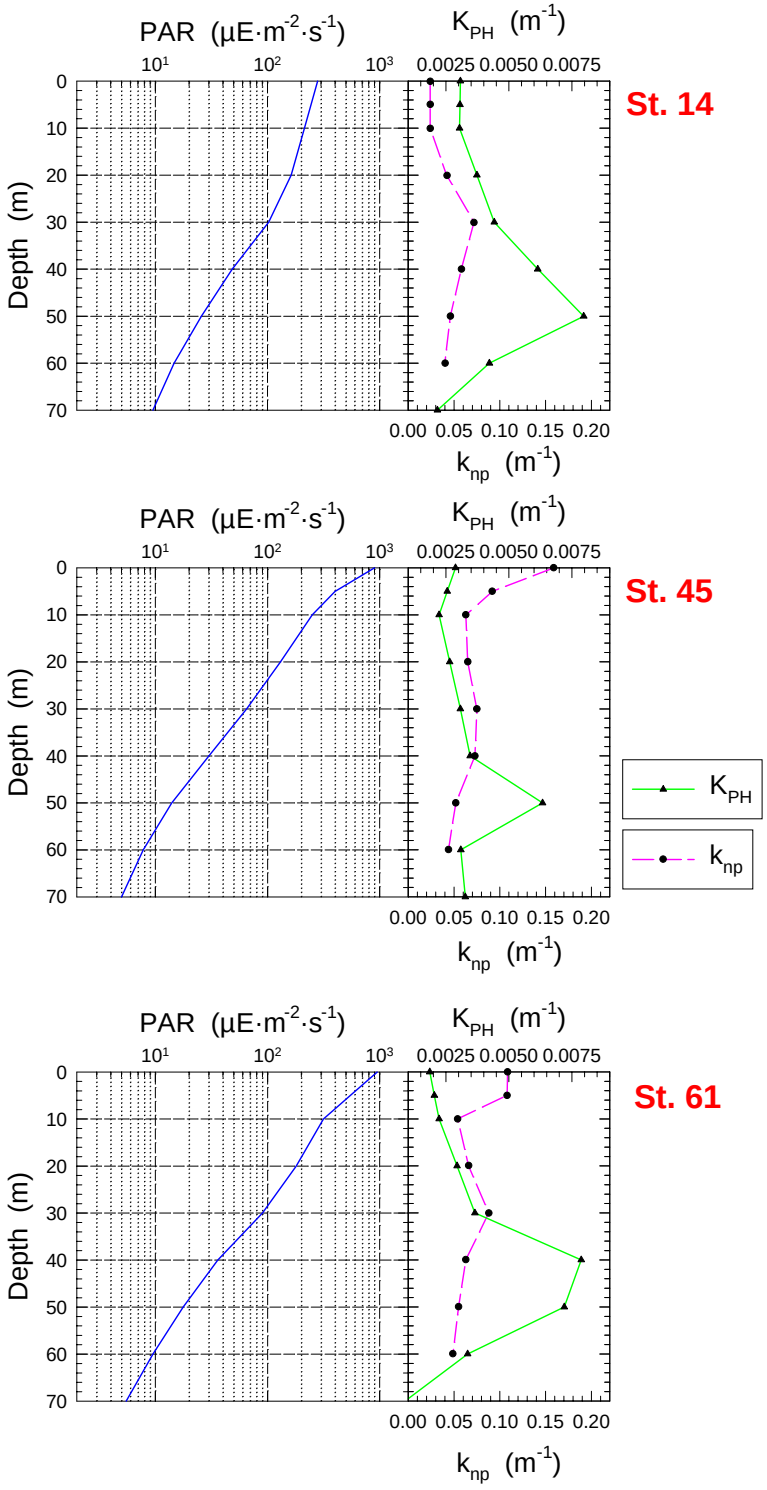

Fig. A.26: The plots show the measured PAR profiles (400-700 nm) in logarithmic scale at the biological stations 14, 45 and 61, of FRONTS'92 Cruise. At the right hand side of each graphic are plotted the estimated vertical attenuation profiles due to phytoplanktonic chlorophyll K_{PH} (triangles), and k_{np} (circles) are the fitted *non-phytoplanktonic* attenuation coefficients. From 70 to 100 meters (no measures) the light field was estimated with the attenuation coefficients of 70 meters.

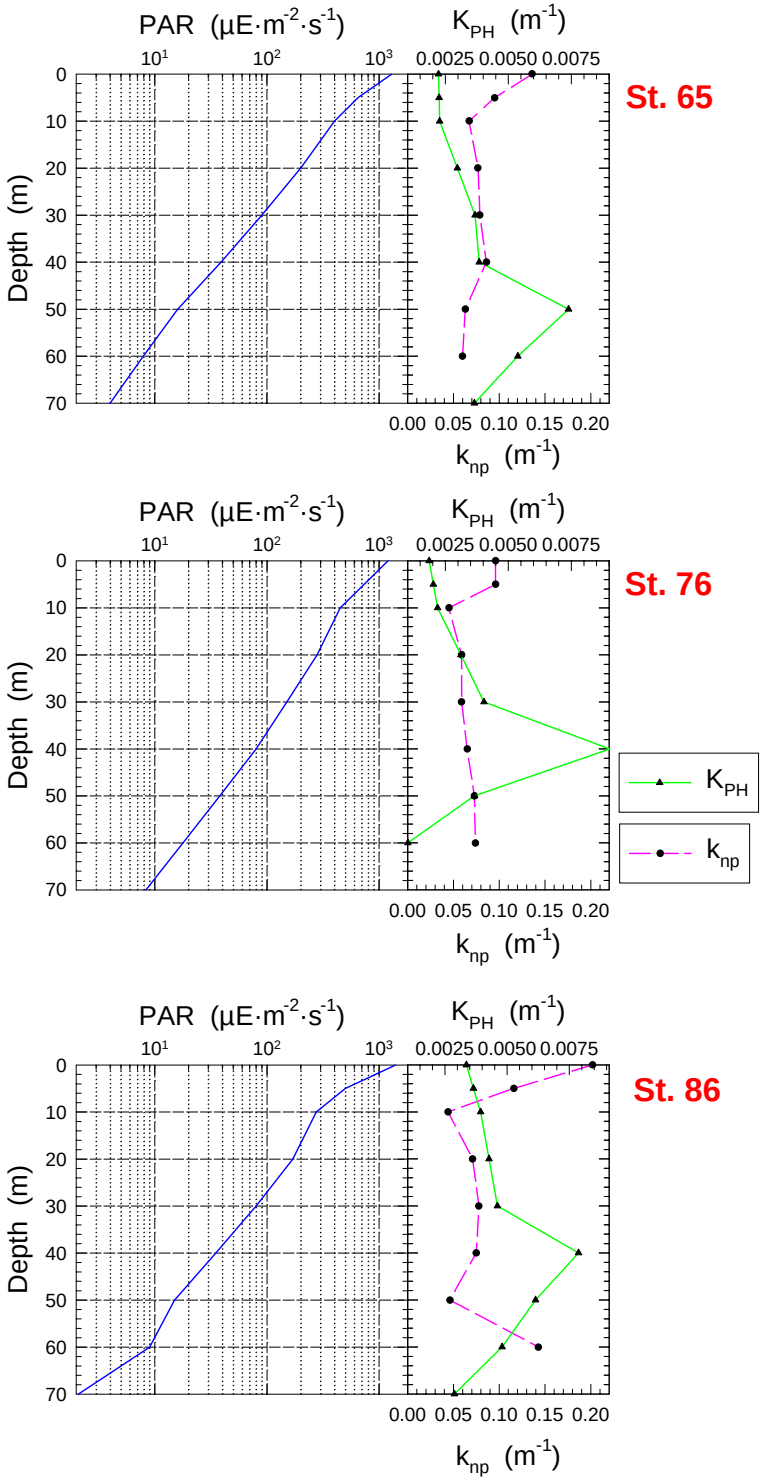

Fig. A.27: (cont.); stations 66, 76 and 86.

B. PARAMETER VALUES

Symbol	Value	Units	
k_c	0.015	m^2 mg Chl a^{-1}	
$\frac{Chl}{C_B}$	0.04	mg Chl a mg C^{-1}	
V_{max10}	0.000348	mg-at N m^{-3} s^{-1}	
K_M	0.17	mg-at N m^{-3}	
$\left(\frac{N}{C}\right)_{min}$	0.000628	mg-at N mg C^{-1}	
α^B	–	$\frac{mg\ C\ mg\ Chl\ a^{-1}\ m^{-3}\ s^{-1}}{\mu Einstein\ m^{-2}\ s^{-1}}$	*see* page 84
β^B	–	$\frac{mg\ C\ mg\ Chl\ a^{-1}\ m^{-3}\ s^{-1}}{\mu Einstein\ m^{-2}\ s^{-1}}$	*see* page 84
P^B_{max10}	–	mg C mg Chl a^{-1} s^{-1}	*see* page 84
Q_{10}	2.3	adim.	
μ_{10}	$1.6\ 10^{-5}$	s^{-1}	
r_A	0.08	adim.	
r_{R10}	$1\ 10^{-9}$	s^{-1}	
m	$1\ 10^{-6}$	s^{-1}	

Tab. B.1: Parameter Values of the Biological Model. *See* chapter 6 for a description of the parameters.

C. VERTICAL ATTENUATION VALUES OF CHLOROPHYLL *A*, K_C (*FROM* SHANZ *et al.*, 1997); [NEXT PAGE]

Used Symbol	Value	Author
k_c	0.020–0.060	Riley, 1960
ε	0.0184	Aruga & Ichimura, 1968
K_s	0.01–0.02	Talling, 1970
K_s	0.01–0.02	Megard, 1972
a^*_{ph}	0.0138	Lorenzen, 1972
K_c	0.016	Bannister, 1974a
ε_s	0.012–0.016	Ganf, 1974
K_1	0.0415	Tyler, 1975
ε_s	0.006	Berman, 1976
ε_s	0.011	Jewson, 1976
K_s	0.0086	Bindloss, 1976
η	0.0043–0.0142	Kirk, 1976
a^*_{ph}	0.020–0.060	Morel & Prieur, 1977
k_c	0.029	Tilzer, 1978
k_c	0.016 ± 0.003	Simth & Baker, 1978a
k_c	0.014	Simth & Baker, 1978b
ε_c	0.009–0.038	Megard *et al.*, 1979
k_c	0.005–0.021	Atlas & Bannister, 1980
a^*_c	0.018–0.077	Prieur & Sathyendranath, 1981
k_c	0.0118–0.0166	Tilzer, 1983
k_c	0.0113–0.0166	Dubinsky *et al.*, 1984
K_c	0.022–0.037	Schanz, 1985
k_c	0.0038–0.021	Dubinsky *et al.*, 1986
k^*_j	0.0061–0.0195	Weidemann & Bannister, 1986
k_c	0.022–0.050	Kishino *et al.*, 1986
k_c	0.0035–0.014	Osborne & Raven, 1986
k_c	0.012–0.026	Schanz, 1986
a_{ph}	0.011–0.023	Maske & Haardt, 1987
k_c	0.0091–0.0422	Wyman *et al.*, 1987
a^*_{ph}	0.017–0.022	Bricaud & Stramski, 1990
ab^*	0.015–0.075	Agustí, 1991
a^*_{ph}	0.03–0.1	Hoepffner & Sathyendranath, 1992
a^*_{ph}	0.0206	Babin *et al.*, 1993

Tab. C.1: Vertical attenuation values of chlorophyll *a*. Values in $m^2 \cdot mg\ Chl\ a^{-1}$.

D. DEDUCTION OF GENERAL *QUANTUM YIELD* EQUATIONS

We begin with the equation (5.15)

$$\phi = \frac{P^B}{k_c \cdot E_d(z)}$$

where the *quantum yield* ϕ is defined in mg C·Einstein^{-1}.

We substitute P^B by the equation (5.2)

$$\phi = \frac{P^B_{max}}{k_c \cdot E_d} \left(1 - e^{-\frac{\alpha^B \cdot E_d}{P^B_{max}}}\right) \cdot \left(e^{-\frac{\beta \cdot E_d}{P^B_{max}}}\right)$$

and multiply the right hand term by ϕ_{max}/ϕ_{max}, and rearrange the ϕ_{max} from the numerator to the left hand term

$$\frac{\phi}{\phi_{max}} = \frac{P^B_{max}}{\phi_{max} \cdot k_c \cdot E_d} \left(1 - e^{-\frac{\alpha^B \cdot E_d}{P^B_{max}}}\right) \cdot \left(e^{-\frac{\beta \cdot E_d}{P^B_{max}}}\right) \tag{D.1}$$

Taking

$$\phi_{max} = \frac{\alpha^B}{k_c} \tag{D.2}$$

$$E_k = \frac{P^B_{max}}{\alpha^B} \tag{D.3}$$

By substituting ϕ_{max} from the right hand term and α^B into D.1, and rearranging, we get

$$\frac{\phi}{\phi_{max}} = \frac{E_k}{E_d} \left(1 - e^{-\frac{E_d}{E_k}}\right) \cdot \left(e^{-\frac{\beta \cdot I}{P^B_{max}}}\right)$$

After moving ϕ_{max} to the right, the yielding equation reads

$$\boxed{\phi = \phi_{max} \cdot \frac{E_k}{E_d} \left(1 - e^{-\frac{E_d}{E_k}}\right) \cdot \left(e^{-\frac{\beta \cdot I}{P^B_{max}}}\right)} \tag{D.4}$$

Part VII

REFERENCES

BIBLIOGRAPHY

[1] **Abraham, E.R.** (1998). The generation of plankton patchiness by turbulent stirring. *Nature*, 391: 577–580.

[2] **Agustí, S.** (1991). Light environment within dense algal populations: cell size influences on self-shading. *J. Plank. Res.*, 13: 863–871.

[3] **Amorocho, J. & J.J. deVries.** (1980). A new evaluation of the wind stress coefficient over water surfaces. *J. Geophys. Res.*, 85: 433–442.

[4] **Ames, W.F.** (1977). Numerical methods for partial differential equations. *Academic Press.* New York.

[5] **Anderson, R.F.** (1969). Subsurface chlorophyll maximum in the northeast Pacific ocean. *Limnol. Oceanogr.*, 14(3): 386–391.

[6] **Anderson, R.F., G.T. Kemp, S. Trumbores and P.E. Biscaye.** (1994). Carbon budget for the mid–slope depocenter in the Middle Atlantic Bight. *Deep–Sea Res.*, 41(2/3): 669–703.

[7] **Arrigo, K.R., D.H. Robinson, D.L. Worthen, R.B. Dunbar, G.R. DiTullio, M. VanWoert and M.P. Lizotte.** (1999). Phytoplankton community structure and the drawdown of nutrients and CO_2 in the South Ocean. *Science*, 283: 365–367.

[8] **Aruga, Y. & I. Ichimura.** 1968. Characteristics of photosynthesis of phytoplankton and primary production in the Kuroshio. *Bull. Mar. Biol. Inst. Kyoto Univ.*, 12: 29–50.

[9] **Atlas, D. & T.T. Bannister.** (1980). Dependence of mean spectral extinction coefficient of phytoplankton on depth, water color and species. *Limnol. Oceanogr.*, 25: 157–159.

[10] **Babin, M., J.-C. Therriault, L. Legendre and A. Condal.** (1993). Variations in the specific absorption coefficient for natural phytoplankton assemblages: Impact on estimates of primary production. *Limnol. Oceanogr.*, 38: 154–177.

[11] **Baker, K.S. & R. Frouin.** (1987). Relation between photosynthetically available radiation and total insolation at the ocean surface under clear skies. *Limnol. Oceanogr.*, 32: 1370–1377.

[12] **Bannister, T.T.** (1974a). Production equation in term of chlorophyll concentration, quantum yield, and upper limit to production. *Limnol & Oceanogr.*, 19: 1–12.

[13] **Bannister, T.T.** (1974b). A general theory of steady state phytoplankton growth in a nutrient saturated mixed layer. *Limnol & Oceanogr.*, 19: 13–30.

[14] **Banse, K.** (1987). Clouds, deep chlorophyll maxima and the nutrient supply to the mixed layer of stratified water bodies. *J. Plank. Res.*, 9(5): 1031–1036.

[15] **Batchelor, G.K.** (1959). Small–scale variation of convected quantities like temperature in turbulent fluid. *J. Fluid Mech.*, 5: 113-133.

[16] **Batchelor, G.K.** (1967). An introduction to fluid dynamics. Cambridge University Press. Cambridge. p. 615.

[17] **Beherenfeld, M.J. & P.G. Falkowski.** (1997). Photosynhetic rates derived from satellite–based chlorophyll concentration. *Limnol. Oceanogr.*, 42(1): 1–20.

[18] **Beherenfeld, M.J. & P.G. Falkowski.** (1997a). A consumer's guide to phytoplankton primary productivity models. *Limnol. Oceanogr.*, 42(7): 1479–1491.

[19] **Belayev, V.I.** (1992). Modelling the influence of turbulence on phytoplankton photosynthesis. *Ecol. Model.*, 60: 11–29.

[20] **Bennett, A.F. & K.L. Denman.** (1985). Phytoplankton patchiness: inferences from particle statistics. *J. Mar. Res.*, 43: 307–335.

[21] **Berg, H.C. & E.M. Purcell.** (1977). Physics of chemoreception. *Biophys. J.*, 20: 193–219.

[22] **Berman, T.** (1976). Light penetrance in Lake Kinneret. *Hydrobiologia*, 49: 41–48.

[23] **Berryman, A.A.** (1992). The origins and evolution of predator–prey theory. *Ecology*, 73(5): 1530–1535.

[24] **Bidigare, R.R., R.C. Smith, K.S. Baker and J. Marra.** (1987). Oceanic primary production estimates from measurements of spectral irradiance and pigment concentration. *Global Biogeochemical Cycles*, 1(3): 171–186.

[25] **Bidigare, R.R., B.B. Prézelin and R.C. Smith.** (1992). Bio–optical models and the problems of scaling. Pages: 175–212. *In:* Falkowski, P.G. & A.V. Woodhead. *Primary productivity and biogeochemical cycles in the sea*. Plenum Press. New York.

[26] **Bienfang, P.K., P.J. Harrison and L.M. Quarmby.** (1982). Sinking rate response to depletion of nitrate, phosphate and silicate. *Mar. Biol.*, 67: 295–302.

[27] **Bindloss, M.E.** (1976). The light-climate of Loch Leven, a shallow Scottish Lake, in relation to primary production by phytoplankton. *Fresh. Biol.*, 6: 501–508.

[28] **Bougeault, P. & J.C. André.** (1986). On the stability of the third–order turbulent closure for the modeling of the stratocumulus–topped boundary layer. *J. Atmos. Sci.*, 43: 1574–1581.

[29] **Bougeault, P. & P. Lacarrère.** (1989). Parametrization of orography–induced turbulence in a meso–beta scale model. *Mon. Weather Rev.*, 117: 1872–1890.

[30] **Boussinesq, J.** (1870). Essai théorique sur les lois trouvées expérimentalement par M. Bazin pour l'écolement uniforme de l'eau dans les canaux découverts. *C. R. Acad. Sci. Paris*, 271: 389–393.

[31] **Bricaud, A. & D. Stramski.** (1990). Spectral absorption coefficients of living phytoplankton and nonalgal biogeneous matter: a comparison between Peru upwelling area and the Sargasso Sea. *Limnol. Oceanogr.*, 35: 562–582.

[32] **Burns, B.D. & J. Beardall.** (1987). Utilization of inorganic carbon by marine microalgae. *J. Exp. Biol. Ecol.*, 107: 75-86.

[33] **Caperon, J.** (1968). Population growth response of *Isochrysis galbana* to nitrate variation at limiting concentration. *Ecology*, 49: 866–872.

[34] **Caperon, J. & J. Meyer.** (1972). Nitrogen-limited growth of marine phytoplankton II. Uptake kinetics and their role in nutrient limited growth of phytoplankton. *Deep-Sea Res.*, 19: 619–632.

[35] **Carpenter E.J. & D.G. Capone.** (1983). Nitrogen in the marine environment. Academic Press.

[36] **Chalup, M.S. and E.A. Laws.** (1990). A test of the assumptions and predictions of recent microalgal growth models with the marine phytoplankter *Pavlova lutheri*. *Limnol. Oceanogr.*, 35: 583–596.

[37] **Charney, J.G.** (1947). The dynamics of long waves in a baroclinic westerly current. *J. Meteor.*, 4: 135–163. (*op. cit.* in Frisch, 1995).

[38] **Cloern, J.E., C. Grenz and L. Videgar–Lucas.** (1995). An empyrical model of the phytoplankton chlorophyll: carbon ratio – the conversion factor between productivity and growth rate. *Limnol. Oceanogr.*, 40(7): 1313–1321.

[39] **Colman, B. & C. Rotatore.** (1995). Photosynthetic inorganic carbon uptake and accumulation in two marine diatoms. *Plant Cell Environ.*, 18: 919-924.

[40] **Colman, B. & K.A. Gehl.** (1983). Physiological characteristics of photosynthesis in *Porphyridium cruentum*: evidence for bicarbonate transport in an unicellular red alga. *J. Phycol.*, 19: 216-219.

[41] **Csandy, G.T.** (1986). Mass transfer to and from small particles in the sea. *Limnol. Oceanogr.*, 31: 237–248.

[42] **Cullen, J.J.** (1990). On models of growth and photosynthesis in phytoplankton. *Deep–Sea Res.*, 37(4): 667–683.

[43] **Cullen, J.J. & R.W. Eppley.** (1981). Chlorophyll maximum layers of the Southern Ocean California Bight and possible mechanisms of their formation and maintenance. *Oceanol. Acta.*, 4(1): 23–32.

[44] **Cullen, J.J., M.R. Lewis, C.O. Davis and R.T. Barber.** (1992). Photosynthetic characteristics and estimated growth rates indicate grazing is the proximate control of primary production in the equatorial Pacific. *J. Geophys. Res.*, 97(C1): 639–654.

[45] **Culver, M.E. & W.O. Smith Jr.** (1989). Effects od environmental variation on sinking rates of marine phytoplankton. *J. Phycol.*, 25: 262–270.

[46] **DeAngelis, D.L.** (1992). Dynamics of nutrient cycling and food webs. Chapman & Hall. United Kingdom. p. 270.

[47] **Denman, K.L. & M. Miyake.** (1973). Upper layer modifications at the ocean station Papa: observations and simulations. *J. Phys. Oceanogr.*, 3: 185–196.

[48] **Denman, K.L. & T. Platt.** (1976). The variance spectrum of phytoplankton in a turbulent ocean. *J. Mar. Res.*, 34: 593–601.

[49] **Denman, K.L., A. Okubo and T. Platt.** (1977). The chlorophyll fluctuation spectrum in the sea. *Limnol. Oceanogr.*, 22: 1033–1038.

[50] **Denman, K.L. & A.E. Gargett.** (1983). Time and space scales of vertical mixing and advection of phytoplankton in the open ocean. *Limnol. Oceanogr.*, 28(5): 801–815.

[51] **de Vahl Davis, G.** (1986). Numerical methods in engineering and science. titAllen & Unwin. London.

[52] **Dillon, T.M., J.G. Richman, C.G. Hausen and M.D. Pearson.** (1981). Near–surface turbulence measurements in a lake. *Nature*, 290: 390–392.

[53] **Dionisio-Sese, M.L. & S. Miyachi.** (1992). The effect of sodium chloride on carbonic anhydrase activity in marine microalgae. *J. Phycol.*, 28: 919-924.

[54] **Dixon, G.K., B.N. Patel and M.J. Merrett.** (1987). Role of intracellular carbonic anhydrase in inorganic carbon assimilation by *Porphyridium purpureum*. *Planta*, 172: 508-513.

[55] **Dixon, G.K. & M.J. Merret.** (1988). Bicarbonate utilization by the marine diatom *Phaeodactylum tricornutum* Bohlin. *New. Phytol.*, 109: 47-51.

[56] **DOE.** (1994). Handbook of methods for the analysis of the various parameters of the carbon dioxide system in sea water; v.2. A.G. Dickson & C. Goyet (eds.), ORNL/CDIAC-74. (`http://www-mpl.ucsd.edu/people/adickson/CO2_QC`).

[57] **Doney, S.C., D.M. Glover and R.G. Najjar** (1996). A new coupled, one–dimension biological–physical model for the upper ocean: applications to the JGOFS Bermuda Atlantic time series study (BATS) site. *Deep–Sea Res.*, 43(2–3): 591–624.

[58] **Droop, M.R.** (1968). Vitamin B_{12} and marine ecology. IV. The kinetics of uptake, growth and inhibition in *Monochrysis lutheri*. *J. Mar. Biol. Ass. U.K.*, 48: 689–733.

[59] **Droop, M.R.** (1973). Some thoughts on nutrient limitation in algae. *J. Phycol.*, 9: 264–733.

[60] **Droop, M.R.** (1974). The nutrient status of algal cells in continuous culture. *J. Mar. Biol. Ass. U.K.*, 54: 825–855.

[61] **Droop, M.R.** (1977). An approach to quantitative nutrition of phytoplankton. *J. Protozool.*, 24: 528–532.

[62] **Droop, M.R.** (1983). 25 years of algal growth kinetics. *Bot. Mar.*, 26: 99–112.

[63] **Droop, M.R., M.J. Mickelson, J.M. Scott and M.F. Turner.** (1982). Light and nutrient status of algal cells. *J. Mar. Biol. Ass. U.K.*, 62: 403–434.

[64] **Dubinsky, Z., T. Berman and F. Schanz.** (1984). Field experiments for *in situ* measurement of photosynthetic efficiency and quantum yield. *J. Plank. Res.*, 6: 339–349.

[65] **Dubinsky, Z., P.G. Falkowski and K. Wyman.** (1986). Light harvesting and utilization by phytoplankton. *Plant Cell Physiol.*, 27: 1335–1349.

[66] **Dubois, D.M.** (1975). Simulation of the spatial structuration of a patch of prey-predator plankton populations in the Southern Bight of the North Sea. *Mém. Soc. R. Sci. Liège*, 6e 7: 75–82.

[67] **Dugdale, R.C.** (1967). Nutrient limitation in the sea: dynamics, identification and significance. *Limnol. Oceanogr.*, 12: 685–695.

[68] **Duce, R.A., P.S. Liss, J.T. Merrill, E.L. Atlas, P. Buat-Menard, B.B. Hicks, J.M. Miller, J.M. Prospero, R. Arimoto, T.M. Church, W. Ellis, J.N. Galloway, L. Hansen, T.D. Jickells, A.H. Knap, K.H. Reinhardt, B. Schneider, A. Soudine, J.J. Tokos, S. Tsunogai, R. Wollast and M. Zhou.** (1991). The atmospheric input of trace species to the world ocean. *Global Biogeoch. Cyc.*, 5(3): 193–259.

[69] **Dugdale, R.C. & J.J. Goering.** (1967). Uptake of new and regenerated forms of nitrogen in primary productivity. *Limnol. Oceanogr.*, 12: 196–206.

[70] **Dugdale, R.C., A. Morel, A. Bricaud and F.P. Wilkerson.** (1989). Modeling new production in upwelling centers: a case of modeling new production from remotely sensed temperature and color. *J. Geophys. Res.*, 94(C12): 18119–18132.

[71] **Durbin, E.G., R.W. Krawiec and T.J. Smayda.** (1975). Seasonal studies on the relative importance of different size fractions on phytoplankton in Narrangasett Bay (USA). *Mar. Biol.*, 32: 271–287.

[72] **Elser, J.J., M.M. Elser, N.A. MacKay and S.R. Carpenter.** (1988). Zooplankton–mediated transitions between N– and P–limited algal growth. *Limnol. Oceanogr.*, 33(1): 1–14.

[73] **Elser, J.J. and R.P. Hassett.** (1994). A stoichiometric analysis of the zooplankton–phytoplankton interaction in marine and freshwater ecosystem. *Nature*, 370: 211–213.

[74] **Eppley, R.W.** (1972). Temperature and phytoplankton growth in the sea. *Fish Bull.*, 70(4): 1063–1085.

[75] **Eppley, R.W. & P.R. Sloan.** (1966). Growth rates of marine phytoplankton: correlation with light absorption by cell chlorophyll *a*. *Physiol. Plant.*, 19: 47–59.

[76] **Eppley, R.W. & B.J. Peterson.** (1979). Particulate organic matter flux and planktonic new production in the deep ocean. *Nature*, 282: 677-680.

[77] **Estrada, M. & E. Berdalet.** (1997). Phytoplankton in a turbulent world. *Sci. Mar.*, 61(Supl. 1): 125-140.

[78] **Evans, G.T. & V. Garçon.** (1997). One-dimensional models of water column biogeochemistry. (eds.) *JGOFS Report*, 23. Homepage: `http://ads.smr.uib.no/jgofs/publications/on-line/report23/coverpage.htm`.

[79] **Falkowski, P.G.** (1981). Light–shade adaptation in marine phytoplankton. In: Falkowski, P.G. *Primary productivity in the sea.* Plenum Press. New York.

[80] **Falkowski, P.G.** (1981). Light–shade adaptation and assimilation numbers. *J. Plank. Res.*, 3(2): 203–216.

[81] **Falkowski, P.G. & A.D. Wookhead.** (1992). Primary prodcutivity and biogeochemical cycles in the sea. (eds.) Plenum Press. New York.

[82] **Fasham, M.J.R., H.W. Ducklow and S.M. McKelvie.** (1990). A nitrogen–based model of plankton dynamics in the ocean mixed–layer. *J. Mar. Res.*, 48: 591–639.

[83] **Fiedler, F. & H.A. Panofsky.** (1970). Atmospheric scales and spectral gaps. *Bull. Amer. Meteor. Soc.*, 51(12): 1114–1119.

[84] **Field, C.B., M.J. Behrenfeld, J.T. Randerson and P. Falkowski.** (1998). Primary production of the biosphere: integrating terrestrial ans oceanic components. *Science*, 281: 237–240.

[85] **Fife, P.C.** (1976). Pattern formation in reacting and diffusing systems. *J. Chem. Phys.*, 64: 554–564.

[86] **Fong, P., T.C. Foin and J.B. Zedler.** (1994). A simulation model of lagoon algae based on nitrogen competition and internal storage. *Ecol. Monogr.*, 64(2): 225–247.

[87] **Franks, P.S. & J. Marra.** (1994). A simple new formulation for phytoplankton photoresponse and an application in a wind–driven mixed–layer model. *Mar. Ecol. Progr. Ser.*, 111: 143–153.

[88] **Fransz, H.G., J.P. Mommaerts and G. Radach.** (1991). Ecological modelling of the North Sea. *Neth. J. Sea Res.*, 28(1/2): 67–140.

[89] **Frisch, U.** (1995). *Turbulence*. Cambridge University Press. Cambridge. U.K.

[90] **Gabaldon, J.E.** (1996). Models matematics en ecologia. Unpublished manuscript. p. 9.

[91] **Gallegos, C.L. & T. Platt.** (1981). Photosynthesis measurements on natural populations of phytoplankton: Numerical analysis. *In* I. Platt (ed.) Physiological bases of phytoplankton ecology. *Can. Bull. Fish. Aquat. Sci.*, 210: 103–111.

[92] **Gama, S., M. Vergassola and U. Frisch.** (1994). Negative eddy viscosity in isotropically forced two–dimensional flow: linear and nonlinear dynamics. *J. Fluid Mech.*, 260: 95–126.

[93] **Ganf, G.G.** (1974). Incident solar irradiance and underwater light penetrance as factors controlling chlorophyll *a* content of a shallow eutrophic lake (Lake George, Uganda). *J. Ecol.*, 62: 593–609.

[94] **Gargett, A.E.** (1984). Vertical eddy diffusivity in the ocean interior. *J. Mar. Res.*, 42: 359–393.

[95] **Gargett, A.E.** (1989). Ocean turbulence. *Ann. Rev. Fluid Mech.*, 21: 419–451.

[96] **Gaspar, P., Y. Grégoris & J.–M. Lefevre.** (1990). A simple eddy kinetic energy model for simulations of the oceanic vertical mixing: tests at station Papa and Long–Term Upper Ocean Study site. *J. Geophys. Res.*, 95(C9): 16179–16193.

[97] **Gavis, J.** (1976). Munk and Riley revisited: nutrient diffusion transport and rates of phytoplankton growth. *J. Mar. Res.*, 34: 161–179.

[98] **Geider, R.J.** (1987). Light and temperature dependence of the carbon to chlorophyll *a* ratio in microalgae and cyanobacteria: Implications for physiology and growth of phytoplankton. *New Phytol.*, 106: 1–34.

[99] **Gibson, C.H. & W.H. Schwarz.** (1963). Detection of conductivity fluctuations in a turbulent flow field. *J. Fluid Mech.*, 20: 357–364.

[100] **Glibert, P.M., M.R. Dennett and J.C. Goldman.** (1985). Inorganic carbon uptake by phytoplankton in Vineyard Sound, Massachusetts. I. Measurements of photosynthesis-irradiance responses of winter and early spring assemblages. *J. Exp. Mar. Biol. Ecol.*, 86: 21–36.

[101] **Goel, N.S., S.C. Maitra and E.W. Montroll.** (1971). On the Volterra and other non-linear models of interaction populations. *Rev. Mod. Phys.*, 43: 231–276.

[102] **Granata, T.C. & T.D. Dickey.** (1991). The fluid mechanics of copepod feeding in turbulent flow: a theoretical approach. *Progr. Oceanogr.*, 26: 243–261.

[103] **Gregg, M.C.** (1987). Dyapicnal mixing in the thermocline: a review. *J. Geophys. Res.*, 92(C5): 5249–5286.

[104] **Gregg, M.C., H. Peters, J.C. Wesson, N.S. Oakey and T.J. Shay.** (1985). Intensive measurements of turbulence and shear in the equatorial undercurrent. *Nature*, 318: 140–144.

[105] **Gregg, M.C., E.A. D'Assaro, T.J. Shay and N. Larson.** (1986). Observations of persistent mixing and near inertial internal waves. *J. Phys. Oceanogr.*, 16: 856–885.

[106] **Gruber, N.** (1998). Anthropogenic CO_2 in the Atlantic Ocean. *Glob. Biogeo. Cycl.*, 12(1): 165–191.

[107] **Gruber, N. & J.L. Sarmiento.** (1997). Global patterns of marine nitrogen fixation and denitrification. *Glob. Biogeo. Cycl.*, 11(2): 235–266.

[108] **Grum, F. & R.J. Becherer.** (1979). Optical radiant energy. Vol. 1. Academic Press. London.

[109] **Häse, C.** (1996). Die Vorhersage der Produktivität des Phytoplanktons im Bodensee unter Berücksichtigung det Temperatur sowie der spektralen Zusammensetzung des Unterwasser–Strahlungsfeldes. *Konstanzer Dissertationen*; Bd. 514. Konstanz Univ. Germany.

[110] **Hastings, A.** (1990). Spatial Heterogenity and ecological models. *Ecology*, 71(2): 426–428.

[111] **Hastings, A.** (1996). Ecosystem modelling: can it be done all? *Ecology*, 77(6),1957.

[112] **Herut, B., M.D. Krom, G. Pan and R. Mortimer.** (1999). Atmospheric input of nitrogen and phosphorus to the Southeast Mediterranean: Sources, fluxes and possible impact. *Limnol. Oceanogr.*, 44(7): 1683–11692.

[113] **Hinze, J.O.** (1959). *Turbulence*. McGraw–Hill. New York.

[114] **Hoepffner, N. & S. Sathyendranath.** (1992). Bio-optical characteristics of coastal waters: absorption spectra of phytoplankton and pigment distribution in the western North Atlantic. *Limnol. Oceanogr.*, 37: 1660–1679.

[115] **Hoge, F.E. & R.N. Swift.** (1993). The influence of chlorophyll pigment upon upwelling spectral radiances from the North Atlantic Ocean: an active-passive correlation spectroscopy study. *Deep-Sea Res.*, 40(1/2): 265–277.

[116] **Hopfinger, E.J.** (1987). Turbulence in stratified fluids: A review. *J. Geophys. Res.*, 92(C5): 5287–5303.

[117] **Howarth, R.W.** (1988). Nutrient limitation of net primary production in marine ecosystems. *Ann. Rev. Ecol. Syst.*, 19: 89–110.

[118] **Jamart, B.M., D.F. Winter, K. Banse, G.C. Anderson and R.K. Lam.** (1977). A theoretical study of phytoplankton growth and nutrient distribution in the Pacific Ocean off the northwestern US coast. *Deep-Sea Res.*, 24: 753–773.

[119] **Jassby, A.D. & T. Platt.** (1976). Mathematical formulation of the relationship between photosynthesis and light for phytoplankton. *Limnnol. & Oceanogr.*, 21: 540–547.

[120] **Jewson, N.G.** (1976). The interaction of components controlling net photosynthesis in a well mixed lake (Lough Neagh, Northern Ireland). *Freshwater Biol.*, 6: 551–576.

[121] **JGOFS Synthesis and Modeling Project.** (1997). U.S. JGOFS Implementation Plan, SCOR.

[122] **Jitts, H.R.** (1963). The simulated *in situ* measurements of oceanic primary production. *Aust. J. Mar. Freshwater Res.*, 14: 139–147.

[123] **Jou, D.** (1997). Intermitent turbulence: a short introduction. *In:* Marrasé, C., E. Saiz and J.M. Redondo (eds.). Lectures on Plankton and Turbulence. *Sci. Mar.*, 61(Supl. 1): 57–62.

[124] **Kármán, T. von** (1930). Mechanische Änlichkeit und Turbulenz. *Nachr. Ges. Wiss. Göttingen, Math–Phys.*, K1: 58–76.

[125] **Karp-Boss, L., E. Boss & P.A. Jumars.** (1996). Nutrient fluxes to planktonic osmotrophs in the presence of fluid motion. *Oceanogr. Mar. Biol.: Ann. Rev.*, 34: 71–107.

[126] **Karp-Boss, L. & P.A. Jumars.** (1998). Motion of diatom chains in a steady shear flow. *Limnol. Oceanogr.*, 43(8): 1767–1773.

[127] **Keller, A.A.** (1989). Modeling the effects of temperature, light and nutrients on primary productivity: An empyrical and mechanistic approach compared. *Limno. Oceanogr.*, 34(1): 82–95.

[128] **Kerby, N.W. & J.A. Raven.** (1985). Transport and fixation of inorganic carbon by marine algae. *Adv. Bot. Res.*, 11: 71-123.

[129] **Kiefer, D.A. & B.G. Mitchell.** (1983). A simple, steady state description of phytoplankton growth based on absorption cross section and quantum efficiency. *Limnol & Oceanogr.*, 28: 770–776.

[130] **Kingsland, S.E.** (1985). Modeling nature. Episodes in the History of Population Ecology. The Univerity of Chicago Press. Chicago. p. 267.

[131] **Kiørboe, T.** (1993). Turbulence, phytoplankton cell size and the structure of pelagic food webs. *Adv. Mar. Biol.*, 29: 1–72.

[132] **Kirstead, H. & L.B. Slobodkin.** (1953). The size of water masses containing plankton bloom. *J. Mar. Res.*, 12: 141–147.

[133] **Kirk, J.T.O.** (1983, 1994 2^{nd} ed.). Light and photosynthesis in aquatic ecosystems. Cambridge University Press. Cambridge. U.K. 509 pages.

[134] **Kishino, M., N. Okami, M. Takahashi and S. Ichimura.** (1986). Light utilization efficiency and quantum yield of phytoplankton in a termally stratified sea. *Limnol. Oceanogr.*, 31: 557–566.

[135] **Kolmogorov, A.N.** (1941). The local structure of turbulence in incompressible viscous fluid for very large Reynolds number. *Dokl. Akad. Nauk S.S.S.R.*, 30: 9-13 (reprinted in *Proc. R. Soc. Lond*, A, 434: 9-13.

[136] **Kraichman, R.H.** (1976). Eddy viscosity in two and three dimensions. *J. Atmos. Sci.*, 33: 1521–1536.

[137] **Kundu, P.K.** (1990). Fluid mechanics. Academic Press. San Diego. p. 639.

[138] **Laws E.A. & T.T. Bannister.** (1980). Nutrient– and light–limited growth of *Thalassiosira fluviatilis* in continuous culture, with implications for phytoplankton growth in the ocean. *Limnol. Oceanogr.*, 25: 457–473.

[139] **Lazier, J.R.N. & K.H. Mann.** (1989). Turbulence and the diffusive layers around small organisms. *Deep–Sea Res.*, 36(11): 1721–1733.

[140] **Levin, S.A.** (1976). Population dynamics in heterogeneous environments. *Ann. Rev. Ecol. Syst.*, 7: 287–310.

[141] **Levin, S.A.** (1978). Population models and community structure in heterogeneous environments. *In:* Levin, S.A. (ed.) *Studies in Mathematical Biology. Part II: Populations and Communities.* Vol. 16. MAA Studies in Mathematics.

[142] **Lewis, E. & D.W.R. Wallace** (1998). Program Developped for CO2 System Calculations. ORNL/CDIAC-105. Carbon Dioxide Information Analysis Center, Oak Ridge National Laboratory, U.S. Department of Energy, Oak Ridge, Tennessee. (`ftp://cdiac.esd.ornl.gov/ftp/co2sys.txt`).

[143] **Li, Y.-H. & S. Gregory.** (1974). Diffusion of ions in sea water and in deep-sea sediments. *Geochim. Cosmochim. Acta*, 38:703-714.

[144] **Li, W.K.W.** (1980). Temperature adaptation in phytoplankton: cellular and photosynthetic characteristics. In: Falkowski, P.G. *Primary productivity in the sea.* Plenum Press. New York. p. 259–279.

[145] **Li, W.K.W., J.C. Smith and T. Platt.** (1981). Temperature response of photosynthetic capacity and carbolxylase activity in Arctic marine phytoplankton. *Mar. Ecol. Progr. Ser.*, 17: 237–243.

[146] **Lilly, D.K., D.E. Waco and S.I. Adelfang.** (1974). Stratospheric mixing estimated from high–altitude turbulence meassurements. *J. Appl. Meteorol.*, 13: 488–493.

[147] **Lomas, M.W. & P.M. Glibert.** (1999). Temperature regulation if nitrate uptake: A novel hypothesis about nitrate uptake and reduction in cool-water diatoms. *Limnol. Oceanogr.*, 44(3): 556–572.

[148] **Longhurst, A.R. and W.G. Harrison.** (1988). Vertical nitrogen flux from the oceanic photic zone by diel migrant zooplankton and nekton. *Deep–Sea Res.*, 35(6): 881–889.

[149] **Lorenzen, C.J.** (1972). Extinction of light in the ocean by phytoplankton. *J. Cons., Cons. Int. Explor. Mer*, 34: 262–267.

[150] **MacIsaac, J.J. & R.C. Dugdale.** (1969). The kinetics of nitrate and ammonia uptake by natural populations of marine phytoplankton. *Deep-Sea Res.*, 16: 45–57.

[151] **MacKenzie, B.R. & W.C. Leggett.** (1991). Quantifying the contribution of small–scale turbulence to the encounter rates between larval fish and their zooplankton prey: effects of wind and tide. *Mar. Ecol. Progr. Ser.*, 73: 149–160.

[152] **Mann, K.H. & J.R.N. Lazier.** (1991). Dynamics of marine ecosystems. Ed. Blackwell Scientific. Boston. p. 466.

[153] **Margalef, R.** (1969). Ecología. Ed. Omega. Barcelona. p. 952.

[154] **Margalef, R.** (1978). Life-forms of phytoplankton as survival alternatives in an unstable environment. *Oceanol. Acta*, 1: 493-509.

[155] **Margalef, R.** (1980). La biosfera: entre la termodinámica y el juego. Ed. Omega. Barcelona. p. 236.

[156] **Margalef, M. & M. Estada.** (1987). Synoptic distribution of summer microplankton (Algae and Protozoa) across the principal front in the Western Mediterranean. *Inv. Pesq.*, 51: 121–140.

[157] **Margalef, R.** (1991). Teoría de los sistemas ecológicos. Publicacions Universitat de Barcelona. Barcelona. p. 290.

[158] **Marrasé, C., J.H. Costello, T. Granata and J.R. Strickler.** (1990). Grazing in a turbulent environment. II. Energy dissipation, encounter rates and efficiency of feeding currents in *Centropages hamatus*. *Proc. Natl. Acad. Sci. USA*, 87: 1653–1657.

[159] **Maske, H. & H. Haardt.** (1987). Quantitative *in vivo* absorption spectra of phytoplankton: detrital absorption and comparison with fluorometric excitation spectra. *Limnol. Oceanogr.,* 32: 620–633.

[160] **Masó, M. & Grupo Varimed.** (1995). Datos oceanográficos Básicos de las Campañas "FRONTS 1992" (octubre–noviembre 1992) y "Variabilidad de Mesoescala en el Mediteráneo Occidental" (junio 1993). *Datos informativos*, 27. Institut de Ciències del Mar. CSIC. p. 117.

[161] **McComb, W.D.** (1990). *The physics of fluid turbulence*. Oxford Science Publications. Oxford. U.K.

[162] **McCreary, J.P.** (1981). A linear, stratified ocean model of the equatorial undercurrent. *Philos. Trans. R. Soc. London, Ser. A,* 298: 603–635.

[163] **McGillicuddy, D.F. Jr & A.R. Robinson.** (1997). Eddy–induced nutrient supply and new production in the Sargasso Sea. *Deep–Sea Res.*, 44(8): 1427–1450.

[164] **McGowan, J.A., D.R. Cayan and L.M. Dorman.** (1998). Climate–ocean variability and ecosystem response in the northeast Pacific. *Science*, 281: 210–217.

[165] **Megard, R.O.** (1972). Phytoplankton, photosynthesis and phosphorous in Lake Minnetonka, Minnesota. *Limnol. Ocenogr.*, 17: 68–87.

[166] **Megard, R.O., W.S. Jr. Combs, P.D. Smith and A.S. Knoll.** (1979). Attenuation of light and integral rates of photosynthesis attained by planctonic algae. *Limnol. Oceanogr.,* 24: 1038–1050.

[167] **Mellor, G.L. & T. Yamada.** (1974). A hierarchy of turbulence closure models for planetary layers. *K. Atmos. Sci.*, 31: 1791–1806.

[168] **Mellor, G.L. & T. Yamada.** (1982). Development of a turbulence closure model for geophysical fluid problems. *Rev. Geophys.*, 20: 851–875.

[169] **Mendelli, E.F., P.R. Burkholder, T.E. Doheny and R. Brody.** (1970). Studies of primary productivity in coastal waters of southern Long Island, New York. *Mar. Biol.*, 7: 153–160.

[170] **Merrett, M.J., L.F. Dong and N.A. Nimer.** (1993). Nitrate availability and calcite production in *Emiliana huxleyi* Lohmann. *Eur. J. Phycol.*, 28: 243-246.

[171] **Millero, F.J. & A. Poisson.** (1981). International one–atmosphere equation of state of seawater. *Deep–Sea Res.*, 28A(6): 625–629.

[172] **Mitchell G. & O. Holm–Hansen.** (1991). Observations and modeling of the Anctartic phytoplankton crop in relation to mixing depth. *Deep–Sea Res.*, 38(8/9): 981–1007.

[173] **Mobley, C.D.** (1994). Light and Water. Academic Press. San Diego.

[174] **Monin, A.S. & A.M. Yaglom.** (1975). Statistical fluid mechanics: mechanics of turbulence. MIT Press. Cambridge.

[175] **Monod, J.** (1950). La technique de la culture continue: Theorie et applications. *Ann. Inst. Pasteur Lille*, 79: 390–410.

[176] **Morel, A. & R.C. Smith.** (1974). Relation between quanta and total energy for aquatic photosynthesis. *Limnol. Oceanogr.*, 19: 591–600.

[177] **Morel, A. & L. Prieur.** (1977). Analysis of variation in ocean color. *Limnol. Oceanogr.*, 22: 709–722.

[178] **Morel, A.** (1991). Light and marine photosynthesis: a spectral model with geochemical and climatological implications. *Progr. Oceanogr.*, 26: 263–306.

[179] **Morel, F.M.M.** (1994). Zinc and carbon co-limitation of marine phytoplankton. *Nature*, 369: 740-742.

[180] **Moum, J.N., D.R. Caldwell and C.A. Paulson.** (1989). Mixing in the equatorial surface layer and thermocline. *J. Geophys. Res.*, 94: 2005–2021.

[181] **Nimer, N.A., M.J. Merrett and C. Brownlee.** (1996). Inorganic carbon transport in relation to culture age and inorganic carbon concentration in a high-calcifying strain *Emiliana huxleyi* (Prymnesiophyceae). *J. Phycol.*, 32: 813-818.

[182] **Nimer, N.A., M.D. Iglesias-Rodríguez and M.J. Merrett.** (1997). Bicarbonate utilization by marine phytoplankton species. *J. Phycol.*, 33: 625-631.

[183] **Nixon, S.W. & M.E.Q. Pilson.** (1983). Nitrogen in estuarine and coastal ecosystems. pages:565–648. *In:* Carpenter E.J. & D.G. Capone [eds.] *Nitrogen in the marine environment.*. Academic Press.

[184] **Oakey, N.S.** (1982). Determination of the rate of dissipation of turbulent energy from simultaneous temperature and velocity shear microstructure measurements. *J. Phys. Oceanogr.*, 12: 256–271.

[185] **Oakey, N.S. & J.A Elliott.** (1982). Dissipation within the surface mixed layer. *J. Pyhs. Oceanogr.*, 12: 83–89.

[186] **Okubo, A.** (1980). Diffusion and ecological problems: Mathematical models. Springer–Verlag. Berlin. p. 254.

[187] **Olsen, Y., A. Jansen, H. Reinertsen and B. Rugstad.** (1983). Comparison of different algal carbon estimates by use of the Droop–model for nutrient limited growth. *J. Plank. Res.*, 5(1): 43–51.

[188] **Olsen, Y., A. Jansen, H. Reinertsen, K.Y. Borsheim, M. Heldal and A. Langeland.** (1986). Dependence of the rate of release of phosphorous by zooplankton on the P: C ratio of food supply, as calculated by a recycling model. *Limnol. Oceanogr.*, 31(1): 34–44.

[189] **Osborn, T.R.** (1980). Estimates of the local rate of vertical diffusion from dissipation measurements. *J. Phys. Oceanogr.*, 10: 83–89.

[190] **Osborn, T.R.** (1996). The role of turbulent diffusion for copepods with feeding currents. *J. Plank. Res.*, 18: 185–195.

[191] **Osborn, T.R. & R.G. Lueck.** (1985). Turbulence measurements with a submarine. *J. Phys. Oceanogr.*, 15: 1502–1520.

[192] **Osborne, B.A. & J.A. Raven.** (1986). Growth light level and photon absorption by cells of *Chlamydomonas rheinhardii, Dunaliella tertiolecta* (Chlorophyceae, Volvocales), *Scenedesmus obliquus* (Chlorophyceae, Chlorococcales) and *Euglena viridis* (Euglenophyceae, Euglenales). titBrit. Phycol. Soc., 21: 303–313.

[193] **Ozmidov, R.V.** (1965). On the turbulent exchange in a stably stratified ocean. (English translation) *Izv. Acad. Sci. USSR Atmos. Oceanic Phys.*, 8: 853–.

[194] **Paerl, H.W.** (1997). Coastal eutrophication and harmful algal blooms: Importance of atmospheric deposition and groundwater as *new* nitrogen and other nutrient sources. *Limnol. Oceanogr.*, 42(5): 1154–1165.

[195] **Pahl–Wostl, C.** (1995). The dynamic nature of ecosystems: chaos and order entwined. Wiley and Sons. New York. p. 267.

[196] **Pahlow, M., U. Riebesell and A. Wolf–Gladrow.** (1997). Impact of cell shape and chain formation on nutrient acquisition by marine diatoms. *Limnol. Oceanogr.*, 42: 1660–1672.

[197] **Painting, S.J., C.L. Moloney and M.I. Lucas.** (1993). Simulation and field measurements of phytoplankton–bacteria–zooplankton interactions in the southern Benguela upwelling region. *Mar. Ecol. Progr. Ser.*, 100: 55–69.

[198] **Pakanowski, R.C. and S.G.H. Philander.** (1981). Parameterization of vertical mixing in numerical models of tropical oceans. *J. Phys. Oceanogr.*, 11: 1443–1451.

[199] **Panofsky, H.A. & J.A. Dutton.** (1984). Atmospheric turbulence. Wiley. New York.

[200] **Pasciak, W.J. & J. Gavis.** (1974). Transport limitation of nutrient uptake in phytoplankton. *Limnol. Oceanogr.*, 19: 881–888.

[201] **Pasciak, W.J. & J. Gavis.** (1975). Transport limited nutrient uptake rates in *Ditylum brightwellii*. *Limnol. Oceanogr.*, 20: 604–617.

[202] **Patten, B.C.** (1968). Mathematical models of plankton production. *Int. Rev. ges. Hydrobiol.*, 53: 357–408.

[203] **Peters, H., & M.C. Gregg and J.M. Toole.** (1988). On the parameterization of equatorial turbulence. *J. Geophys. Res.*, 93: 1199–1218.

[204] **Peters, F. & J.M. Redondo.** (1997). Turbulence generation and measurement: application to studies on plankton. *In:* Marrasé, C., E. Saiz and J.M. Redondo (eds.). Lectures on Plankton and Turbulence. *Sci. Mar.*, 61(Supl. 1): 205–228.

[205] **Pielou, E.C.** (1969). An introduction to mathematical ecology. J. Wiley & Sons. New York.

[206] **Pielou, E.C.** (1977). Mathematical ecology. J. Wiley & Sons. New York.

[207] **Platt, T.** (1972). Local phytoplankton abundance and turbulence. *Deep-Sea Res.*, 19: 183–187.

[208] **Platt, T. & K.L. Denman.** (1975). A general equation for the mesoscale distribution of phytoplankton in the sea. *Mém. Soc. R. Sci. Liège*, 7: 31–42.

[209] **Platt, T, C.L. Gallegos and W.G. Harrison.** (1980). Photoinhibition of photosynthesis in natural assamblages of marine phytoplankton. *J. Mar. Res.*, 38: 687–701.

[210] **Platt, T., D.F. Bird and S. Sathyendranath.** (1991). Critical depth and marine primary production. *Proc. R. Soc. Lond., B*, 246: 205–217.

[211] **Ploug, H., M. Kühl, B. Buchholz-Cleven and B.B. Jørgensen.** (1997). Anoxic aggregates — an ephemeral phenomenon in the pelagic environment? *Aquat. Microb. Ecol.*, 13: 285-294.

[212] **Ploug, H., W. Stolte, E.H.G. Epping and B.B. Jørgensen.** (1999a). Diffusive boundary layers, photosynthesis, and respiration of the colony-forming plankton algae, *Phaeocystis* sp. *Limnol. Oceanogr.*, 44(8): 1949-1958.

[213] **Ploug, H., W. Stolte and B.B. Jørgensen.** (1999b). Diffusive boundary layers of the colony-forming plankton alga, *Phaeocystis* sp.— implicationsfor nutrient uptake and cellular growth *Limnol. Oceanogr.*, 44(8): 1959-1967.

[214] **Powell, T.M., P.J. Richerson, T.M. Dillon, B.A. Agee, B.J. Dozier, D.A. Godden and L.O. Myrup.** (1975). Spatial scales of current speed and phytoplankton biomass fluctuations in Lake Tahoe. *Science*, 189: 1088–1089.

[215] **Powell, T.M. & A. Okubo.** (1994). Turbulent diffusion and patchiness in the sea. *Phil. Trans. R. Soc. London Ser. B*, 343: 11–18.

[216] **Prandtl, A.** (1925). Bericht über Untersuchungen zur ausgebildeten Turbulenz. *Zs. angew. Math. Mech.*, 5: 136-139.

[217] **Press, W.H., S.A. Teukolsky, W.T. Vetterling and B.P. Flannery.** (1992). Numerical recipes in C. The art of scientific calculation. 2nd Ed. Cambridge University Press. Cambridge.

[218] **Prieur, L. & S. Sathyendranath.** (1981). An optical classification of coastal and oceanic waters based on the specific spectral absorption curves of phytoplankton pigments, dissolved organic matter, and other particulate materials. *Limnol. Oceanogr.*, 26: 671–689.

[219] **Prospero, J.M., K. Barrett, T. Church, F. Dentener, R.A. Duce, J.N. Galloway, H. Levy II, J. Moody and P. Quinn.** (1996). Atmospheric deposition of nutrients to the North Atlantic Basin. *Biogeochem.*, 35:27–73.

[220] **Purcell, E.M.** (1977). Life at low Reynolds number. *Amer. J. Phys.*, 45: 3-11.

[221] **Purcell, E.M.** (1977). The effect of fluid motionson the absorption of molecules by suspended particles *J. Fluid Mech.*, 84: 551-559.

[222] **Radach, G. & E. Maier–Reimer.** (1975). The vertical structure of phytoplankton growth dynamics. A mathematical model. *Mém. Soc. R. Sci. Liège*, 6e 7: 113–146.

[223] **Rau, G.H., U. Riebesell and D. Wolf-Gladrow.** (1996). A model of photosynthetic ^{13}C fractionation by marine phytoplankton based on diffusive molecular CO_2 uptake. *Mar. Ecol. Progr. Ser.*, 133: 275-285.

[224] **Raven, J.A.** (1984). Energetics and Transport in Aquatic Plants. Liss Press. New York.

[225] **Raven, J.A. & F.A. Smith.** (1980). *In*: Spanswick, R.M., W.J. Lucas and J. Dainty (eds.) Plant membrane transport: current concenptuals issues. Elsevier. Amsterdam.

[226] **Raven, J.A., A.M. Johnson and D.H. Turpin.** (1993). Influence of changes in CO_2 concentration and temperature on marine phytoplankton $^{13}C/^{12}C$ ratios: an analysis of possible mechanisms. *Global Planet. Change*, 8: 1-12.

[227] **Redondo, J.M.** (1990). The structure of density interfaces. PhD Thesis. University of Cambridge. Cambridge. U.K.

[228] **Reynolds, O.** (1895). On the dynamical theory of incompressible viscous fluids and the determination of the criterion. *Phil. Trans. R. Soc. London*, Ser. A, 186: 1–123.

[229] **Richtmyer, R.D. & K.W. Morton.** (1967). Difference methods for initial value problems. *Wiley-Intescience.* New York.

[230] **Riebesell, U.** (1991a). Particle aggregation during a diatom bloom. I. Physical aspects. *Mar. Ecol. Progr. Ser.*, 69: 273–280.

[231] **Riebesell, U.** (1991b). Particle aggregation during a diatom bloom. II. Biological aspects. *Mar. Ecol. Progr. Ser.*, 69: 281–291.

[232] **Riebesell, U.** (1992). The formation of large marine snow and its sustained residence in surface waters. *Limnol. Oceanogr.*, 37(1): 63–76.

[233] **Riebesell, U., D.A. Wolf–Gladrow and V. Smatacek.** (1993). Carbon dioxide limitation of marine phytoplankton growth rates. *Nature*, 361: 249–251.

[234] **Riley, G.A.** (1956). Oceanography of Long Island Sound 1952–54. Production and utilization of organic matter. *Bull. Bingham Oceanogr. Collect.*, 15: 324–343.

[235] **Roughgarden, J.** (1998). Primer of ecological theory. Prentice–Hall. Upper Sadle River, New Jersey. p. 456.

[236] **Rotatore, C., B. Colman and M. Kuzma.** (1995). The uptake of carbon dioxide by the marine diatoms *Phaeodactylum tricornutum* and *Cyclotella* sp. *Plant Cell Environ.*, 18: 913-918.

[237] **Rott, N.** (1990). Note on the history of the Reynolds number. *Ann. Rev. Fluid Mech.*, 22: 1–11.

[238] **Saiz, E., M. Alcaraz and G.–A. Paffenhöfer.** (1992). Effects of small–scale turbulence on feeding rate and gross–growth efficiency of three *Acartia* species (Copepoda: Calanoida). *J. Plank. Res.*, 14: 1085–1097.

[239] **Saiz, E.** (1994). Observations on the free–swimming behaviour of the copepod *Acartia tonsa*: effects of food concentration and turbulent water. *Limnol. Oceangr.*, 39: 1566–1578.

[240] **Saiz, E. & T. Kiørboe.** (1995). Predatory and suspension feeding of the copepod *Acartia tonsa* in turbulent environments. *Mar. Ecol. Progr. Ser.*, 122: 147–158.

[241] **Sakshaug, E., K. Andresen and D.A. Kiefer.** (1989). A steady state description of growth and light absorption in the marine planktonic diatom *Skeletonema costatum*. *Limnol. Oceanogr.*, 34: 198–205.

[242] **Starr, V.P.** (1968). *Physics of negative viscosity phenomena*. McGraw–Hill, New York.

[243] **Schanz, F.** (1985). Vertical light attenuation and phytoplankton development in Lake Zürich. *Limnol. Oceanogr.*, 30: 299–310.

[244] **Schanz, F.** (1986). Depth distribution of phytoplankton and associated spectral changes in downward irradiance in Lake Zürich. *Hydrobiol.*, 134: 183–192.

[245] **Schanz, F., P. Senn and Z. Dubinsky.** (1997). Light absorption by phytoplankton and the vertical light attenuation: ecological and physiological significance. *Oceanogr. Mar. Biol.*, 35: 71–95.

[246] **Schlesinger, W.H.** (1997). Biogeochemistry. An analysis of global change. (2nd Edition). Academic Press. San Diego. p. 588.

[247] **Segel, L.A. & J. Jackson.** (1972). Dissipative structure: an explanation and an ecological example. *J. Theor. Biol.*, 37: 545–559.

[248] **Seuront, L., F. Schmitt, Y. Lagedeuc, D. Schertzer and S. Lovejoy.** (1999). Universal multifractal analysis as a tool to characterize multiscale intermittent patterns: example of phytoplankton distribution in turbulent coastal waters. *J. Plank. Res.*, 21(1):1–46.

[249] **Skellam, J.G.** (1951). Random dispersal in theoretical populations *Biometrika*, 38: 196–218.

[250] **Smith, R.C. & K.S. Baker.** (1978a). The bio-optical state of ocean waters and remote sensing. *Limnol. Oceanogr.*, 23: 247–259.

[251] **Smith, R.C. & K.S. Baker.** (1978b). Optical classification of natural waters. *Limnol. Oceanogr.*, 23: 260–267.

[252] **Solé, R.V., J. Bascompte and J. Valls.** (1992). Stability and complexity of spatially extended two–species competition. *J. Theor. Biol.*, 159: 469–480.

[253] **Sreenivasan, K.R.** (1991). Fractals and multifractals in fluid turbulence. *Ann. Rev. Fluid Mech.*, 23: 539–600.

[254] **Steele, J.H. & E.W. Henderson.** (1992). A simple model for plankton patchiness. *J. Plank. Res.*, 14: 1397–1403.

[255] **Stumm, W. & J.J. Morgan.** (1996). Aquatic chemistry: chemical equilibria and rates in natural waters. (3rd ed.) John Wiley & Sons. New York.

[256] **Sundby, S. & P. Fossum.** (1990). Feeding conditions of arctonorwegian cod larvae compared with the Rothschild–Osborn theory on small–scale turbulence and plankton contact rates. *J. Plank. Res.*, 12: 1153–1162.

[257] **Talling, J.F.** (1960). Self–shading in natural populations of aq planktonic diatom. *Wetter und Leben*, 12: 235–242.

[258] **Talling, J.F.** (1970). Generalized and specialized features of phytoplankton as a form of photosynthetic cover. In: *Prediction and measurement of photosynthetic productivity.* Centre for Agricultural Publishing abd Documentation. Wageningen. The Netherlands. p. 431–445.

[259] **Taylor, G.I.** (1921). Diffusion by continuous movements. *Proc. Lond. Math. Soc.*, 20: 196–211.

[260] **Taylor, G.I.** (1932). The transport of vorticity and heat through fluids in turbulent motion. *Proc. Royal Soc. London A*, 135: 685–701.

[261] **Taylor, K.E. & J.E. Penner.** (1994). Response of the climate system to atmospheric aerosols and greenhouse gases. *Nature*, 369: 734-737.

[262] **Tennekes, H. & J.L. Lumley.** (1972). A first course in turbulence. *The MIT Press.* p.300.

[263] **Tett, P., A. Edwards and K. Jones.** (1986). A model for the growth of shelf–sea phytoplankton in summer. *Est. Coast. Shelf Sci.*, 23: 641–672.

[264] **Thingstad, F. & E. Sakshaug.** (1990). Control of phytoplankton growth in nutrient recycling ecosystems. Theory and terminology. *Mar. Ecol. Progr. Ser.*, 63: 261–272.

[265] **Thomas, W.H. & C.H. Gibson.** (1992). Effects of quantified small–scale turbulence on the dinoflagellate *Gymnodinium sanguineum (splendens)*: contrasts with *Gonyaulax (Lingulodinium) polyedra*, and the fishery implications. *Deep Sea Res.*, 39: 1249–1437.

[266] **Tilzer, M.M.** (1978). Prediction of productivity changes in lake Tahoe at increasing phytoplankton biomass. *Int. Ver. Theor. Ang. Limnol. Verh.*, 20: 407–413.

[267] **Tilzer, M.M.** (1983). The importance of fractional light absorption by photosynthetic pigments for phytoplankton productivity in Lake Constance. *Limnol. Oceanogr.*, 28: 833–846.

[268] **Tortell, P.D., J.R. Reinfelder and F.M.M. Morel.** (1997). Active uptake of bicarbonate by diatoms. *Nature*, 390: 243-244.

[269] **Turing, A.** (1952). The chemical basis of morphogenesis. *Philos. Trans. Roy. Soc. London*, Ser. B., 237: 37–72.

[270] **Tyler, J.E.** (1975). The *in situ* quantum efficiency of natural phytoplankton populations. *Limnol. Oceanogr.*, 20: 976–980.

[271] **Tyrrell, T.** (1999). The relative influences of nitrogen and phosphorus on oceanic primary production. *Nature*, 400: 525–531.

[272] **Ulanovicz, R.E.** (1980). An hypothesis on the development of natural communities. *J. Theor. Biol.*, 85: 223–245.

[273] **Ulanovicz, R.E.** (1986). Growth and development. Ecosystems phenomenology. Springer Verlag. New York. p. 203.

[274] **Valiela, I.** (1995) Marine ecological processes. Springer Verlag. New York. p. 686.

[275] **Varela, R., A. Cruzado, J. Tintoré, and E. García–Ladona.** (1992). Modelling the deep–chlorophyll maximum. A coupled physical–biological approach. *J. Mar. Res.*, 50: 441–463.

[276] **Vergassola, M., S. Gama and U. Frisch.** (1993). Proving the existence of negative isotropic eddy viscosity. *In:* Proctor, M.R.E., P.C. Mathews & A.M. Rucklidge. (eds.) NATO–ASI: Solar and Planetary dynamos. Cambridge University Press.

[277] **Verity, P.G.** (1981). Effects of temperature, irradiance and daylength on the marine diatom *Leptocylindricus danicus* Cleve. 1. Photosynthesis and cellular composition. *J. Exp. Mar. Biol. Ecol.*, 55: 79–81.

[278] **Verity, P.G.** (1982). Effects of temperature, irradiance and daylength on the marine diatom *Leptocylindricus danicus* Cleve. 4. Growth. *J. Exp. Mar. Biol. Ecol.*, 60: 209–222.

[279] **Waite, A.M., P.A. Thompson and P.J. Harrison.** (1992). Does energy control the sinking rates of marine diatoms? *Limnol. Oceanogr.*, 37(3): 468–477.

[280] **Walsh, J.J.** (1975). A spatial simulation model of the Peru upwelling ecosystem. *Deep–Sea Res.*, 22: 201–236.

[281] **Weidemann, A.D. & T.T. Bannister.** (1986). Absorption and scattering coefficient in Irondequoit Bay. *Limnol. Oceanogr.*, 31: 567–583.

[282] **Weinstock, J.** (1978). Vertical turbulent diffusion in a stably stratified fluid. *J. Atmos. Sci.*, 35: 1022–1027.

[283] **Weinstock, J.** (1987). The turbulence field generated by a linear gravity wave. *J. Atmos. Sci.*, 44: 410–420.

[284] **Whitakker, R.H.** (1975). Communities and ecosystems. Macmillan. London.

[285] **Williams, R.B. & M.B. Murdoch.** (1966). Phytoplankton production and chlorophyll concentration in the Beaufort Channel, North Carolina. *Limnol. Oceanogr.*, 11: 73–82.

[286] **Wyman, K.D., Z. Dubinsky, J. Porter and P.G. Falkowski.** (1987). Light absorption and utilization among hermatypic corals: a study in Jamaica, West Indies. *Mar. Biol.*, 96: 283–292.

[287] **Yaglom, A.M.** (1994). A.N Kolmogorov as a fluid mechanician and founder of a school in turbulence research. *Ann. Rev. Fluid Mech.*, 26: 1–22.

[288] **Yentsch, C.S. & D.W. Menzel.** (1963). A method for determination of phytoplankton chlorophyll and phaeophytin by fluorescence *Deep–Sea Res.*, 10: 221–231.

[289] **Yoder, J.A.** (1979). Effect of temperature on light–limited growth and chemical composition of *Skeletonema costatum* (Bacillariophyceae). *J. Phycol.*, 15: 362–370.

[290] **Zeigler, B.P.** (1976). Theory of modelling and simulation. Wiley and Sons. New York. p. 435.

[291] **Zimmerman, R.C., J.N. Kremer and R.C. Dugdale.** (1987). Acceleration of nutrient uptake by phytoplankton in a coastal upwelling ecosystem: a modeling analysis. *Limnol. Oceanogr.*, 32(2): 359–367.

[292] **Zonneveld, C., H.A. van der Berg and S.A.L.M. Kooijman.** (1997). Modeling carbon cell quota in light–limited phytoplankton. *J. Theor. Biol.*, 188: 215–226.